


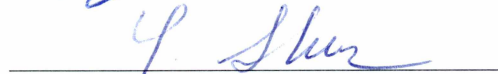
LONG-TERM PERFORMANCE OF WICKING FABRIC TO REDUCE DAMAGE IN
ALASKAN PAVEMENTS


By

Wendy Presler

RECOMMENDED:


Billy Connor



Yuri Shur

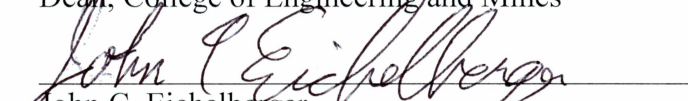

Juanyu Liu



Xiong Zhang
Advisory Committee Chair


Leroy Hulsey, Department Chair,
Department of Civil and Environmental Engineering

APPROVED:


Douglas Goering
Dean, College of Engineering and Mines


John C. Eichelberger
Dean of the Graduate School


Date 15 April 2016

APPLICATION OF WICKING FABRIC TO REDUCE DAMAGE IN ALASKAN
PAVEMENTS

A
THESIS

Presented to the Faculty
of the University of Alaska Fairbanks

in Partial Fulfillment of the Requirements
for the Degree of

MASTER OF SCIENCE

By

Wendy A. Presler, B.S.

Fairbanks, Alaska

May 2016

Abstract

Beaver Slide is located near kilometer 177.8 (mile 110.5) on the Dalton Highway. The road is sloped downhill when heading north. The road gradient is approximately 11%, and the road prism is on a side hill. Each year, soft spots usually appear in the pavement structure in late April and remain all summer. These soft spots have been called “frost boils”. The “frost boils” have resulted in extremely unsafe driving conditions and frequent accident occurrences. Conventional repair methods have not worked. A newly developed geosynthetic wicking fabric was installed in the road structure in August 2010. The fabric has a high specific surface area (consequently high wettability and high capillary action) and high directional permittivity. Test results over the initial two year period proved the effectiveness of the wicking fabric to mitigate “frost boils” and the subsequent road softening issue. Data collected during the past four years were analyzed to evaluate the long-term performance of the wicking fabric. A scanning electron microscope (SEM) was used to explore the interaction between the wicking fabric and in situ soils, and to determine the condition of the fabric five years after installation.

Table of Contents

Signature Page	i
Title Page	iii
Abstract	v
Table of Contents	vii
List of Figures	ix
List of Tables	xiii
Acknowledgements	xv
CHAPTER I INTRODUCTION	1
Problem Statement	1
Research Objectives	2
Research Methodology	3
CHAPTER II LITERATURE REVIEW	5
Mechanisms Causing Soft Spots	5
Previously Developed Methods of Mitigating Ice Formation	5
Use of Geotextile Materials to Mitigate ice Formation	6
CHAPTER III CONSTRUCTION OF TEST SECTION AND INSTRUMENTATION ... 11	
Construction Process	11
Instrumentation	17
Existing Site Conditions	19
CHAPTER IV DATA DISCUSSION AND ANALYSIS 23	
Temperature and Moisture Contours	23
General Climate Conditions	47
Temperature Data	47
Soil Temperature Changes	49
Soil Moisture Changes	53
CHAPTER V LONG TERM PERFORMANCE OF WICKING FABRIC	59
During Rainfall Events	59
During Freezing Process	67
During Thawing Process	71
SEM Analysis	77

CHAPTER VI CONCLUSIONS.....	83
REFERENCES.....	85

List of Figures

	Page
Figure 1.1 : Pressurized Ground Water Flow in Spring.....	1
Figure 1.2 : Soft Spots at Beaver Slide on May 12, 2010 (Looking North).....	2
Figure 2.1 : Wicking Fabric 2-layer Weave.....	8
Figure 2.2 : Water Movement in Fabric at Zero Hydraulic Gradient.....	9
Figure 3.1 : Excavation of East Lane (Looking North)	11
Figure 3.2 : Excavation of Pit at Center of Road (Sensor 13)	12
Figure 3.3 : Temperature and Moisture Sensor	13
Figure 3.4 : Bottom Layer of Wicking Fabric after Placement.....	14
Figure 3.5 : East Lane of Road after Construction	15
Figure 3.6 : Excavation of West Lane of Road.....	15
Figure 3.7 : First Layer of Wicking Fabric on West Side of Road	16
Figure 3.8 : Covering Wicking Fabric with Crushed Rock at the East Shoulder	17
Figure 3.9 : Construction of Data Collection Station	18
Figure 3.10 : Sensor Locations, Groundwater and Soil Stratigraphy	18
Figure 3.11 : Sieve Analysis for Soils Obtained During Construction.....	19
Figure 3.12 : Water in Existing Ditch on East Side of Road on August 5, 2010	20
Figure 3.13 : Water Along Tree Line on West Side of Road on August 5, 2010	20
Figure 4.1 : Temperature and Moisture Contours at Noon on August 18, 2010	24
Figure 4.2 : Hourly Relative Humidity Data for August 18-22, 2010	25
Figure 4.3 : Temperature and Moisture Contours at Noon on August 19, 2010	25
Figure 4.4 : Temperature and Moisture Contours at Noon on August 26, 2010	26
Figure 4.5 : Temperature and Moisture Contours at Noon on September 4, 2010.....	26
Figure 4.6 : Temperature and Moisture Contours at Noon on October 10, 2010	28
Figure 4.7 : Temperature and Moisture Contours at Noon on October 17, 2010	28
Figure 4.8 : Temperature and Moisture Contours at Noon on October 26, 2010.....	29
Figure 4.9 : Temperature and Moisture Contours at Noon on November 9, 2010	29
Figure 4.10 : Temperature and Moisture Contours at Noon on March 12, 2011	30
Figure 4.11 : Temperature and Moisture Contours at Noon on April 26, 2011	31

Figure 4.12 :	Temperature and Moisture Contours at Noon on May 15 2011.....	32
Figure 4.13 :	Temperature and Moisture Contours at Noon on May 22, 2011.....	32
Figure 4.14 :	Temperature and Moisture Contours at Noon on May 29, 2011.....	33
Figure 4.15 :	Temperature and Moisture Contours at Noon on May 30, 2011.....	34
Figure 4.16 :	Temperature and Moisture Contours at Noon on June 10, 2011.....	35
Figure 4.17 :	Temperature and Moisture Contours at Noon on July 1, 2011	36
Figure 4.18 :	Temperature and Moisture Contours at Noon on July 5, 2011	36
Figure 4.19 :	Temperature and Moisture Contours at Noon on July 18, 2011	37
Figure 4.20 :	Temperature and Moisture Contours at Noon on July 21, 2011	38
Figure 4.21 :	Temperature and Moisture Contours at Noon on July 31, 2011	39
Figure 4.22 :	Temperature and Moisture Contours at Noon on August 3, 2011	39
Figure 4.23 :	Temperature and Moisture Contours at Noon on August 15, 2011	40
Figure 4.24 :	Temperature and Moisture Contours at Noon on August 24, 2011	40
Figure 4.25 :	Temperature and Moisture Contours at Noon on September 23, 2011.....	41
Figure 4.26 :	Temperature and Moisture Contours at Noon on October 14, 2011	42
Figure 4.27 :	Temperature and Moisture Contours at Noon on October 23, 2011	43
Figure 4.28 :	Temperature and Moisture Contours at Noon on October 31, 2011	43
Figure 4.29 :	Temperature and Moisture Contours at Noon on November 6, 2011	44
Figure 4.30 :	Temperature and Moisture Contours at Noon on February 21, 2012.....	44
Figure 4.31 :	Temperature and Moisture Contours at Noon on April 16, 2012	45
Figure 4.32 :	Temperature and Moisture Contours at Noon on May 12, 2012.....	46
Figure 4.33 :	Temperature and Moisture Contours at Noon on May 22, 2012.....	46
Figure 4.34 :	Temperature and Moisture Contours at Noon on May 29, 2012.....	47
Figure 4.35 :	Hourly Temperature Data.....	48
Figure 4.36 :	Hourly Relative Humidity Data.....	49
Figure 4.37 :	Soil Temperature vs. Depth.....	50
Figure 4.38 :	Soil Temperature 0.45 Meters (1.5 Feet) below the Road Surface	51
Figure 4.39 :	Soil Temperature 0.76 Meters (2.5 Feet) below the Road Surface	51
Figure 4.40 :	Soil Temperature 1.06 Meters (3.5 Feet) below the Road Surface	52
Figure 4.41 :	Soil Temperature 1.97 Meters (6.5 Feet) below the Road Surface	53
Figure 4.42 :	Soil Moisture Content 0.45 Meters (1.5 Feet) below the Road Surface ...	54

Figure 4.43 :	Soil Moisture Content 0.76 Meters (2.5 Feet) below the Road Surface ...	55
Figure 4.44 :	Soil Moisture Content 1.06 Meters (3.5 Feet) below the Road Surface ...	57
Figure 4.45 :	Soil Moisture Content 1.97 Meters (6.5 Feet) below the Road Surface ...	58
Figure 5.1 :	Soil Moisture Contours before Short Duration Rainfall	65
Figure 5.2 :	Soil Moisture Contours 1 Hour after Short Duration Rainfall	65
Figure 5.3 :	Soil Moisture Contours 1 Day after Short Duration Rainfall	66
Figure 5.4 :	Soil Moisture Contours before Long Duration Rainfall	66
Figure 5.5 :	Soil Moisture Contours 1 Hour after Long Duration Rainfall	66
Figure 5.6 :	Soil Moisture Contours 1 Day after Long Duration Rainfall	67
Figure 5.7 :	Temperature and Moisture Contours on October 4, 2012	67
Figure 5.8 :	Temperature and Moisture Contours on October 20, 2012	68
Figure 5.9 :	Temperature and Moisture Contours on December 4, 2012	69
Figure 5.10 :	Moisture Contours on September 20, 2010	70
Figure 5.11 :	Moisture Contours on September 25, 2011	70
Figure 5.12 :	Moisture Contours on October 11, 2012	70
Figure 5.13 :	Moisture Contours on October 5, 2013	71
Figure 5.14 :	Temperature and Moisture Contours on May 9, 2013	72
Figure 5.15 :	Temperature and Moisture Contours on May 25, 2013	73
Figure 5.16 :	Temperature and Moisture Contours on June 26, 2013	74
Figure 5.17 :	Temperature and Moisture Contours on July 30, 2013	75
Figure 5.18 :	Moisture Contours on May 25, 2011	76
Figure 5.19 :	Moisture Contours on May 25, 2012	76
Figure 5.20 :	Moisture Contours on May 25, 2013	76
Figure 5.21 :	Moisture Contours on May 25, 2014	77
Figure 5.22 :	Intact Sample (Sample 4)	78
Figure 5.23 :	Surface Clogging (Sample 20)	78
Figure 5.24 :	Beneath Sample (Sample 25)	78
Figure 5.25 :	Wicking Fiber Comparison	78
Figure 5.26 :	New Wicking Fabric	79
Figure 5.27 :	Permanent Deformation	79
Figure 5.28 :	Top View	80

Figure 5.29 : Front View.....	80
Figure 5.30 : Sample 17.....	80
Figure 5.31 : Sample 23.....	80
Figure 5.32 : Sample 3.....	81
Figure 5.33 : Sample 11.....	81
Figure 5.34 : Sample 21.....	82
Figure 5.35 : Sample 26.....	82

List of Tables

	Page
Table 2.1: Technical Data for Wicking Fabric.....	10
Table 5.1: Rainfall Event Summary.....	59-64

ACKNOWLEDGMENTS

The author wishes to express her appreciation to Dr. Xiong Zhang for his enthusiasm and guidance, Alaska Department of Transportation & Public Facilities (AKDOT&PF) and Tencate Geosynthetics (North America) for their support throughout this study, as well as Alaska University Transportation Center (AUTC) for the funding that made this project and thesis possible. The author would also like to thank the project advisory committee members Billy Connor, Jenny Liu and Yuri Shur, and graduate students Lin Li and Chuang Lin whose efforts have contributed significantly to this work.

CHAPTER I

INTRODUCTION

Roadway pavement degradation due to thaw weakening of the structure is a common condition in northern regions. Soft spots, often referred to as frost boils, are the result of spring thawing of ice lenses that were formed inside the pavement structure through the previous winter. While their exact mechanism of formation may vary, they can result in unsafe driving conditions and cause vehicle accidents.

Problem Statement

Beaver Slide is located at kilometer 177.8 (mile 110.5) on the Dalton Highway, and is about 8 kilometers (5 miles) south of the Arctic Circle. The road is downhill when heading north, at approximately 11% gradient. The road is constructed on a steep side slope, where shallow groundwater drains down the slope starting each spring and lasts until early winter. The excess water comes up into the road embankment, causing soft spots and subsequent road damage, as illustrated in Figure 1.1.



Figure 1.1 Pressurized Ground Water Flow in Spring

Crews from AKDOT&PF have observed soft, loose aggregate at the surface of the road during spring thawing (Figure 1.2). Operators of heavy trucks tend to apply their brake on the downhill slope when encountering the soft spots and make the condition even worse. The soft spots have resulted in extremely unsafe driving conditions and frequent accident occurrences. Alaska Department of Transportation and Public Facilities (AKDOT&PF) maintenance crews

have added material to the road, re-graded the road surface, and have rebuilt the road section in the past to try to alleviate the problem. These conventional methods of repair have not been successful.

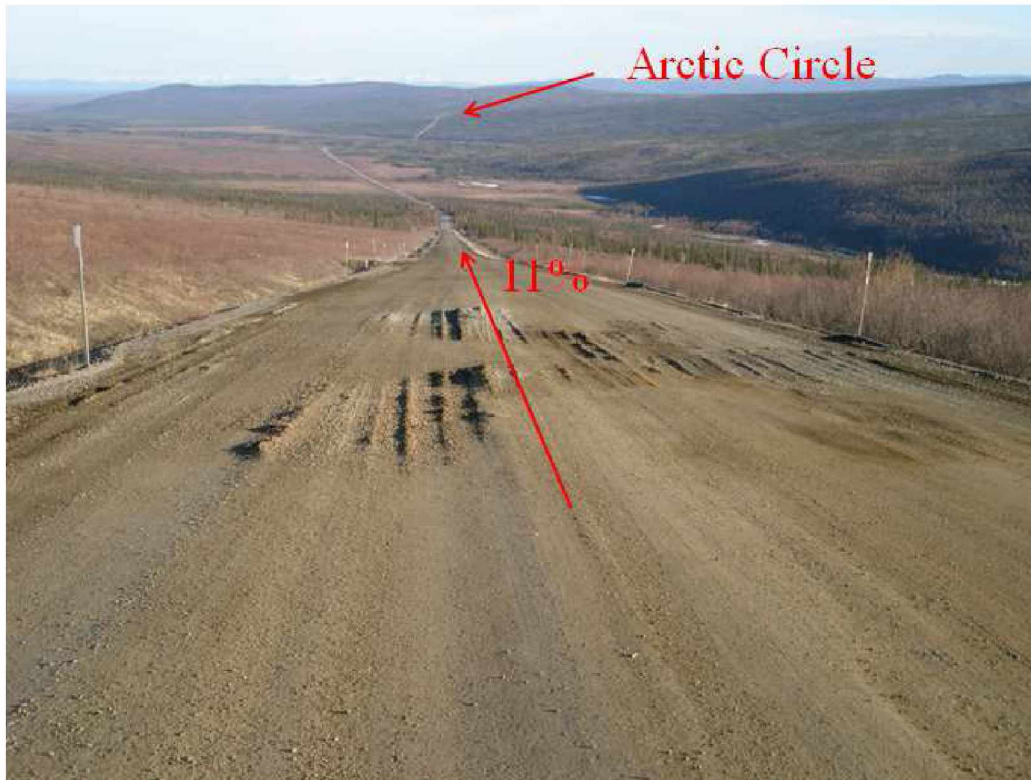


Figure 1.2 Soft Spots at Beaver Slide on May 12, 2010 (Looking North)

Research Objectives

A new type of geotextile is recently developed and can potentially be used to mitigate the issue discussed above. This type of geotextile is a dual function geotextile product, which contains a high modulus polypropylene yarn for reinforcement and a nylon wicking yarn to absorb and transport water laterally under unsaturated conditions. Since this geotextile material is relatively new, there is no direct evidence to prove that the wicking fabric will work in the field to improve performance of pavement. In addition, there are also some concerns whether the wicking fabric will work in the harsh climate of Alaska, because water is frozen in the winter and may potentially cause the wicking fabric to lose the ability to transport water. After several discussions including the engineers at AKDOT&PF, researchers at the University of Alaska

Fairbanks, and representatives from the fabric manufacturer, it was decided that it was worthwhile to construct a test section including the wicking fabric at Beaver Slide to verify the fabric's effectiveness in mitigating the frost heave and subsequent thaw weakening problems in Alaskan pavements.

In this study, the following objectives are addressed:

- To systematically evaluate the mechanisms causing soft spots in the road at the site,
- To construct a test section at the site in order to monitor the improved performance of the test section by implementing two layers of geotextile wicking fabric;
- To evaluate the effectiveness of the wicking fabric in mitigating the frost heave and subsequent thaw weakening problems; and
- To assess the severity of potential issues, such as the effect of salinity, the effect of clogging, permanent deformation and aging of the wicking fabric.

Research Methodology

To meet the objectives of this study, the following major tasks are accomplished:

- Task 1: Literature Review
- Task 2: Construction of Test Section
- Task 3: Data Collection and Analyses
- Task 4: Conclusions and Recommendations

Task 1: Literature Review

A comprehensive literature review was conducted to gather information related to this study. The literature review focused on a previous study on the use of geosynthetics to reduce the occurrence of soft spots at the road surface.

Task 2: Construction of Test Section

A 60-foot section of the Dalton Highway, known as Beaver Slide, was reconstructed and included the installation of two layers of a newly developed wicking fabric. Temperature and moisture content sensors were installed in the roadway section, and were connected to a data logger. A weather station was installed at the site to monitor air temperature and relative humidity.

Task 3: Data Collection and Analyses

Gradation tests were performed in the laboratory on materials collected at the site during construction of the test section, to determine if the soils present were frost-susceptible. Data was collected from the data logger at the site two or three times per year, over a four year period. The data collected was analyzed to evaluate the performance of the test section, and to determine the mechanisms responsible for the frost heave and thaw weakening prior to improvement.

Samples of the wicking fabric were collected from the site during the summer of 2015. The samples were analyzed using a scanning electron microscope (SEM) to determine if soil clogging or aging is impacting the performance of the fabric.

Task 4: Conclusions and Recommendations

Based on the tasks above, a summary of conclusions were presented in this task. Also, recommendations were given regarding the future use of the wicking fabric to address similar problems in northern pavements.

CHAPTER II

LITERATURE REVIEW

The soft spots were believed to be related to the formation of ice lenses in the soil and subsequent thaw-weakening. As a result, a portion of the literature review focus is on previous studies on the use of geosynthetic materials to reduce ice formation and thaw-weakening. The geotextile used in this project is relatively new; therefore, previous studies regarding the characterization of geotextiles are investigated to grasp the basic hydraulic properties of the new material.

Mechanisms Causing Soft Spots

The three elements necessary for ice lenses to form, which may result in soft spots after thawing, are (Holtz and Kovacs 1981): 1) the presence of frost susceptible soil, 2) subfreezing temperatures, and 3) water supply from shallow groundwater table, infiltration, an aquifer, or held within the voids of fine-grained soils. All three of these conditions are met in many northern regions. Removal of any of the three conditions above eliminates, or at least minimizes, ice formation and thaw weakening. Numerous techniques have been developed to mitigate the damage to pavements and airfields caused by ice formation and thaw weakening.

Previously Developed Methods of Mitigating Ice Formation

The most common and widely employed technique is to remove the frost susceptible soils and replace them with non-frost susceptible soils. The non-frost susceptible soils are placed in layers thick enough to reduce the strain in the frost susceptible soil layers beneath to an acceptable level. This method is the removal of condition 1, above. To address this issue, AKDOT&PF stipulates that granular materials with fines content less than 6% must be used as base course material (AKDOT&PF, 2004).

To remove condition 2 above, a common method is to include the use of insulation in the pavement section to reduce the freeze and thaw depth (Esch 1994). In many remote areas where the removal of frost susceptible soils and the reduction of subfreezing temperatures are difficult and expensive, removal of available water could lead to savings in construction costs.

By breaking the capillary flow path, which will remove condition 3 above, ice formation will be less severe. A capillary barrier is a layer of coarse-grained soils or geosynthetic material that is placed in a frost susceptible soil to: 1) reduce upward capillary flow of soil water due to the suction gradient generated by evaporation or freezing, and (or) 2) reduce or prevent water from infiltrating from the overlying fine-pored, unsaturated soil into the soil below the capillary barrier (Henry and Holtz 2001). In the latter case, if the capillary barrier is sloped, the infiltrating water flows in the fine soil downwards along the interface with the capillary barrier. Granular capillary barriers have been used to successfully reduce ice formation in roads. Taber (1929) found that placing a layer of coarse sand above the water supply in frost-susceptible soil specimens being frozen from the top down eliminated ice formation. He also noted that ice formation requires substantially more water than is naturally available in the soil pores. Casagrande (1938) and Beskow (1946) described placing a layer of sand or gravel above the water table in road construction to reduce ice formation in overlying fine-grained soil. Later, Rengmark (1963) and Taivenen (1963) documented using a sand layer above the water table to help prevent ice formation in overlying frost susceptible soil.

Use of Geotextile Materials to Mitigate Ice Formation

In recent years, geotextiles and geocomposites were evaluated to determine their effectiveness, when used as capillary barriers, to reduce frost damage in pavement structures. Geosynthetic drainage nets have been found to serve as good capillary barriers under most conditions because of their large pore sizes. The performance of nonwoven geotextiles as a capillary barrier appears to be compromised by soil intrusion into their interiors, decreasing the pore size and increasing the affinity of the material to water. Hoover et al. (1981) and Allen et al. (1983) independently performed experiments indicating that certain geotextiles reduced ice formation when they were placed horizontally in upright, cylindrical soil specimens that were frozen from the top down with water freely available at the base. Henry (1988) noted the importance of the surface properties of the geotextiles, i.e., that hydrophobic geotextiles were much more effective in reducing ice formation than hydrophilic geotextiles. Henry (1996) concluded that properly selected geotextiles reduce ice formation in soils by functioning as capillary barriers and summarized guidelines for granular capillary barriers. It was also concluded that in addition to

serving as capillary barriers during freezing, and to reinforce or separate and filter subgrade layers, geotextiles probably can be used for a combination of functions to reduce frost-related damage during thaw.

Guthrie and Hermansson (2006) reported test results which indicated that unsaturated granular base material became saturated due to water vapor flow during freezing. Henry et al. (2002) proposed the use of a geocomposite capillary barrier drain (GCBD) as a promising method to reduce frost damage in pavement structures under unsaturated conditions. A GCBD consists of a capillary barrier layer sandwiched between transport layers. The function of the capillary barrier layer is to impede unsaturated flow, either upward or downward. The GCBD is similar to drains commonly used to minimize the impacts of frost. However, conventional drainage systems are not wholly effective in reducing water-related problems in partially saturated soils (Beskow 1946, translated by Osterberg 1991), while soil above the ground water table is unsaturated, and ice formation occurs through the capillary rise of water. The GCBD is used to perform as a capillary break and as a drainage system that can suck water out of soil—that is, provide drainage while the soil is unsaturated. The key to the success of such a system is the use of a material with high wettability, which means it can absorb water from unsaturated soils, and high permittivity, which means it can transport the absorbed water out of the pavement structure quickly. The transport layer used in Henry et al. (2002) was a very heavy, woven, multifilament material with a mass per unit area of 2,370 grams per square meter, a thickness of 3.2 millimeters, and an O95 size of 0.075 millimeters. The infiltration test results indicated that the use of the GCBD to limit moisture changes in pavement subgrades and bases was very promising. Furthermore, the GCBD prevented the moistening of the subgrade at many of the infiltration rates tested. Whether the capillary barrier will reduce or prevent ice formation by preventing upward flow during freezing was not tested.

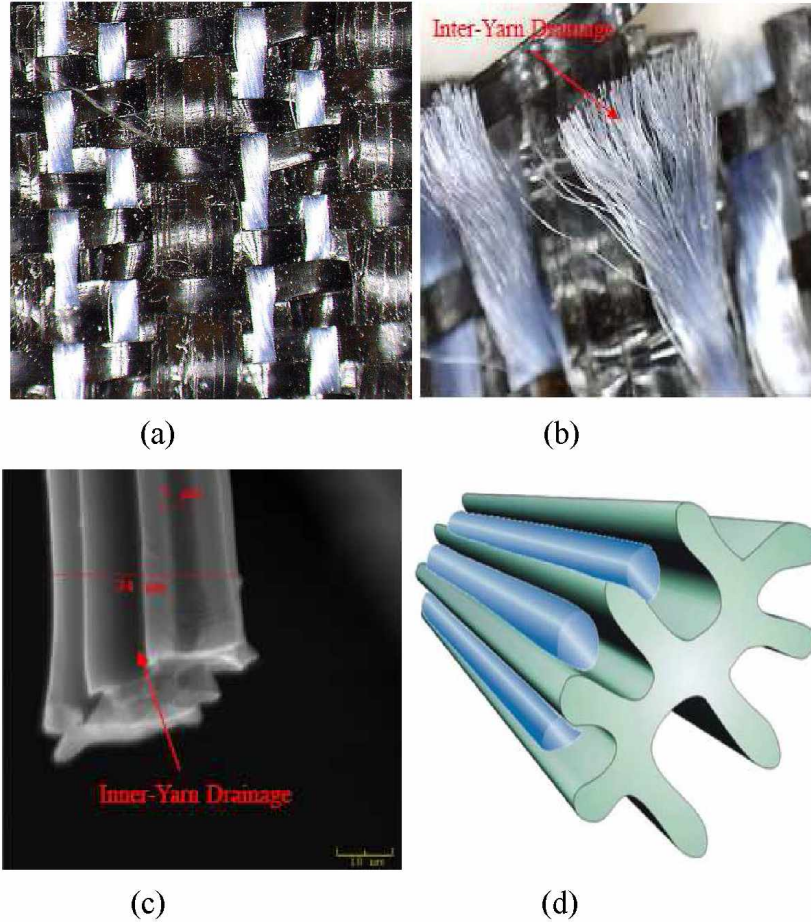


Figure 2.1 Wicking Fabric 2-layer Weave

A recently developed type of wicking fabric is made of nylon yarns and polypropylene yarns as shown in Figure 2.1(a). The black polypropylene yarns tend to repel water and have high tensile strength, which provide reinforcement and confinement properties. The special hydrophilic and hygroscopic 4DG™ yarns (white fibers) shown in Figure 2.1(b) have a high specific surface area (consequently high wettability and high capillary action) and high permittivity. A microscopic image of a 4DG™ fiber, Figure 2.1(c), indicates that the average diameter of each wicking fiber is about 34 microns, and the groove spacing is approximately 7 microns. The multichannel cross-section has one of the highest available shape factors and has the greatest number of channels per fiber, which give the wicking fabric great potential for maximizing capillary action and water transport in an unsaturated environment, as illustrated in Figure 2.1(d). The specific surface area of the wicking fabric is 3,650 square centimeters per

gram, and it has a permittivity of 0.24 per second, which is equivalent to a flow rate of 611 liters per minute per square meter (about 12.5 gallons per minute per square foot).

Table 2.1 presents the technical data sheet information for the wicking fabric. Zhang and Belmont (2009) performed a series of laboratory tests to investigate the performance of the wicking fabric to mitigate the frost heave and thaw-weakening problems in Alaska's harsh climate. The test results generally showed that the wicking fabric can potentially be used as a capillary barrier to mitigate frost heave. Although the results on the frost heave test were inconclusive, there were some definitive results indicating that the wicking fabric transports water under unsaturated conditions.

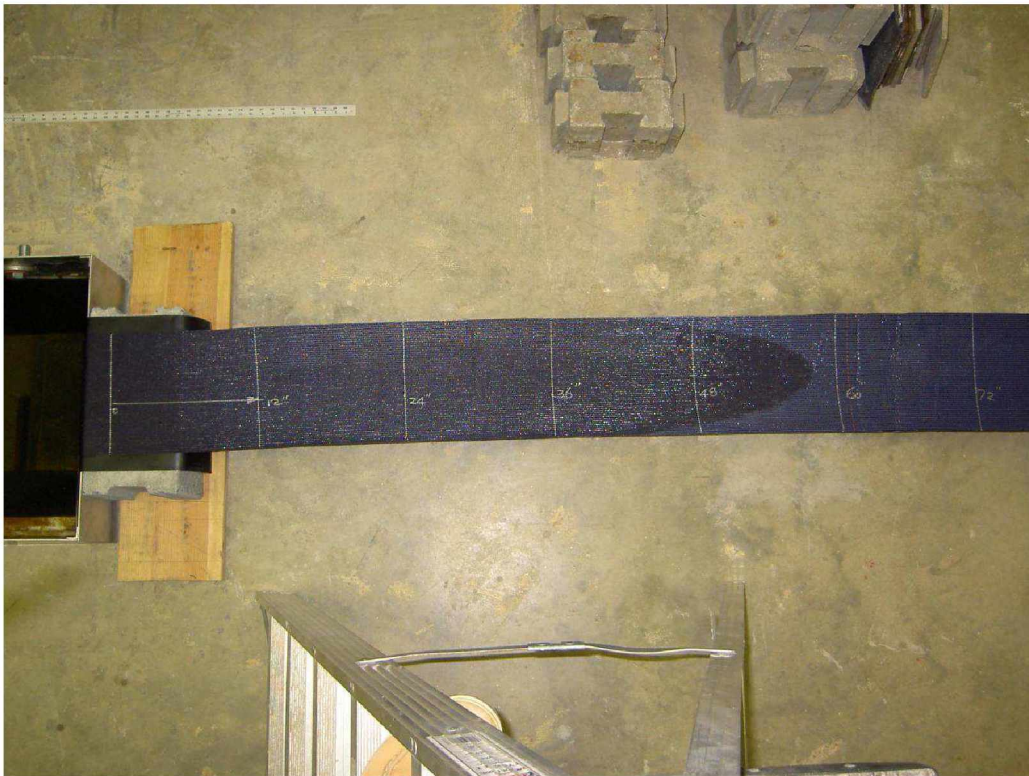


Figure 2.2 Water Movement in Fabric at Zero Hydraulic Gradient

Table 2.1 presents the technical data sheet information for the wicking fabric. Zhang and Belmont (2009) performed a series of laboratory tests to investigate the performance of the wicking fabric to mitigate the frost heave and thaw-weakening problems in Alaska's harsh climate. The test results generally showed that the wicking fabric can potentially be used as a

capillary barrier to mitigate frost heave. Although the results on the frost heave test were inconclusive, there were some definitive results indicating that the wicking fabric transports water under unsaturated conditions. However, there was no direct evidence to prove that the wicking fabric will work in the field to improve the performance of pavement. In addition, there were some concerns regarding whether the wicking fabric would work in the harsh climate of Alaska, because water is frozen in the winter and may potentially cause the wicking fabric to lose the ability to transport water. After several discussions including the engineers at AKDOT&PF, researchers at the University of Alaska Fairbanks, and representatives from the fabric manufacturer, it was decided that it was worthwhile to construct a test section including the wicking fabric at Beaver Slide to verify the fabric effectiveness in mitigating the frost heave and subsequent thaw weakening problems in Alaskan pavements.

Table 2.1 Technical Data for Wicking Fabric

Mechanical Properties	Test Method	Unit	Minimum Average Roll Value	
			MD	CD
Tensile Strength (at ultimate)	ASTM D4595	lbs/in (kN/m)	450 (78.8)	450 (78.8)
Tensile Strength (at 2% strain)	ASTM D4595	lbs/in (kN/m)	45 (7.9)	75 (13.1)
Tensile Strength (at 5% strain)	ASTM D4595	lbs/in (kN/m)	135 (23.6)	325 (56.9)
CBR Puncture Strength	ASTM D6241	lbs (N)	2300 (10235)	
Permittivity	ASTM D4491	sec ⁻¹	0.24	
Pore Size (O ₅₀)	ASTM D6767	microns	85	
Pore Size (O ₉₅)	ASTM D6767	microns	195	
Apparent Opening Size (AOS) ¹	ASTM D4751	U.S.Sieve (mm)	40 (0.43)	
Flow Rate	ASTM D4491	gal/min/ft ² (L/min/m ²)	15 (611)	
Wet Front Movement ² (24 minutes)	ASTM C1559 ³	inches	6.0 Vertical direction	
Wet Front Movement ² (983 minutes) Zero Gradient	ASTM C1559 ³	inches	73.3 Horizontal direction	

¹ASTM D4751: AOS is a maximum opening diameter value

²At standard temperature and pressure

³Modified

CHAPTER III

CONSTRUCTION OF TEST SECTION AND INSTRUMENTATION

This chapter consists of a description of the construction process at the test section, installation of instrumentation and data collection equipment, and observations of existing site conditions.

Construction Process

A test section of 18.1 meters (60 feet) was constructed at Beaver Slide from August 3, 2010 through August 5, 2010. The construction was performed according to the following procedure.

The east (northbound) lane of the road was excavated to a depth of 1.06 meters (3.5 feet) below the original road surface, while the west (southbound) lane of the road was not excavated, to maintain the traffic flow.



Figure 3.1 Excavation of East Lane (Looking North)

Before installing the first layer of wicking fabric, three pits were excavated below the centerline, the edge of the original road, and the edge of the excavation limit, as shown in Figure 3.10 below. These pits were about 1.97 meters (6.5 feet) below the original road surface, or about

0.91 meters below the mass excavation level. At the bottom of the excavation pits, three pairs of sensors were installed and are numbered 13, 6, and 2, respectively.

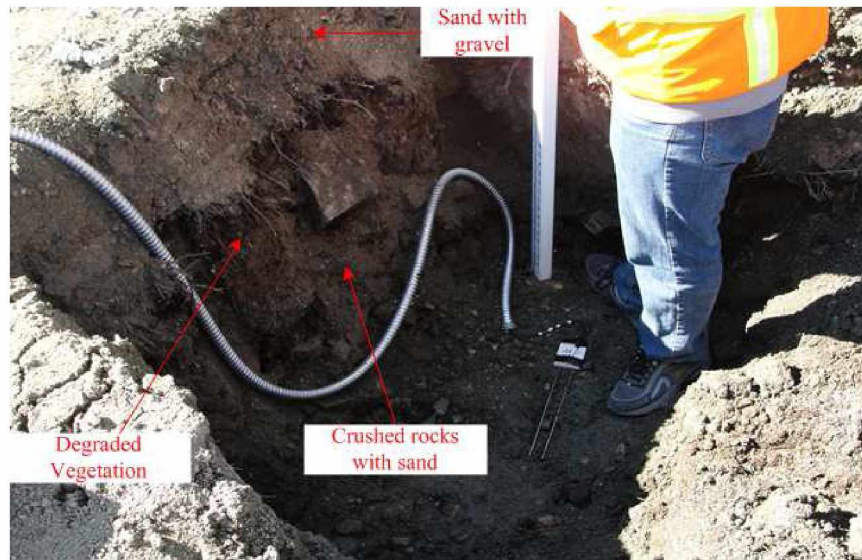


Figure 3.2 Excavation of Pit at Center of Road (Sensor 13)

Each pair of sensors consists of a Campbell Scientific 107-L temperature sensor and a CS616-L water content reflectometer.

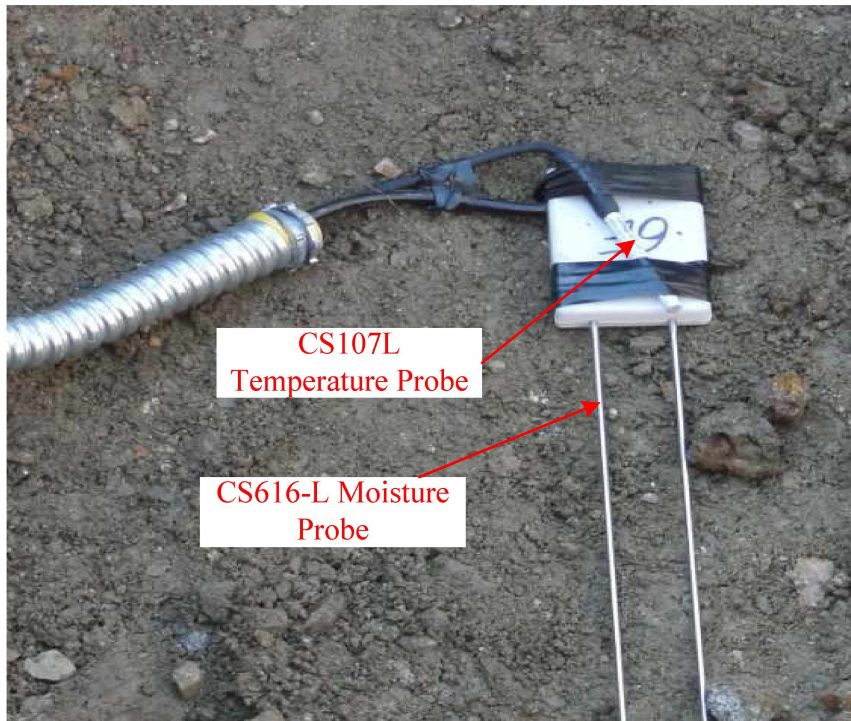


Figure 3.3 Temperature and Moisture Sensor

The excavation pits were then backfilled with soils originally taken out, and were compacted according to AKDOT&PF general construction procedures. Sensor pairs 1, 5, 9, and 12 were then carefully installed and the first layer of wicking fabric was installed. Since water transportation in the wicking fabric is directional, care was taken to make sure the direction of the wicking fabric was along the transverse direction of the road section, so that water in the road structure was transported horizontally to the road shoulder.



Figure 3.4 Bottom Layer of Wicking Fabric after Placement

The excavated soils were brought back to backfill the excavation area with a thickness of approximately one foot. The backfill was then graded and compacted on top of the wicking fabric. After the soils were compacted, sensors 4 and 8 were installed. Then a second layer of wicking fabric was installed as shown in Figure 3.10. A portion of the two layers of wicking fabric is exposed to the air, about 1.21 meters (4 feet), at the road shoulder. After the second layer of wicking fabric was placed properly, the excavated soils were used to backfill the excavation area with a thickness of approximately one foot. The backfill was then graded and compacted, and then sensors 3 and 7 were installed. The rest of the soil was brought back to backfill the excavation in the east lane to its original elevation.

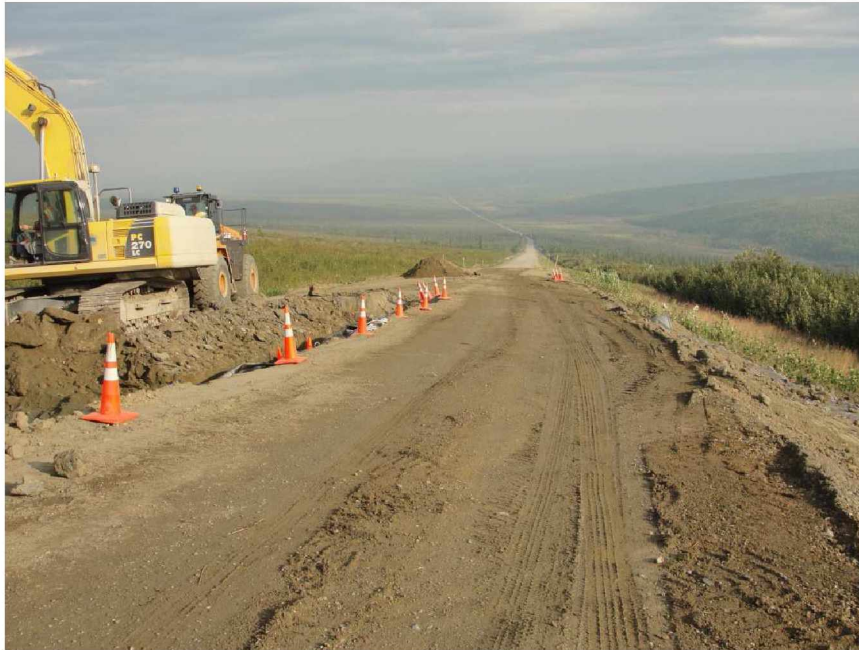


Figure 3.5 East Lane of Road after Construction

The next step in the construction process began with digging out the west (southbound) lane of the road to a depth of approximately 1.06 meters (3.5 feet). To avoid the possible introduction of water from the ditch into the road section, the west road shoulder was not excavated.



Figure 3.6 Excavation of West Lane of Road

After the bottom of the excavation was graded, a pit was then excavated at about 5.44 meters (18 feet) from the center of the road to install sensor 20. The excavation pit was backfilled, and sensors 16, 19 and 22 installed, followed by a layer of the wicking fabric. The same procedures as those described above were followed. The excavated soils were used to backfill the excavation area with a thickness of approximately 0.30 meters (one foot). The backfill was then graded and compacted. After the soils were compacted, sensors 11, 15, and 18 were installed. A second layer of wicking fabric was installed and the excavated soils were brought back to backfill the excavation area with a thickness of approximately another one foot.



Figure 3.7 First Layer of Wicking Fabric on West Side of Road

The backfill was then graded and compacted and then sensors 10, 14, and 17 were installed. After that, the rest of the soil was brought back to backfill the excavation to its original elevation. Approximately four feet of fabric was left exposed to the air on the east shoulder, the down-slope side of the embankment, where water will be allowed to drain out of the fabric and flow down the hill.



Figure 3.8 Covering Wicking Fabric with Crushed Rock at the East Shoulder

Instrumentation

All of the wires for the sensors were protected using aluminum conduit to prevent damage from the traffic loads. The aluminum conduits were grouped together, buried in a small ditch in the transverse direction, and connected to a Campbell Scientific CR1000 datalogger. In addition to the temperature and moisture sensors inside the test section, an HMP45C Air Temperature/Relative Humidity weather station was installed to monitor the air temperature and relative humidity at the test site. The panel temperature of the datalogger was monitored by the CR1000. All of the data acquisition devices were organized into an ENC14/16 -NC-NM weather-resistant enclosure, which was installed on the tundra on the west side of the road.



Figure 3.9 Construction of Data Collection Station

The locations of the sensors were surveyed using a Leica NA720. TBMW1 and TBMW2 presented in Figure 3.10 were temporary benchmark locations.

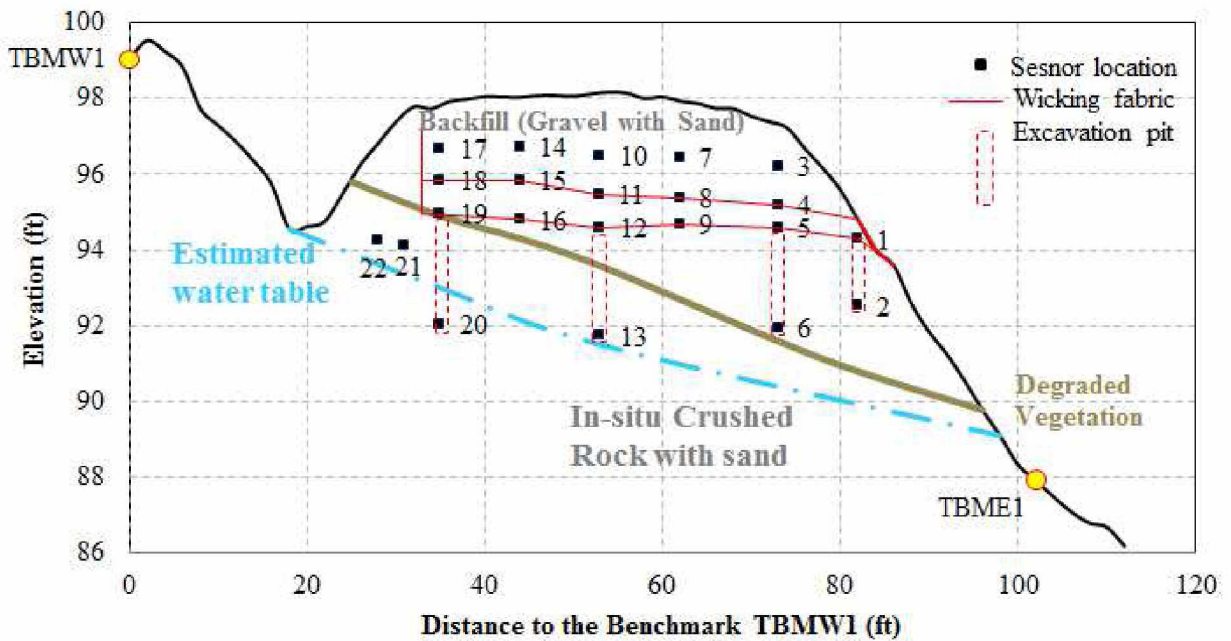


Figure 3.10 Sensor Locations, Groundwater and Soil Stratigraphy

Existing Site Conditions

Figure 3.10 shows the soil stratigraphy at the test section location, based upon the observations made during the construction process. It was found that the road section was built directly on the original tundra on the hill, using the degraded granite which was classified as silt with gravel, according to USCS classifications. Sieve analysis of the soils indicated that some soils have fines contents greater than 6%, indicating that some soils at the site may be frost susceptible.

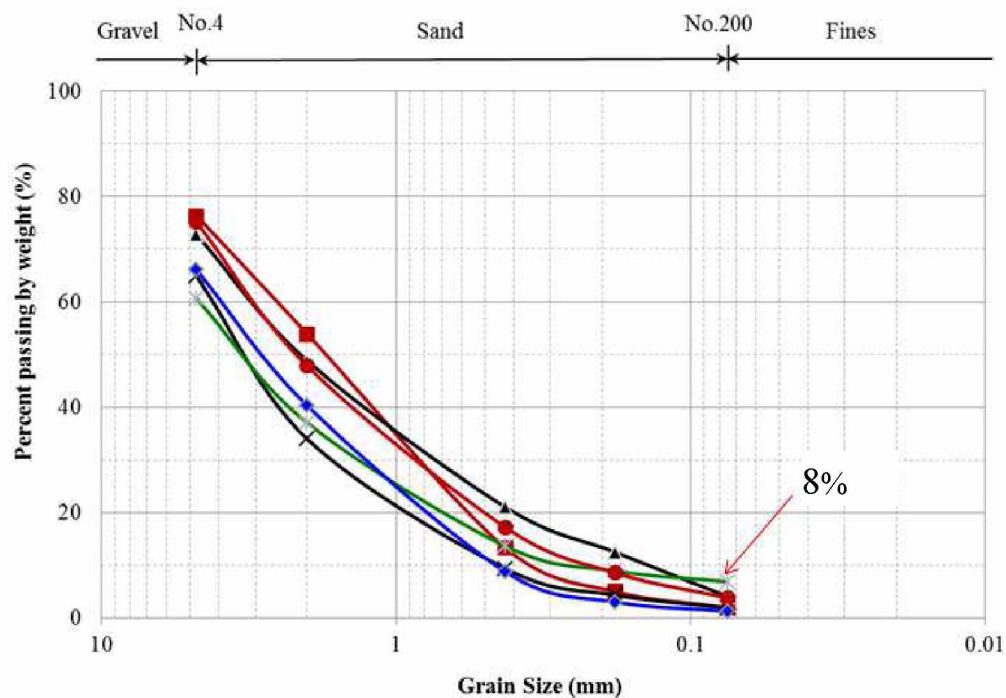


Figure 3.11 Sieve Analysis for Soils Obtained During Construction

The original tundra was encountered at about 0.91 meters (3.0 feet) below the ground surface at the west edge of the road, and at 1.36 meters (4.5 feet) below the surface at the centerline of the road section. It was about 2.72 meters (9 feet) lower than the road surface where it extended to the tree line at the west shoulder of the road. The buried vegetation encountered was degraded into a dark-yellow layer, which was about 0.05-0.1 meters (1-2 inches) thick. *In situ* crushed rocks with sand were encountered below the vegetation. Ground water was observed 0.15 meters (6 inches) below the tundra surface, once the tundra was removed. Additionally,

standing water was observed during the construction process in the existing drainage ditch along the west side of the road. On the east side of the road, water was sporadically present along the tree line.



Figure 3.12 Water in Existing Ditch on East Side of Road on August 5, 2010



Figure 3.13 Water Along Tree Line on West Side of Road on August 5, 2010

Ground water was also encountered when installing sensor 20. Figure 3.10 above shows the approximate ground water table based upon these observations.

CHAPTER IV

DATA DISCUSSION AND ANALYSIS

In this chapter, general climate conditions, soil temperature changes, soil moisture changes, and performance of the wicking fabric are discussed.

Temperature and Moisture Contours

The hourly temperature and moisture data at different sensor locations were used to generate temperature and moisture contours to analyze the spatial distributions of the temperature and moisture to evaluate the performance of the wicking fabric. As shown in Figure 4.1, on August 18, 2010, two weeks after the test section was constructed, the soils at 1.83 meters (6 feet) below the road surface were completely unfrozen. The soil temperatures decreased with an increase of depth, varying from 12° C to 4° C. The isothermal lines were approximately parallel to the configuration of the road section. The moisture content contour was not related to the temperature contour, but depended upon the groundwater flow. At sensor locations 19 through 22, close to the ditch, the soils were saturated. Soils at sensor locations 12 through 13 were also saturated, while the soils at sensor locations 14 through 16 were unsaturated. The saturated soil protrusion coincided with the excavation of the pit for sensor installation at the center of the road, which implied that compaction at the excavation pit was not good and resulted in a channel with relatively high permeability. At the east shoulder of the road from sensors 5 to 2, there was a narrow zone of soils with high moisture content. This location is near the edge of the wicking fabric on the drainage side.

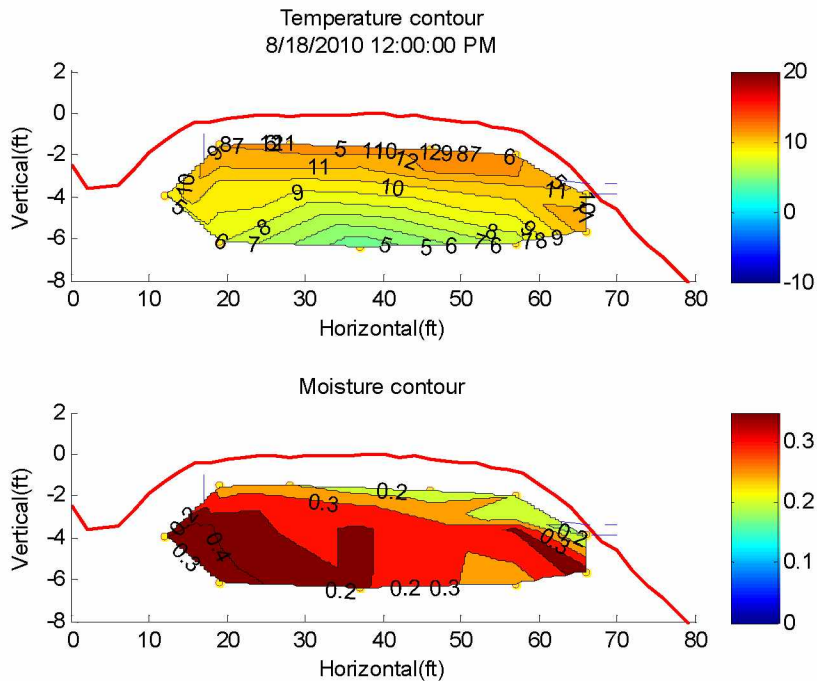


Figure 4.1 Temperature and Moisture Contours at Noon on August 18, 2010

As shown in Figure 4.2, the relative humidity on August 19, 2010 from 3:00 am to 9:00 am was 100%, indicating that there was a rainfall event. This was consistent with changes in the moisture content contour at noon on August 19, 2010, as shown in Figure 4.3. Compared with the previous day, there was a clear increase in the moisture content in the test section, especially along the wicking fabric layer at 0.91 meters (3 feet) below the road surface. At the east shoulder of the road from sensors 5 to 2, moisture contents increased in soils close to the drainage edge of the wicking fabric. This was a clear indication that the wicking fabric provided a good channel for water transport.

In the following two weeks, there was no rainfall, as indicated by the relative humidity data. Compared with Figures 4.4 and 4.5, the moisture content in the test section clearly decreased, especially in the east lane of the road. The soils at the drainage edge of the wicking fabric were the driest. The decrease in moisture content in the west lane of the road was clear but not as dramatic. The high moisture content protrusion at the center of the road was reduced significantly until August 26, 2010 (Figure 4.15) and nearly

disappeared on September 4, 2010 (Figure 4.5). The soils remained saturated at sensor locations 20 through 22, close to the ditch.

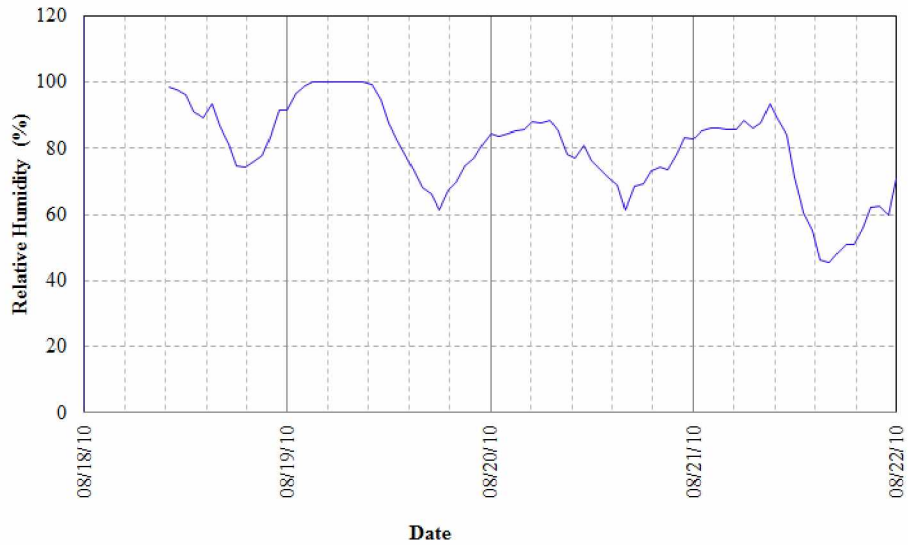


Figure 4.2 Hourly Relative Humidity Data for August 18-22, 2010

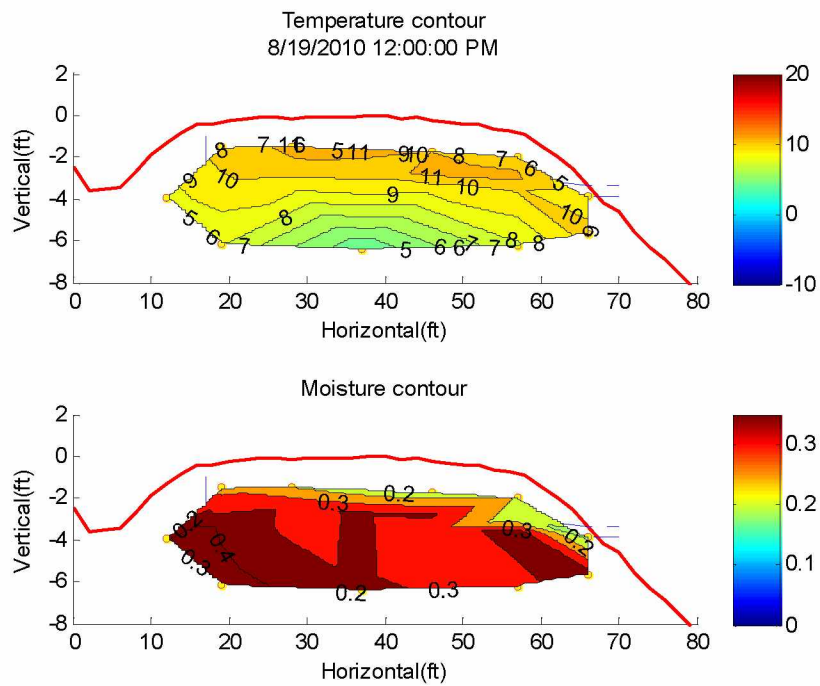


Figure 4.3 Temperature and Moisture Contours at Noon on August 19, 2010

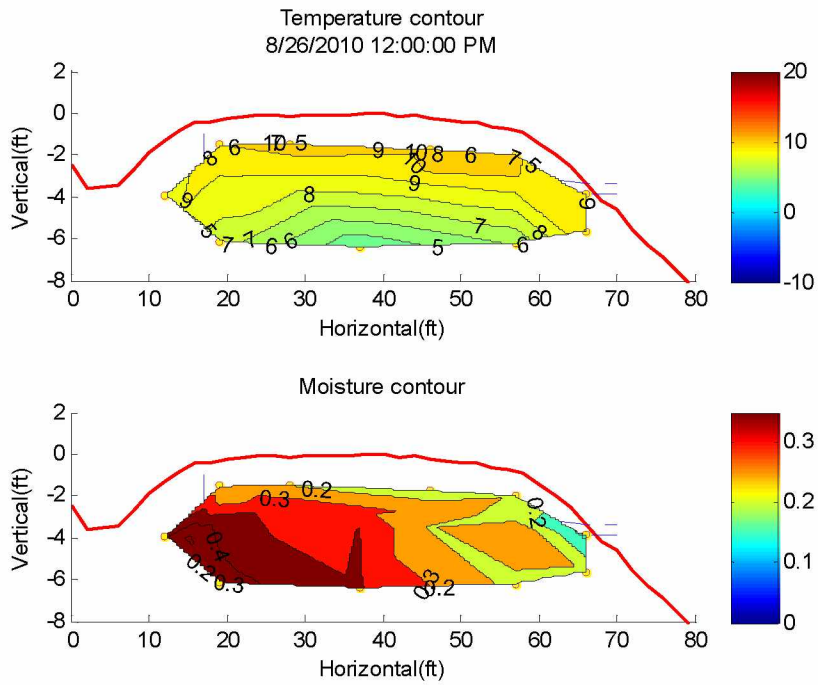


Figure 4.4 Temperature and Moisture Contours at Noon on August 26, 2010

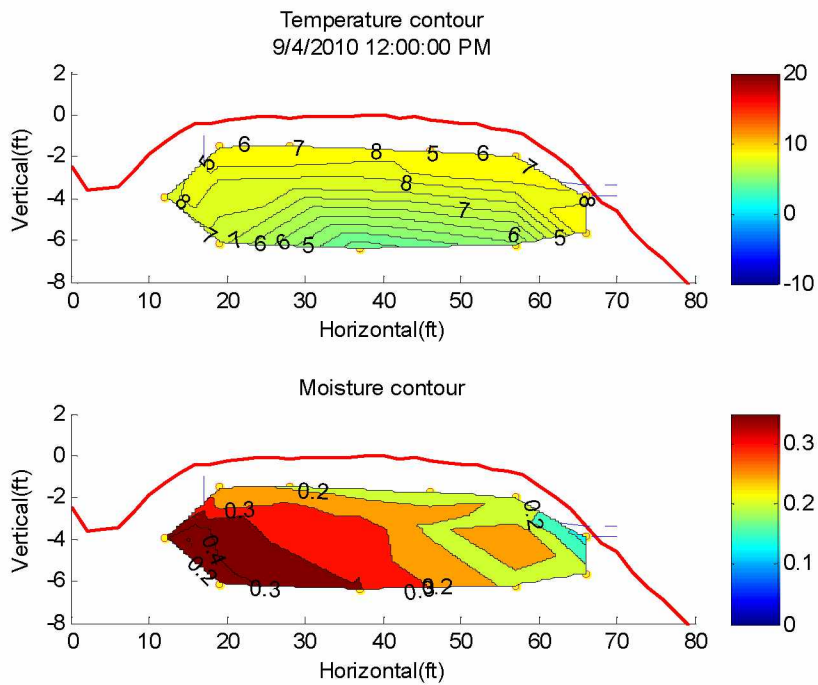


Figure 4.5 Temperature and Moisture Contours at Noon on September 4, 2010

Figures 4.6 through 4.9 show the temperature and moisture content contours for the road section when the freezing front penetrated to approximately 0.46 meters, 0.76 meters, 1.07 meters and 1.83 meters (1.5 feet, 2.5 feet, 3.5 feet, and 6 feet) below the road surface on October 10, 2010, October 17, 2010, October 26, 2010, and November 9, 2010, respectively. It can be seen from these figures that the temperature and moisture contours for frozen soils are similar (as shown later, it seemed that unfrozen moisture content for partially frozen soils depended upon temperature only). For soils in the unfrozen zone, there was no clear relationship between the temperature and moisture content contours. It was also found that before the soils were frozen, the moisture contents had been significantly reduced in all figures. Possible reasons for this included: (1) reduced water supply from the upward tundra, (2) increased drainage due to dryer environment, and (3) upward movements of water due to frost heaving. The third possibility is related to the frost boils/soft spots problem. Analysis of the 2011 Spring thawing data indicated that there were no frost heave occurrences for this period. As a result, the explanation is that there was reduced water supply from the upward tundra.

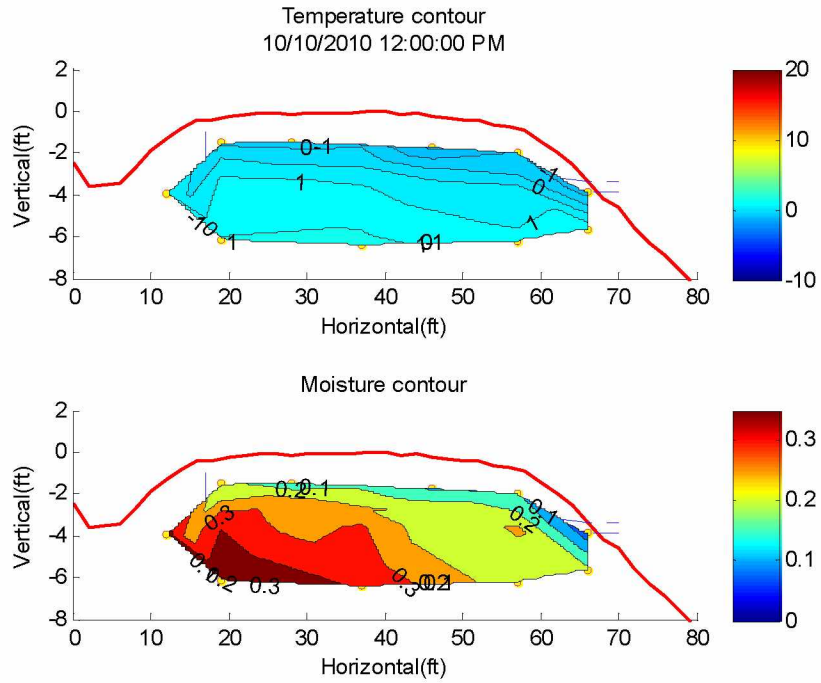


Figure 4.6 Temperature and Moisture Contours at Noon on October 10, 2010

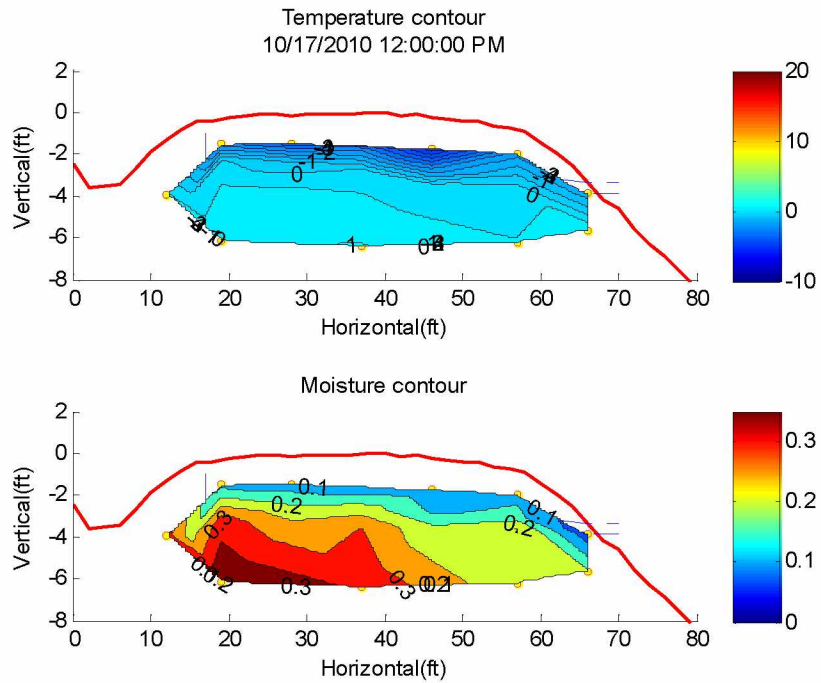


Figure 4.7 Temperature and Moisture Contours at Noon on October 17, 2010

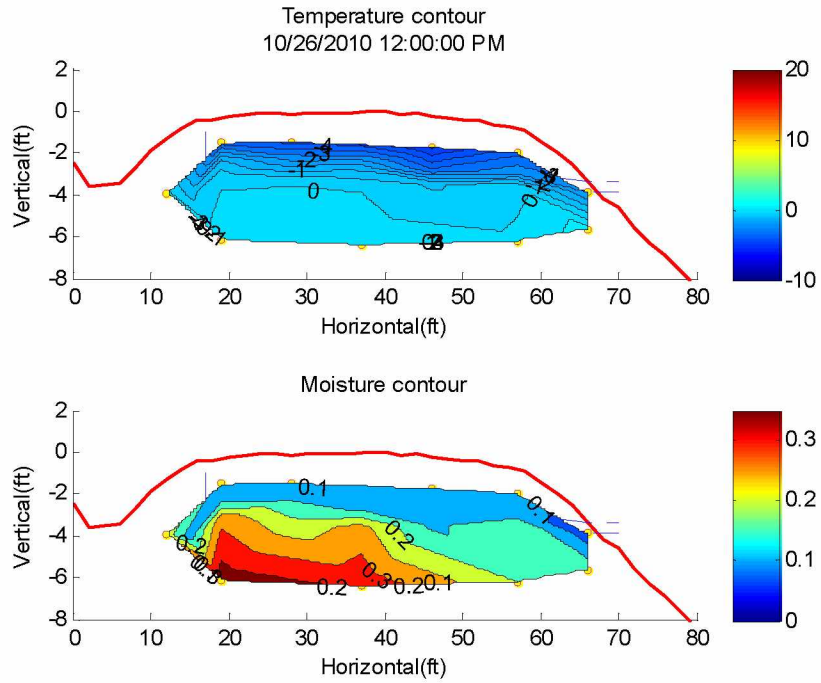


Figure 4.8 Temperature and Moisture Contours at Noon on October 26, 2010

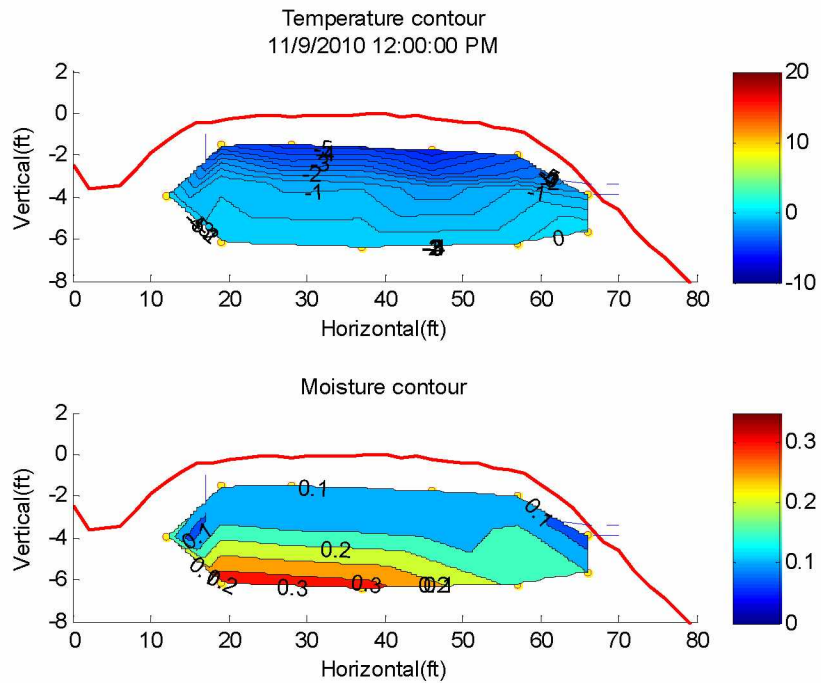


Figure 4.9 Temperature and Moisture Contours at Noon on November 9, 2010

Figure 4.10 shows the temperature and moisture content contours for the road section on March 12, 2011, when the whole road section was completely frozen at the time of a site visit. The moisture content was not greater than 10% at any sensor location.

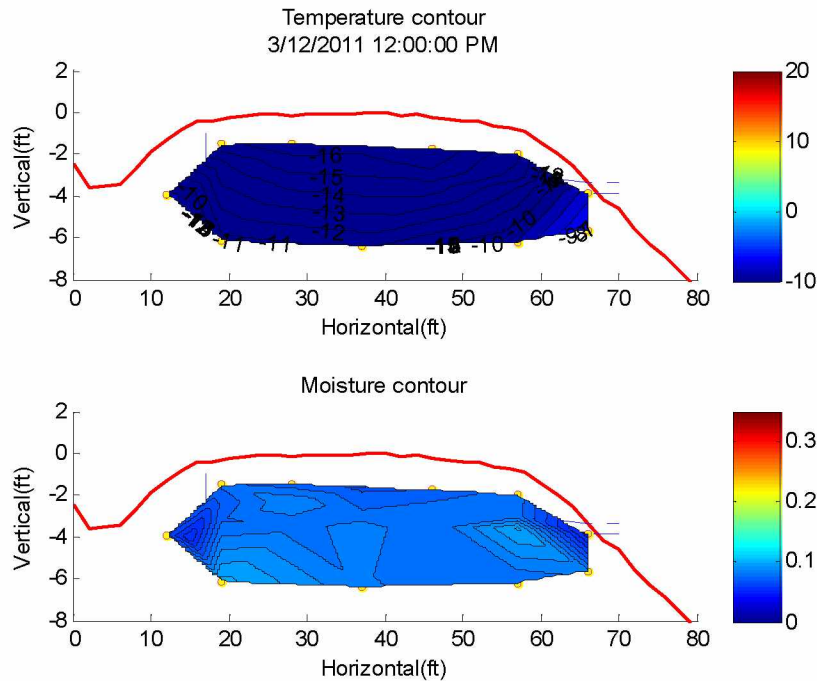


Figure 4.10 Temperature and Moisture Contours at Noon on March 12, 2011

When the air temperature rose to above 0° C on April 26, 2011, the entire road section remained frozen, and the unfrozen moisture content was very low, as shown in Figure 4.11. Figures 4.12 and 4.13 show the temperature and moisture contours of the road section on May 15 and May 22 of 2011, when the thawing depths were 0.46 meters and 0.76 meters (1.5 feet and 2.5 feet) below the road surface. Soils at sensor 22 near the ditch remained frozen. It is also worth noting that in previous years, the frost boils and soft spots had appeared during this time of year. It is therefore concluded that the frost boils/soft spots which had occurred in early Spring each year at the Beaver Slide were not likely to be caused by the groundwater, but more likely to be caused by thawing of in-situ water in the soils. Since excess amounts of water are needed to form frost boils/soft spots, it must come from the thawing of ice lenses created by frost heave. Figures 4.12 and 4.13

indicate that the soil moisture content in the road section remained low, which implied that there was no frost heave 0.76 meters (2.5 feet) below the road surface. In other words, the wicking fabric successfully eliminated the frost heave and subsequent thaw weakening in the spring of 2011.

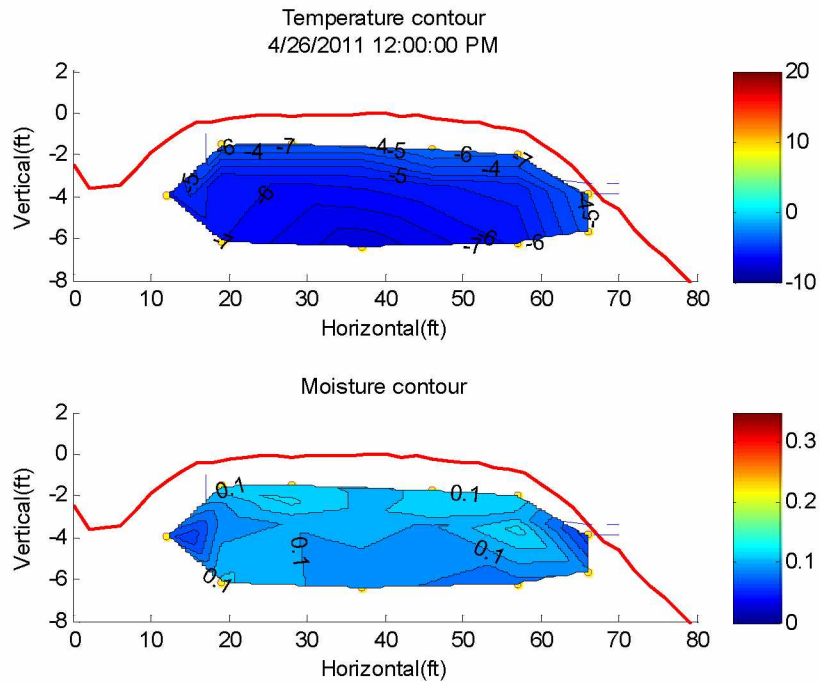


Figure 4.11 Temperature and Moisture Contours at Noon on April 26, 2011

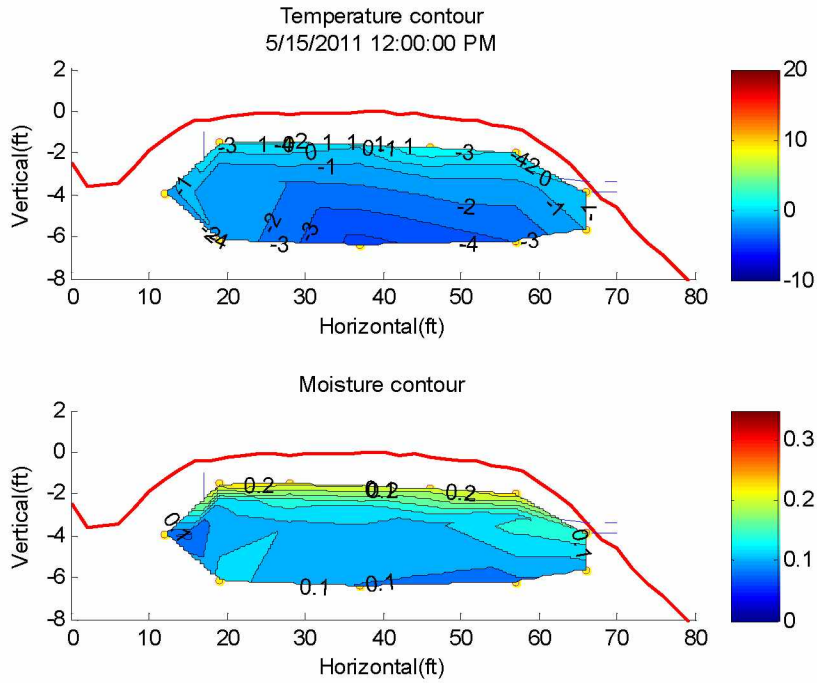


Figure 4.12 Temperature and Moisture Contours at Noon on May 15, 2011

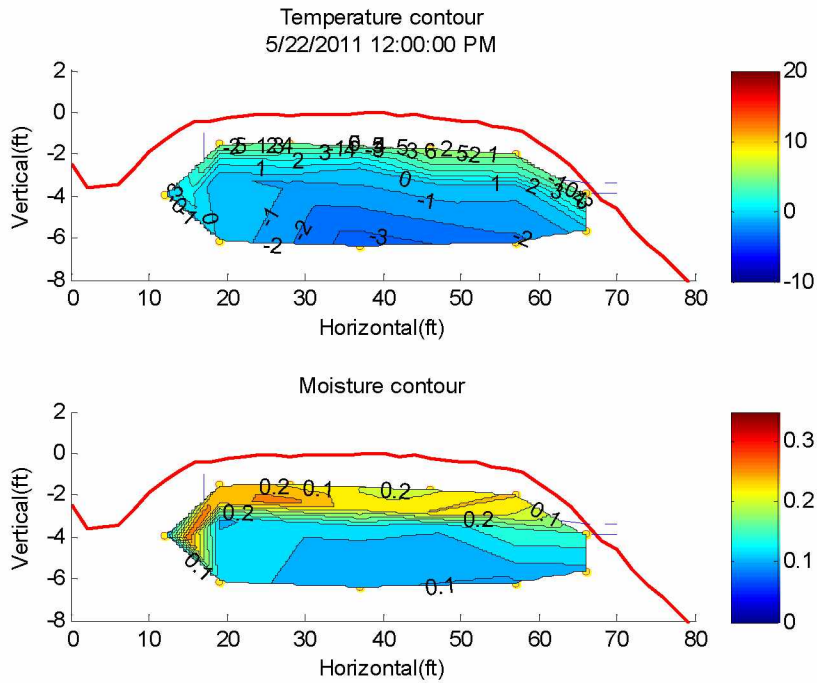


Figure 4.13 Temperature and Moisture Content at Noon on May 22, 2011

Figure 4.14 shows the temperature and moisture content contours of the road section on May 29, 2011. Soil temperatures were higher in east lane of the road section and were thawed to a depth of 1.83 meters (6 feet) below the road surface, while the west lane of the road was thawed to a depth of 1.37 meters (4.5 feet). It can be seen that soils at sensor locations 2, 5, 8, 9, 19, 21 and 22 were nearly saturated. There was a frozen soil protrusion around sensor locations 20, 16, 11, 12, and 13. This can be seen more clearly in Figure 4.15, which shows the temperature and moisture content contours of the road section on May 30, 2011. The frozen soil protrusion was reduced at the center of the road where sensors 12 and 13 are located. On both sides of the frozen soil protrusion, the soils were near saturation at the depth of 1.22 meters (4 feet) below the road surface. Comparing Figure 4.14 and Figure 4.15, the soils in the east lane of the road were much drier one day later. The soils at 1.83 meters (6 feet) below the road surface remained frozen.

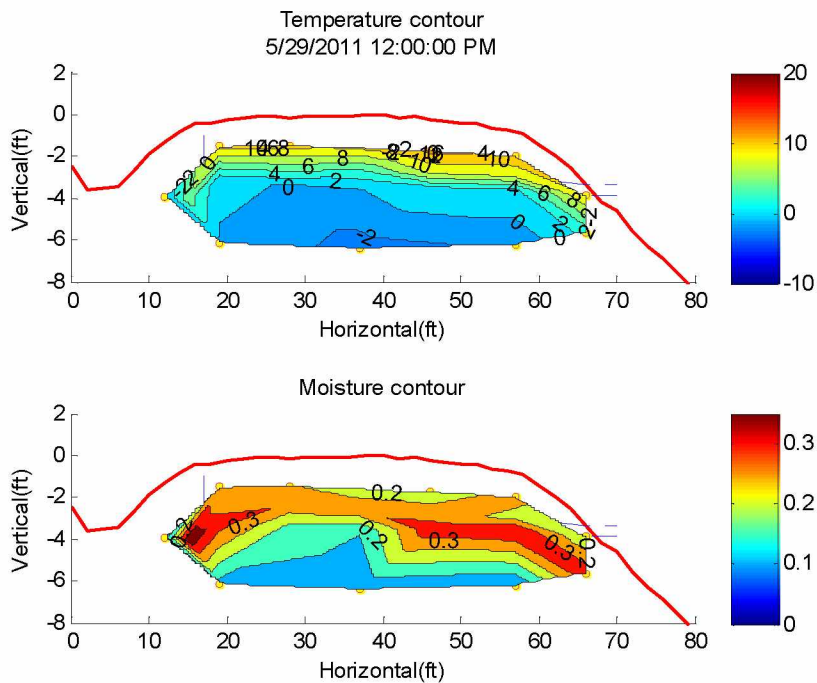


Figure 4.14 Temperature and Moisture Contours at Noon on May 29, 2011

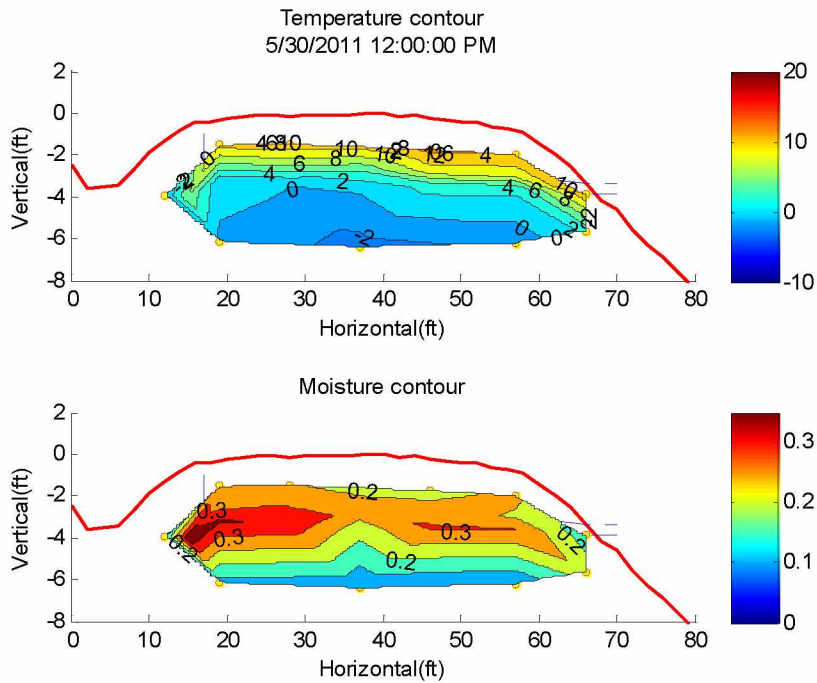


Figure 4.15 Temperature and Moisture Contours at Noon on May 30, 2011

From April 17, 2011 to June 8, 2011 there was no clear indication of any significant rainfall. The groundwater present was mainly the result of thawing of frozen soils from the hill. During the morning of June 9, 2011, there was a rainfall event. As a result, there was an increase in water content in the road section. As shown in Figure 4.16, there was a high water content channel at 0.91 to 1.52 meters (3 to 5 feet) below the road surface, where the two layers of wicking fabric were installed. The soils at 1.52 meters (5 feet) below the road surface remained frozen, which can be considered an impermeable layer. The soils above 0.91 meters (3 feet) below the road surface had moisture contents of less than 30%.

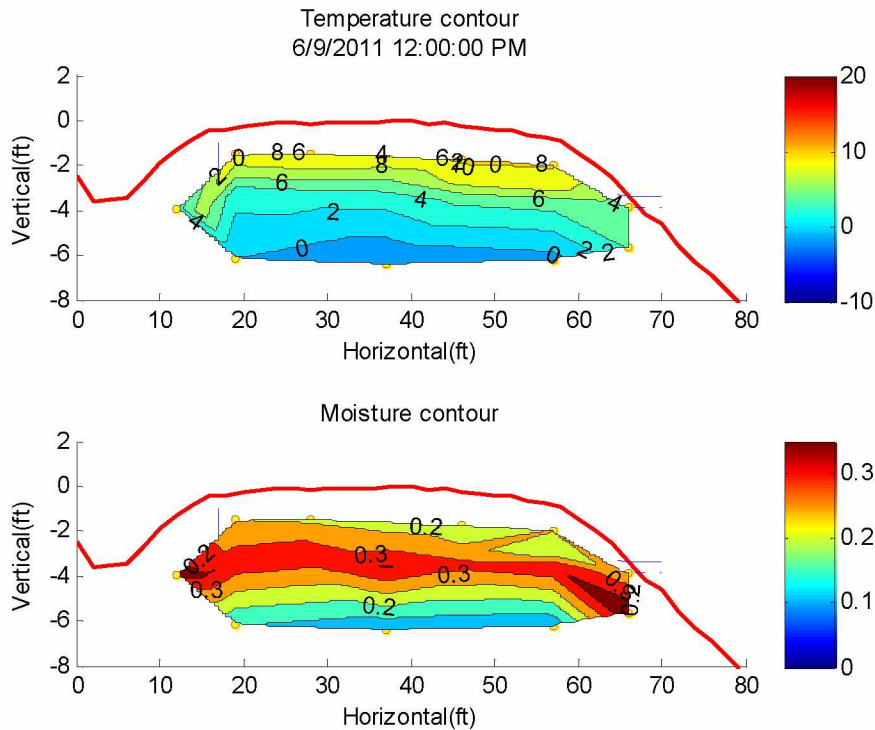


Figure 4.16 Temperature and Moisture Contours at Noon on June 10, 2011

Figure 4.17 shows the temperature and moisture contours at noon on July 1, 2011 after a possible rainfall event in the morning of the same day. There were three saturated soil zones in the moisture contour: one near the ditch, one at the center, and one at the east lane. Below the saturated soil zone at the center was a frozen soil core with low (unfrozen) water content. This seemed to imply that the non-uniform thawing of the soils caused ponding of water at the center of the road. With the installed wicking fabric, the road section dried out in a few days. Figure 4.18 shows the temperature and moisture contours at noon on July 5, 2011. Comparing Figures 4.17 and 4.18, it can be seen that the wicking fabric can act as a siphon to drain the ponded water caused by non-uniform thawing. This is also consistent with the results from the laboratory tests discussed in Chapter II.

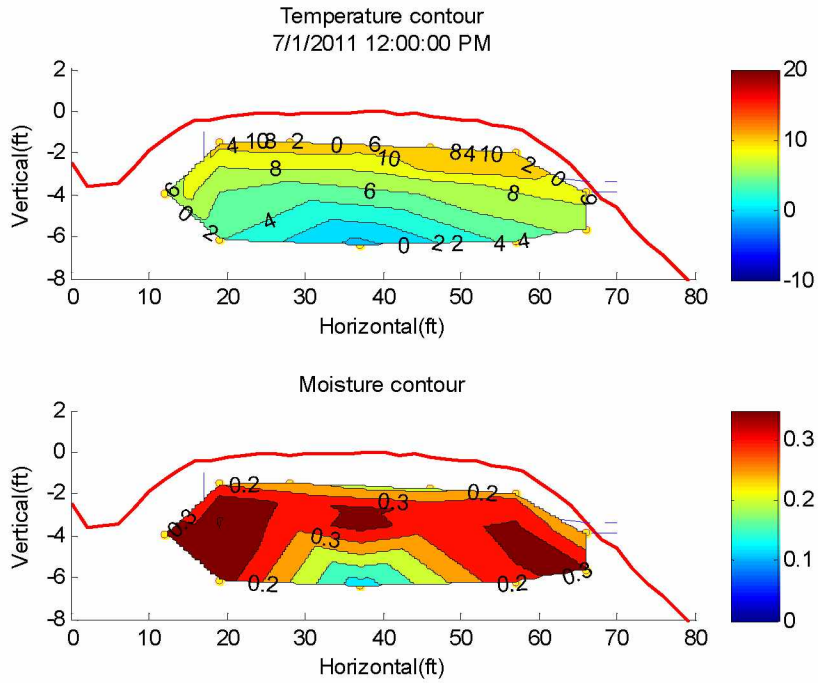


Figure 4.17 Temperature and Moisture Contours at Noon on July 1, 2011

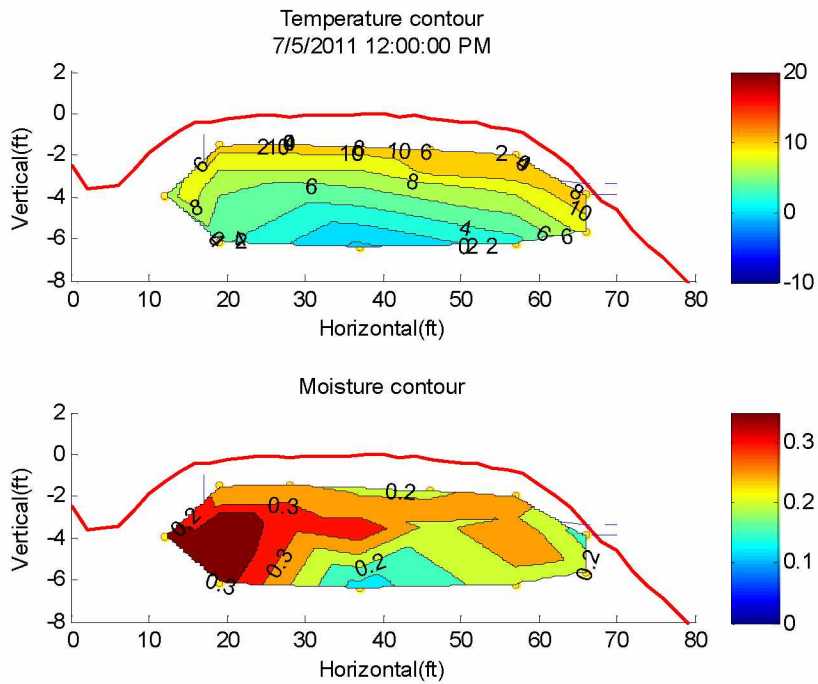


Figure 4.18 Temperature and Moisture Contours at Noon on July 5, 2011

Figure 4.19 shows the temperature and moisture contours at noon on July 18, 2011 after a possible rainfall event in the morning of the same day. There were three saturated soil zones at the same locations as those shown in Figure 4.17, which confirmed the conclusion that the wicking fabric can work as a siphon to drain the ponded water caused by non-uniform thawing. Comparing Figures 4.18 and 4.19, it can also be seen that the frozen soil core had been reduced significantly.

Figure 4.20 shows the temperature and moisture contours at noon on July 21, 2011, when the road section was completely thawed. The soils at 1.83 meters (6 feet) below the center of the road became saturated. The moisture content contour was similar but not the same as those in the previous year. The difference might imply that the freeze-thaw cycle changed the soil structure in the road section. Specifically, it seemed that the soils at the west lane of the road between sensor locations 13 and 22 had been loosened and had higher moisture content compared with the previous year. The soils at the east lane of the road were significantly drier than soils at the west lane.

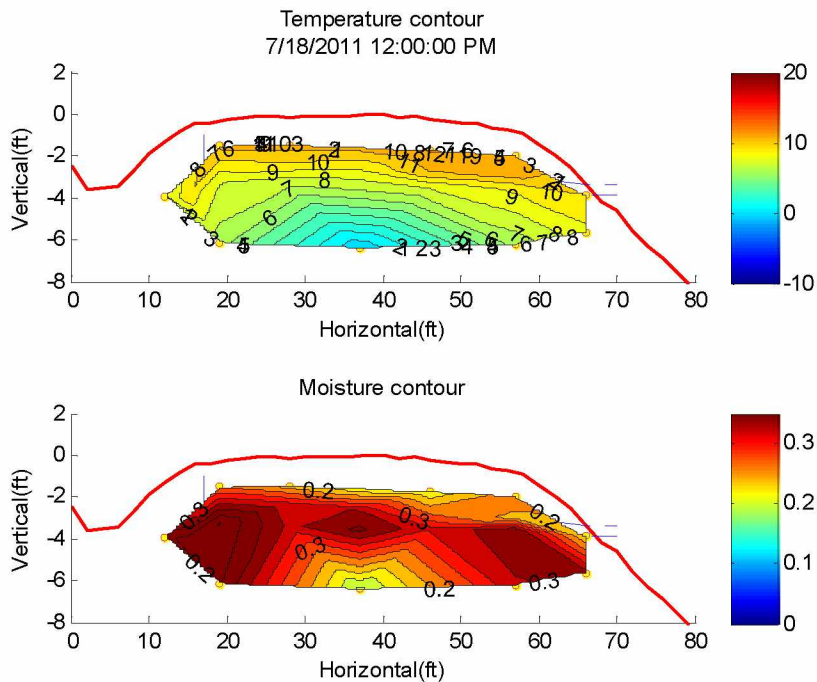


Figure 4.19 Temperature and Moisture Contours at Noon on July 18, 2011

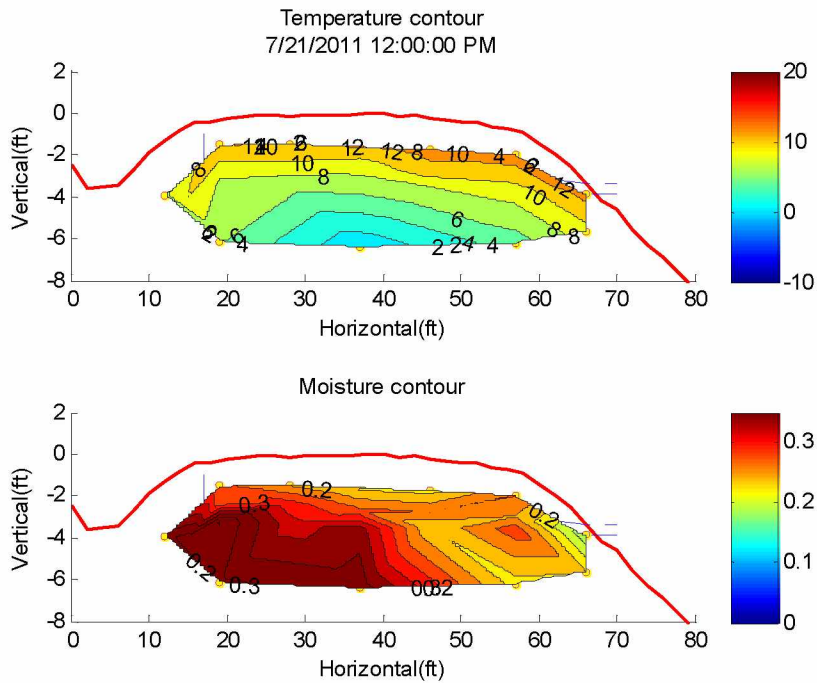


Figure 4.20 Temperature and Moisture Contours at Noon on July 21, 2011

Several rainfall events and the continuous thawing of the frozen soils on the hill kept the road section relatively wet in August and early September of 2011. Figures 4.21 through 4.24 show the temperature and moisture content contours at noon on July 31, August 3, August 15, and August 24, 2011 after a rainfall event on each day, respectively. The first 0.91 meters (3 feet) of soil below the surface remained unsaturated, with lower water content than deeper soils. In addition, after a rainfall event, the east lane of the road embankment dried out in a few days along the horizontal direction where the wicking fabric layers were installed. All of the moisture contours clearly show that the water was moving along the wicking fabric, out of the pavement structure.

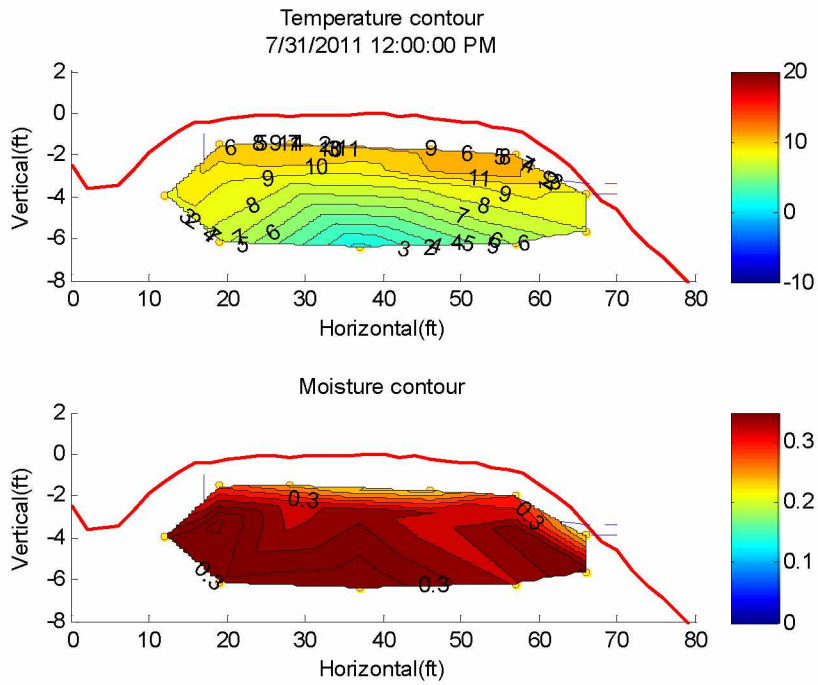


Figure 4.21 Temperature and Moisture Contours at Noon on July 31, 2011

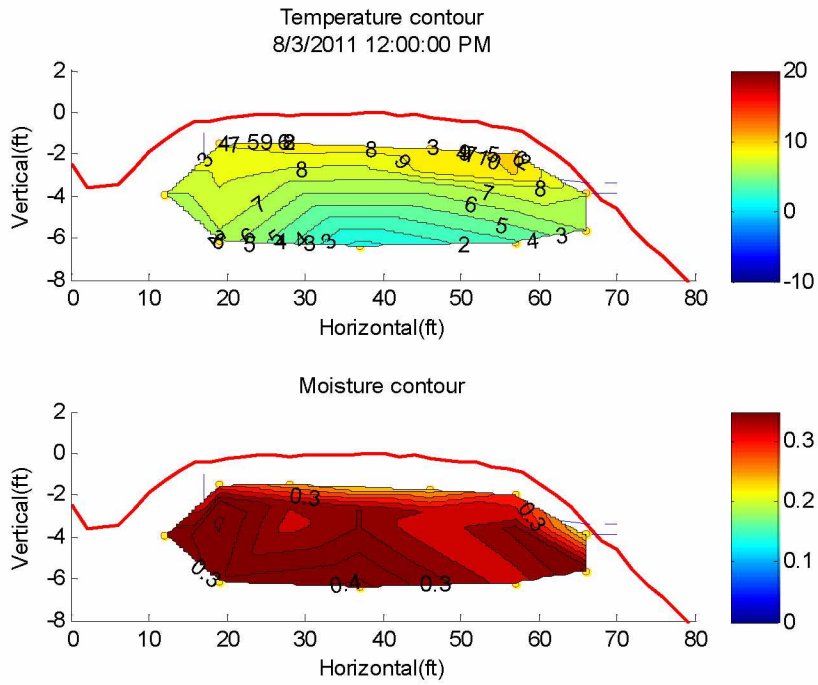


Figure 4.22 Temperature and Moisture Contours at Noon on August 3, 2011

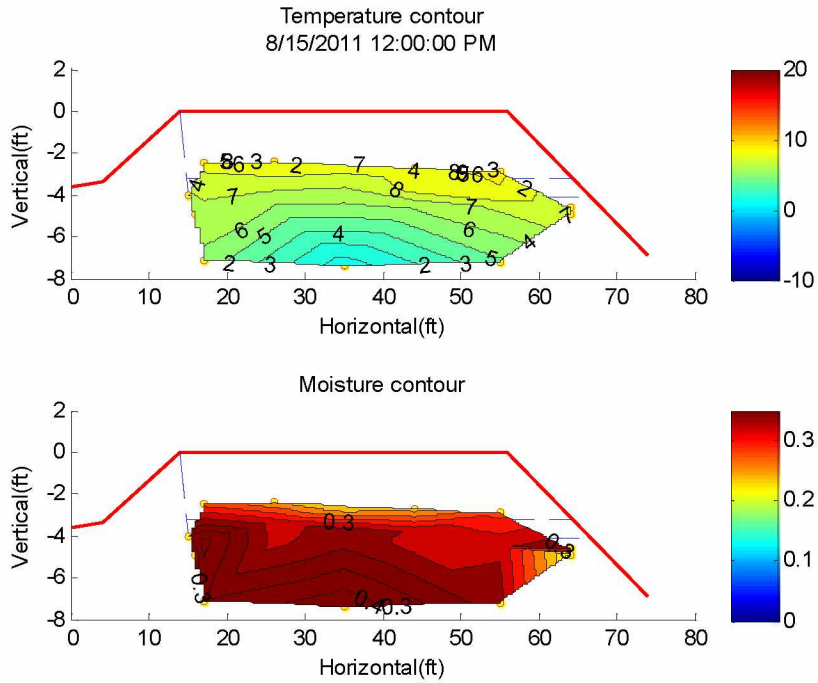


Figure 4.23 Temperature and Moisture Contours at Noon on August 15, 2011

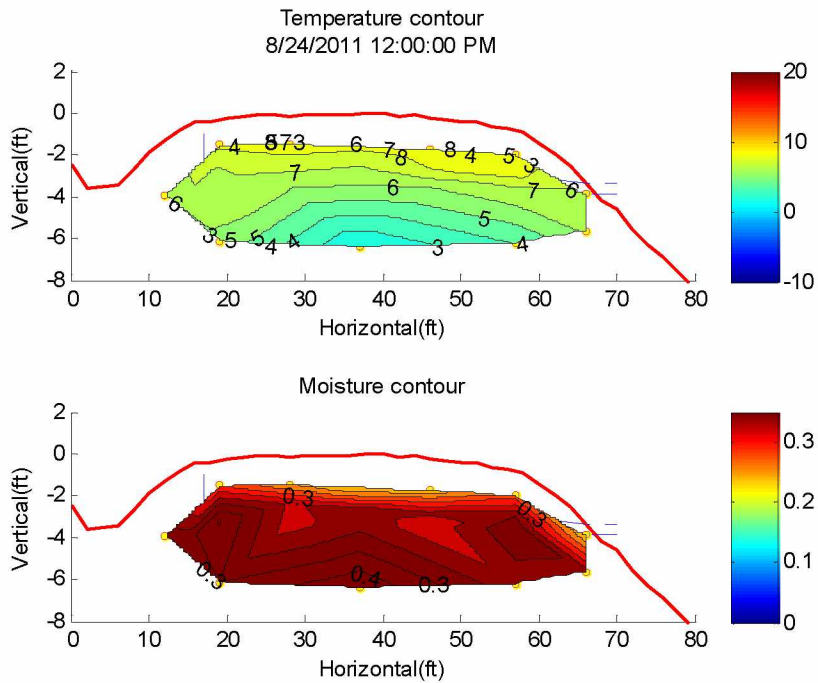


Figure 4.24 Temperature and Moisture Contours at Noon on August 24, 2011

In 2011, the air temperature dropped to 0° C on September 23. The corresponding temperature and water content contours are shown in Figure 4.25. Before any soil freezing occurred, water had been drained out of the embankment and the moisture content in most of the road section was low, especially in the first 1.07 meters (3.5 feet) below the road surface. The soil moisture content in the soils above 1.07 meters (3.5 feet) was generally less than 20 percent, which corresponded to a degree of saturation of less than 50 percent. Because the soils were relatively dry, it was unlikely frost heave would occur in the top 1.07 meters (3.5 feet) of soils.

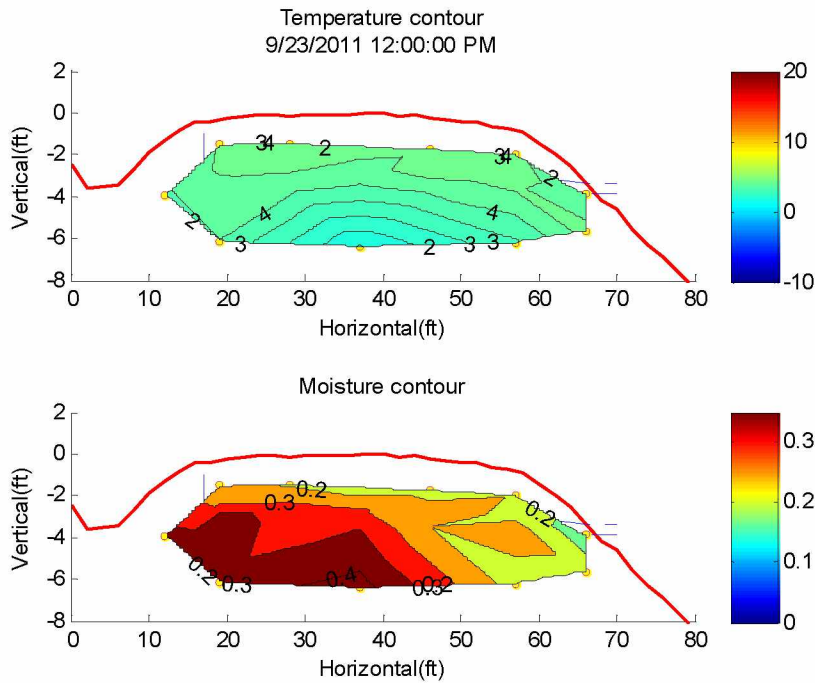


Figure 4.25 Temperature and Moisture Contours at Noon on September 23, 2011

Figures 4.26 through 4.29 present the temperature and moisture contours as the freezing front penetrated to 0.46, 0.76, 1.07 and 1.83 meters (1.5, 2.5, 3.5 and 6 feet) below the road surface, respectively. There was concern that the wicking fabric would lose function when the drainage exit at the east edge was frozen, however it appeared that the fabric was working during freezing conditions. Even after the air temperature dropped to 0° C and the soils began freezing, the water supply at the uphill slope seemed to be reduced. Consequently, the soil water content in the road section was reduced during the

freezing process, as shown in Figures 4.26 through 4.29. Figure 4.30 shows the temperature and moisture contours when the road section was completely frozen. The unfrozen moisture content in the entire road section dropped to 10 percent or less.

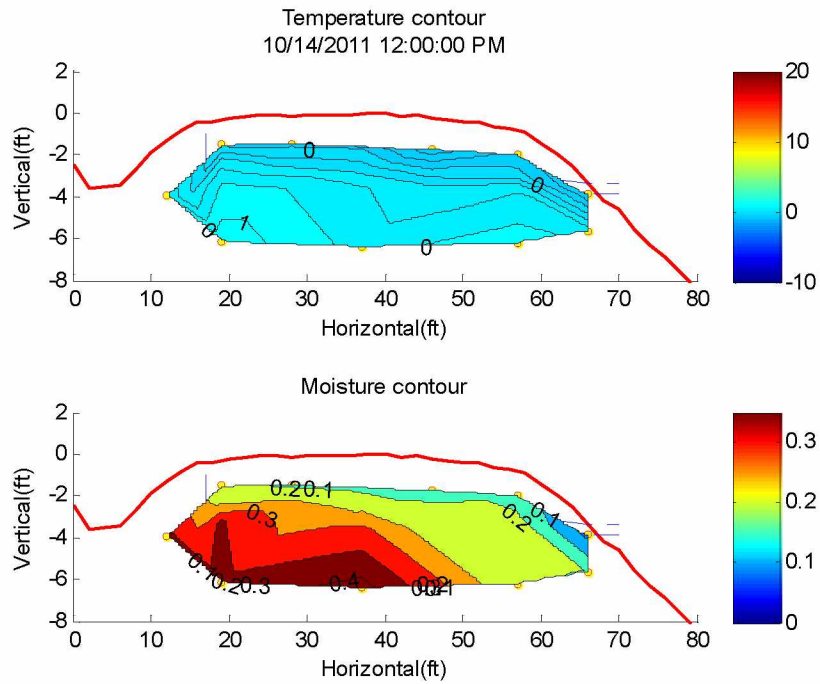


Figure 4.26 Temperature and Moisture Contours at Noon on October 14, 2011

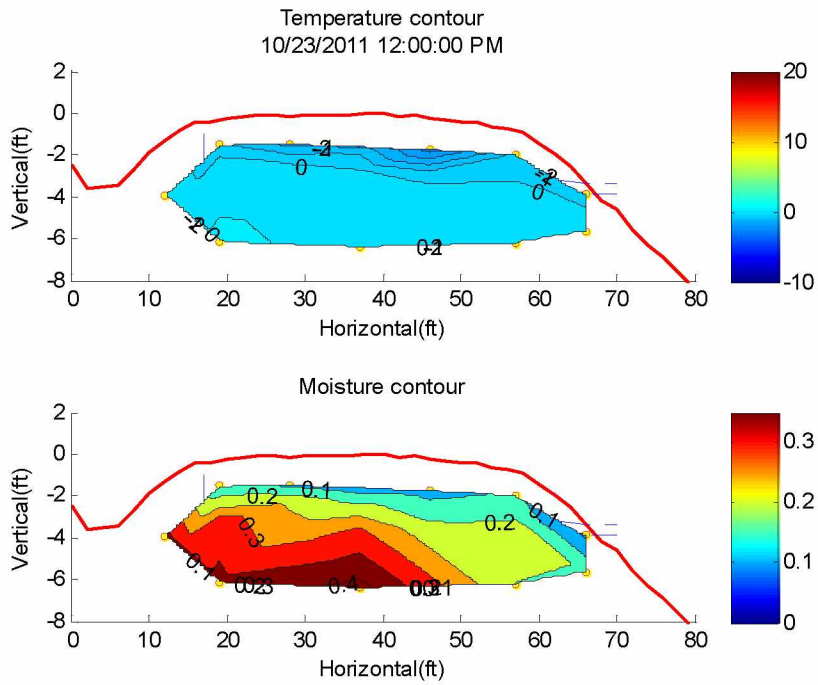


Figure 4.27 Temperature and Moisture Contours at Noon on October 23, 2011

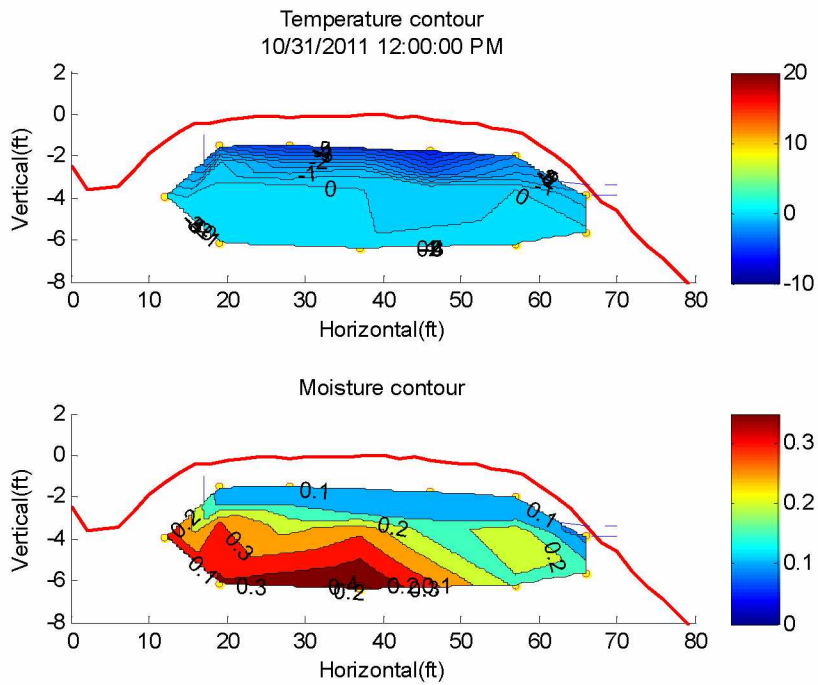


Figure 4.28 Temperature and Moisture Contours at Noon on October 31, 2011

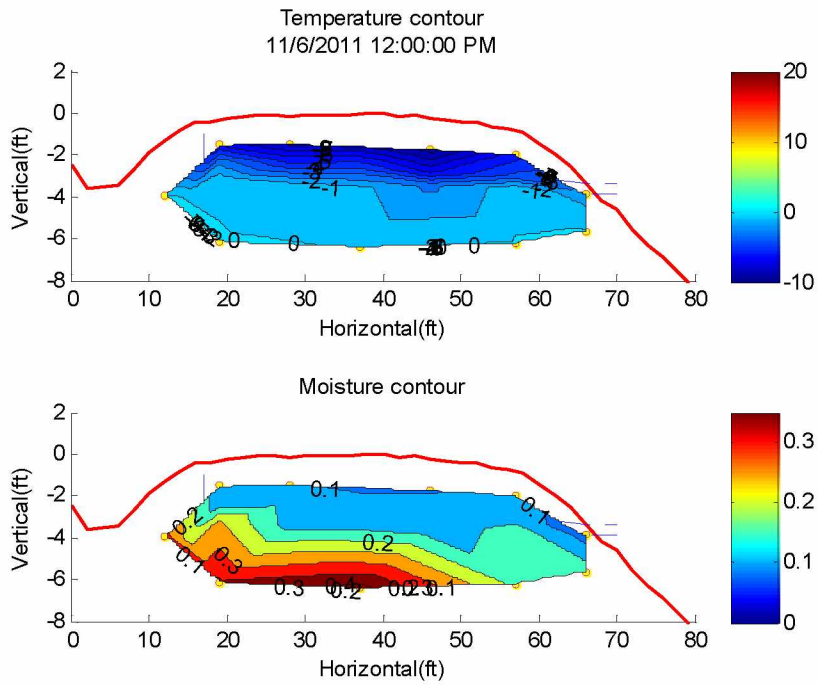


Figure 4.29 Temperature and Moisture Contours at Noon on November 6, 2011

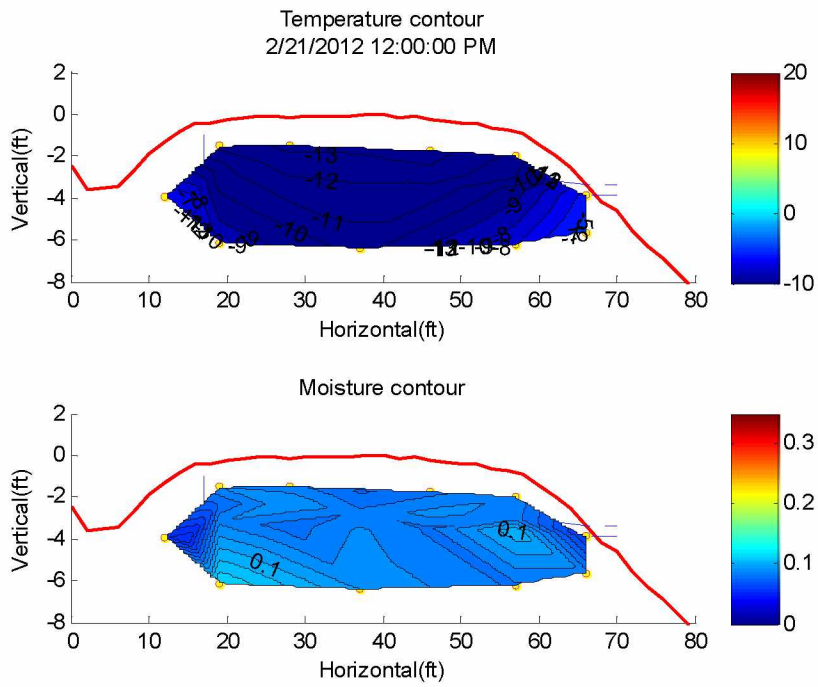


Figure 4.30 Temperature and Moisture Contours at Noon on February 21, 2012

Figure 4.31 shows the temperature and moisture contours when the air temperature first rose to above 0° C in 2012. It was found that the road section was completely frozen, and that the unfrozen moisture content was 10 percent or less. Figures 4.32 and 4.33 show the temperature and moisture contours when the thawing front penetrated to 0.46 and 0.76 meters (1.5 and 2.5 feet) below the road surface on May 12 and 22, 2012, respectively. This period corresponded to the time period when the frost boils usually appeared, in early spring. The moisture contours during this period did not indicate any saturated soil zone, which was confirmation that no frost heave had occurred in the previous year. Figure 4.34 shows the temperature and moisture contours when the thawing front penetrated to 1.07 meters (3.5 feet) below the road surface on May 29, 2012. Soils at sensor locations 19 and 21 near the ditch were saturated, while soils at other locations were below saturation. Similar to what was observed in 2011, there was a frozen soil core at the bottom center of the road. The moisture content contour indicated that water was flowing from the ditch to the east edge of the embankment along the wicking fabric layers.

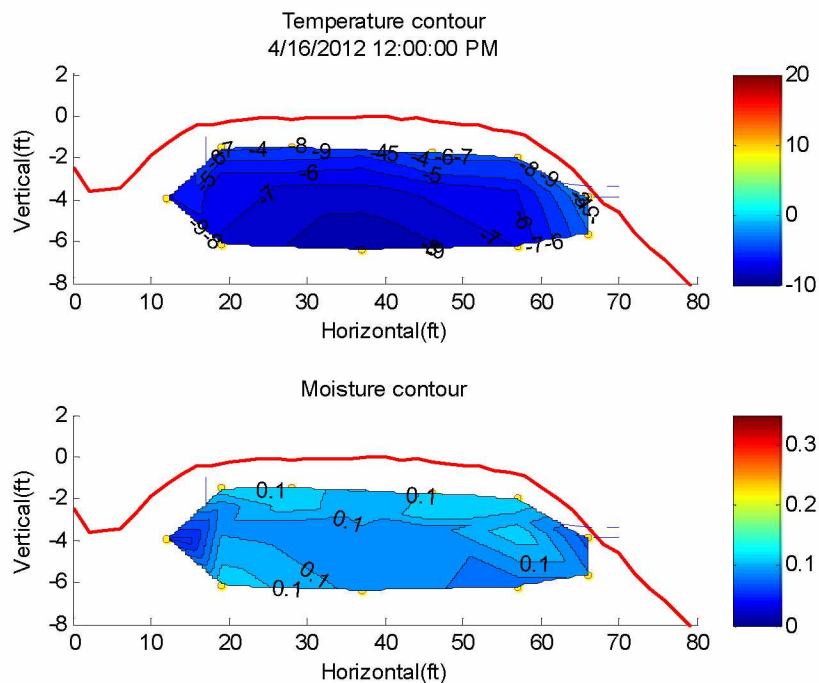


Figure 4.31 Temperature and Moisture Contours at Noon on April 16, 2012

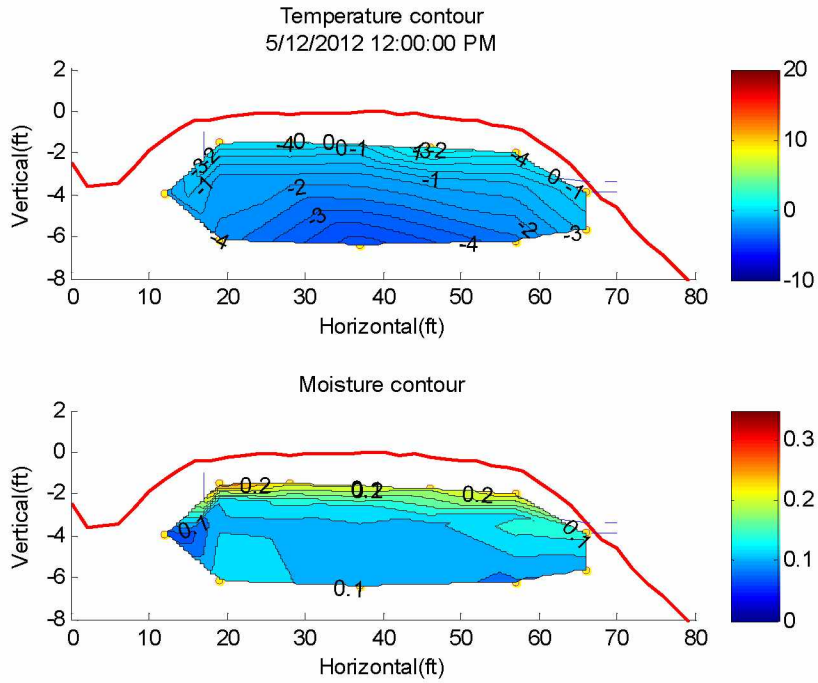


Figure 4.32 Temperature and Moisture Contours at Noon on May 12, 2012

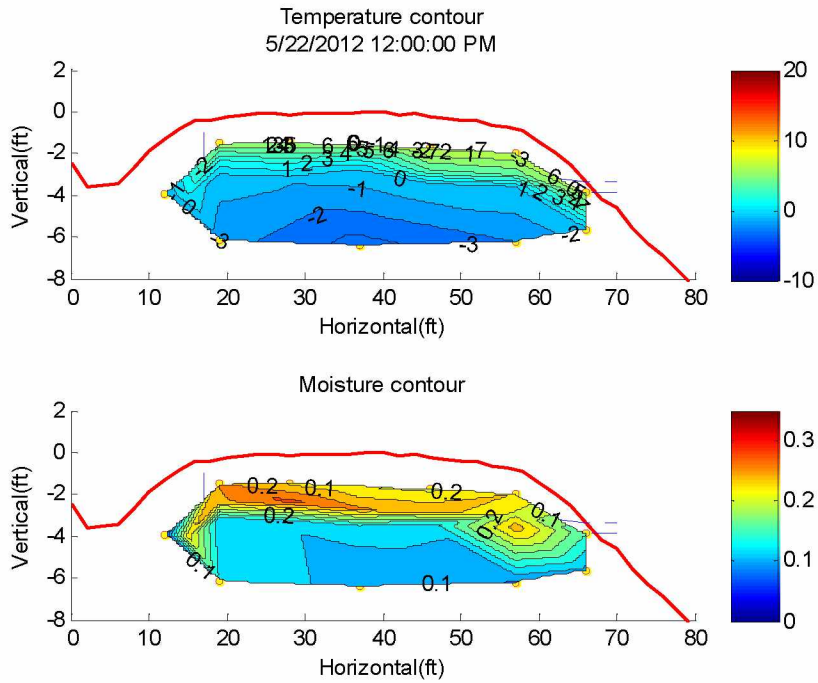


Figure 4.33 Temperature and Moisture Contours at Noon on May 22, 2012

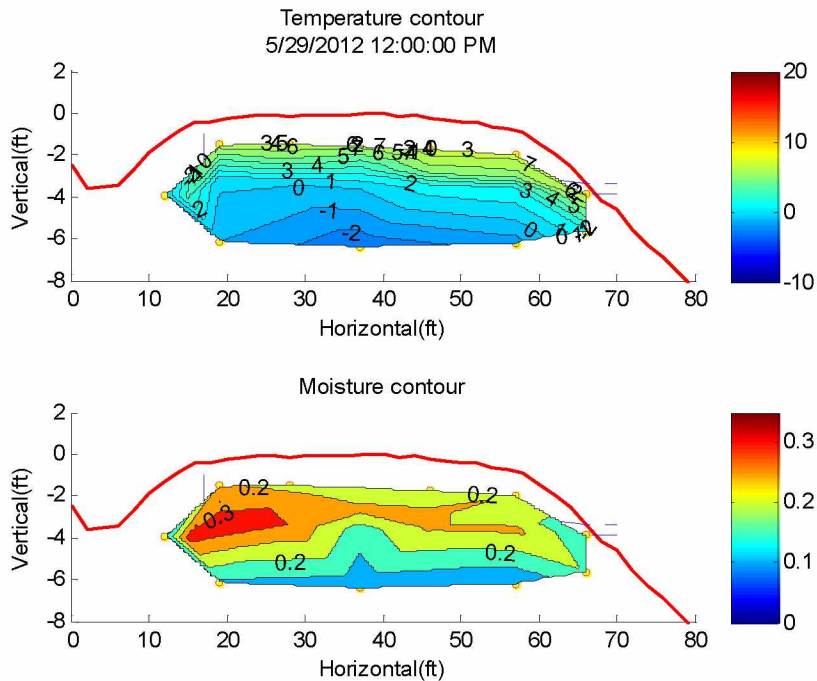


Figure 4.34 Temperature and Moisture Contours at Noon on May 29, 2012

The freezing and thawing processes at the test site have continued as described above. It was discovered during the process of these analyses that the 0°C isotherm generally corresponds to a moisture content of about 20 percent. The drainage of water from the embankment through the wicking fabric may be the explanation for lower average moisture contents in the roadway structure.

General Climate Conditions

Temperature Data

Figure 4.35 shows hourly air temperature data at the test section between August 2010 and August 2014. In general, summer air temperatures increased from 2011 to 2013, followed by a decrease in 2014. The average winter air temperature increased year during the same period. Each year, the air temperature dropped below 0°C in late September, and rose to above 0°C in mid- to late April. The lowest temperature was recorded on January 29, 2011, which was -39.8°C . Most winter temperatures are approximately -20°

C. The highest temperature observed was 26.2° C, which occurred on June 19, 2013. The daily temperature variation in the summer months was smaller than the daily temperature variation in winter months.

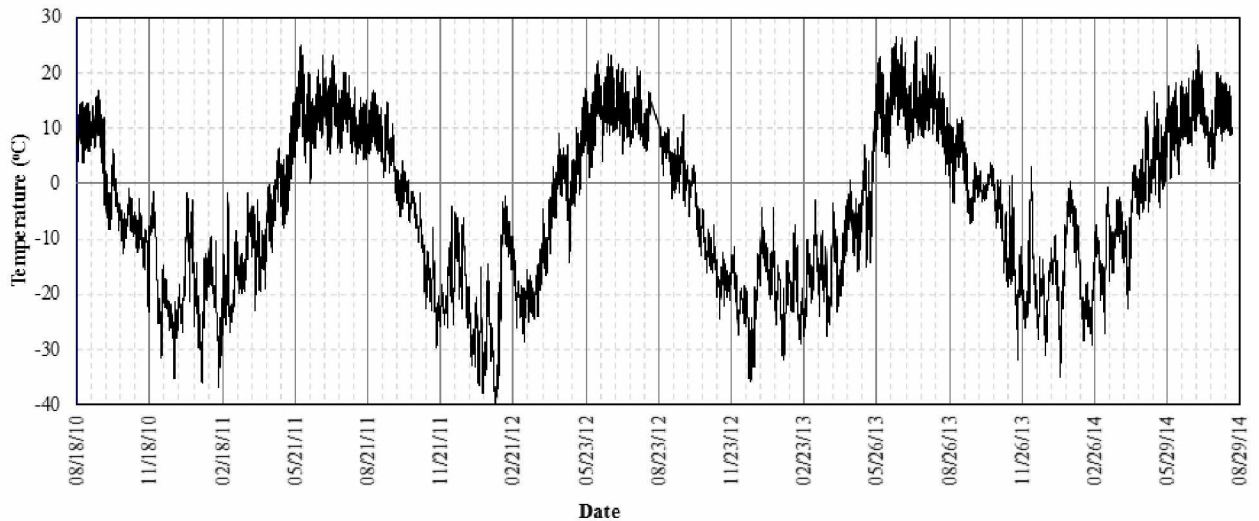


Figure 4.35 Hourly Temperature Data

Figure 4.36 shows hourly relative humidity data at the test section from August 2010 to August 2014. In the winter months, the relative humidity generally varied from 70% to 90%, while in the summer months, the relative humidity had a larger variation, from 20% to 90%. There were some days during this period where the relative humidity was higher than 95% for short periods. These periods were assumed to be rainfall events; there was no rain gauge installed at the test section. This assumption was verified by a site visit on June 21, 2011 when there was a rainfall during the site visit, and the recorded relative humidity during the visit was between 95% and 98%.

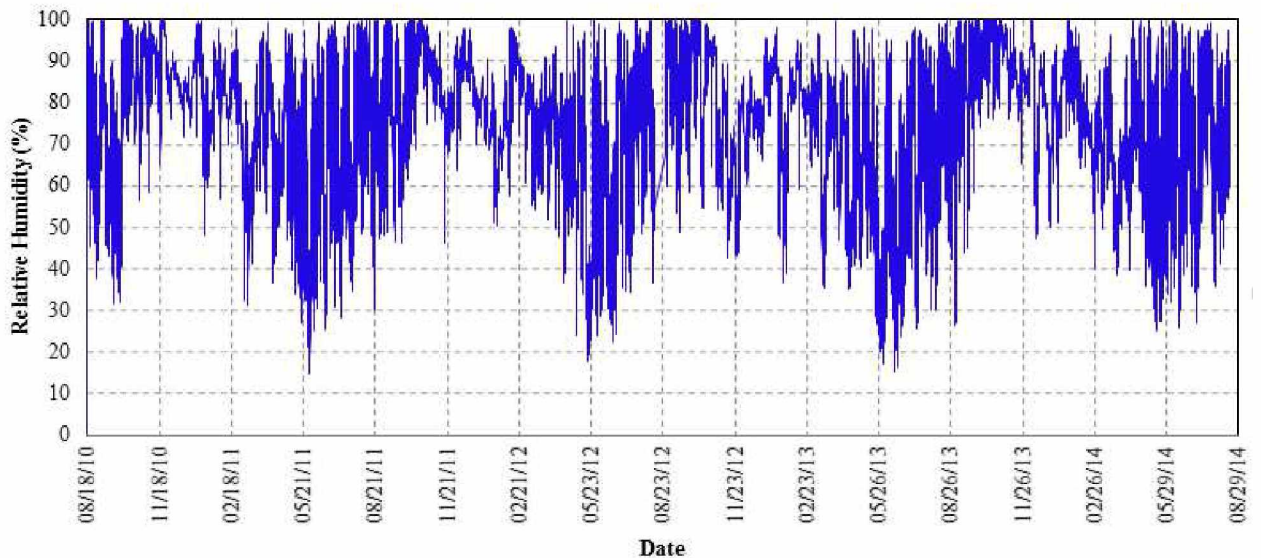


Figure 4.36 Hourly Relative Humidity Data

Soil Temperature Changes

Figure 4.37 presents the soil temperature variations from November 2010 through August 2014 at sensor locations 10, 11, 12 and 13 compared to the air temperature variations at the site. These sensor locations are at the center of the embankment. The sensors were buried at 0.45, 0.76, 1.06 and 1.97 meters (1.5, 2.5, 3.5, and 6.5 feet), respectively, below the road surface. In general, the trend of temperature changes in the soil followed the air temperature trend. The temperature change in the soil decreased in magnitude as depth increased, due to the insulating effect of the soil above the sensor. For instance, sensor 10 was located 0.45 meters (1.5 feet) below the surface, which was the closest sensor to the road surface, and its temperature variation followed the air temperature change very closely during the summer. During the winter months, the temperatures at sensor 10 were higher than the air temperatures, due to the insulating effect of snow on the road surface. In comparison, the temperature variation at sensor 13, which was installed 1.97 meters (6.5 feet) below the road surface, ranged from -12 °C to 3 °C for the entire year. The variation at sensor 13 was much smaller than that for the air temperature, which was as much as 30 °C in winter and 16 °C in summer. It was also observed that the soil temperature 1.97 meters (6.5 feet) below the road surface only experienced temperatures

above 0 °C for less than 3 months each year (ie. July 20, 2012 to October 30, 2012). This indicates that the soil at 1.97 meters (6.5 feet) below the road surface can be considered a permeable layer for 3 months, and that it is an impermeable layer the rest of the year.

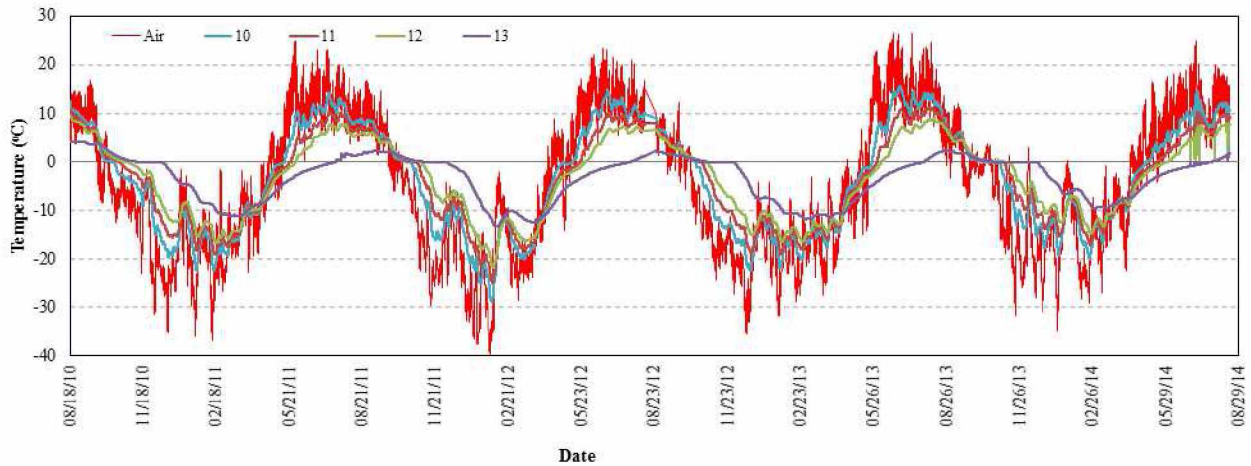


Figure 4.37 Soil Temperature vs. Depth

Figure 4.38 through Figure 4.41 show the temperature changes at the sensor locations 0.45, 0.76, 1.06 and 1.97 meters (1.5, 2.5, 3.5, and 6.5 feet) below the road surface, respectively, for the past four years.

Figure 4.38 presents temperature data for the sensors located near the road surface, at 0.45 meters (1.5 feet). In general, the soil temperature changes followed the air temperature trend during the summer, and were warmer than the air temperature in winter. Thus, soils above 0.45 meters (1.5 feet) below the road surface can be considered a permeable layer during the summer. Additionally, the soil temperatures observed in the center of the road were lower than temperatures at the edges during winter months; soil temperatures at the west side of the road were lower than that at the east side. There are two reasons to explain this phenomenon: (1) snow was routinely removed and piled on the shoulders, insulating the shoulders to make them warmer than the center of the road. Therefore, the soils near the shoulder experienced a higher temperature in the winter; and (2) the roadway on the east side received more solar energy than the west side, therefore temperatures at the east side of the roadway were higher than at the west side.

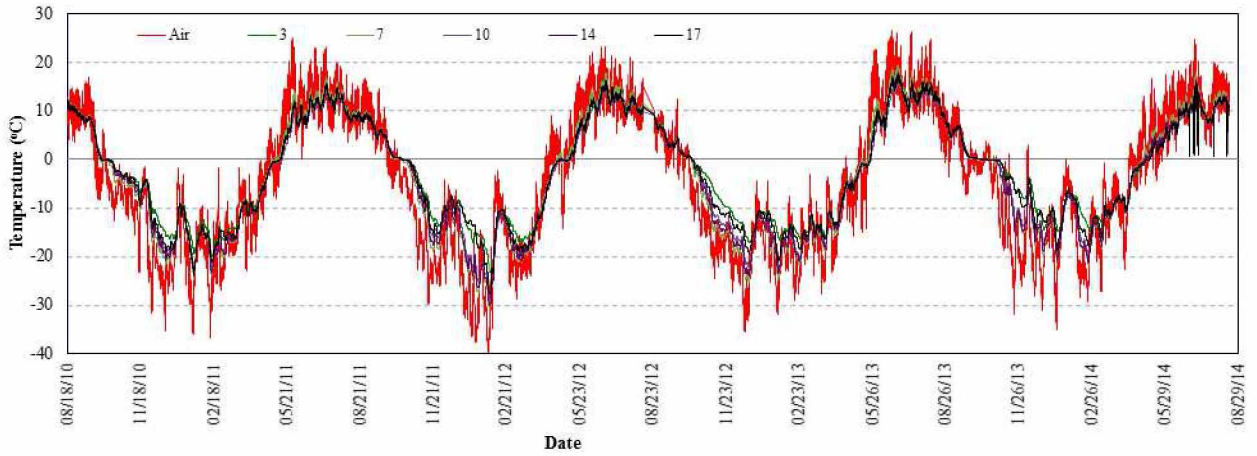


Figure 4.38 Soil Temperature 0.45 Meters (1.5 Feet) below the Road Surface

Figure 4.39 shows the temperature variation for sensors at 0.76 meters (2.5 feet) below the road surface. Compared with Figure 4.38, the amplitude of temperature change at 0.76 meters (2.5 feet) was smaller than that at 0.45 meters (1.5 feet). The time periods that the soil temperatures were below and above zero were similar to the air temperatures, indicating that the air temperature has an influence to a depth of at least 0.76 meters (2.5 feet) below the road surface. When the air temperature rose above 0 °C in late April, the soils at 0.76 meters (2.5 feet) below the road surface were unfrozen and can be considered a permeable layer, able to drain the melting snow at the surface of the roadway.

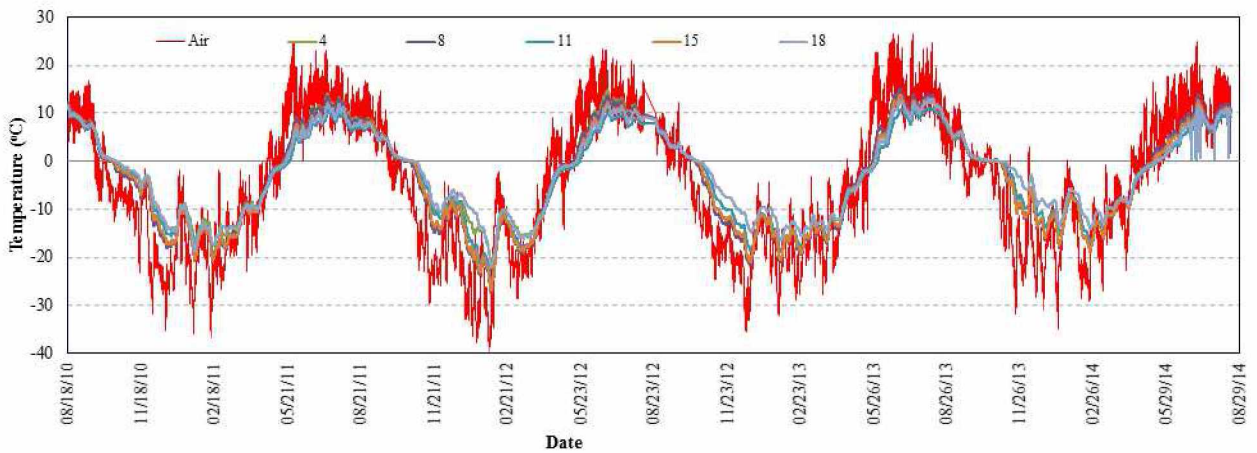


Figure 4.39 Soil Temperature 0.76 Meters (2.5 Feet) below the Road Surface

Figure 4.40 shows the temperature change for sensors at 1.06 meters (3.5 feet) below road surface. As can be seen in Figure 4.40, soil temperatures in this layer experienced approximately a 1 month time lag compared with the air temperature change. This phenomenon indicates that during the early spring (late April or early May), the soils at a depth of 1.06 meters (3.5 feet) and below were still frozen and could not be considered a drainage layer until 1 month later. In other words, since the second layer of wicking fabric was installed at this depth, it would not be able to drain the water out of the embankment until early June. The first snowfall at the site is expected in early October each year, allowing the second layer of wicking fabric to remain functional until early November, when the soils at this depth become frozen.

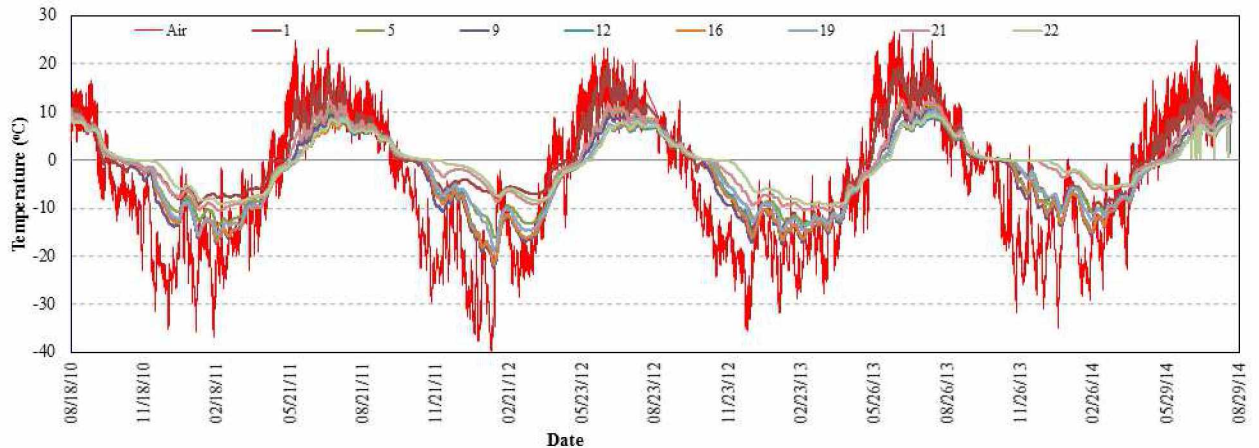


Figure 4.40 Soil Temperature 1.06 Meters (3.5 Feet) below the Road Surface

Figure 4.41 presents the temperature changes for sensors at 1.97 meters (6.5 feet) below road surface. The temperature variation amplitude at this depth was smaller than the amplitude in the soils at 1.06 meters (3.5 feet). The insulation effect becomes more obvious as the depth below the surface increases. Moreover, since this layer is deeper than the sensors at 1.06 meters (3.5 feet), the time lag of temperature change was more obvious than in the previous discussions. For example, sensor 13 was located at the center of the roadway, and the temperature did not rise above 0° C until July, 30 2013, and fell below 0° C on October 19, 2013. Since the snow that was piled at the shoulder

started to melt in late April or early May, there were about 3 months of time lag before the soils at a depth of 1.97 meters (6.5 feet) below the surface were thawed and could be considered a permeable layer, able to drain the water from the road section.

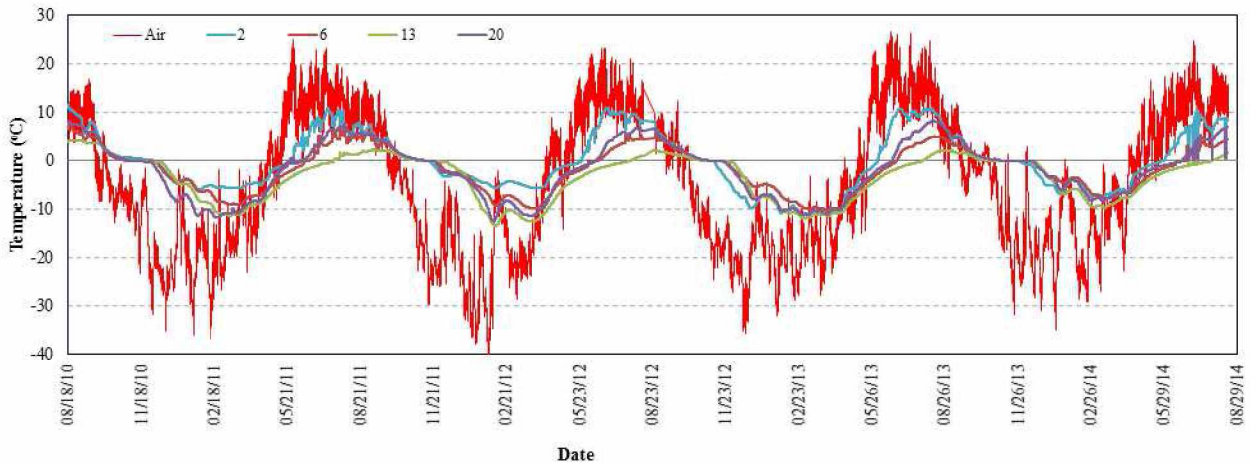


Figure 4.41 Soil Temperature 1.97 Meters (6.5 Feet) below the Road Surface

Soil Moisture Changes

As can be seen in Figure 3.10, sensor 22 was buried at about 1.20 meters (3.94 feet) below the road surface, and was 1.50 meters (4.92 feet) away from the up-slope drainage ditch. Its elevation was 0.1 meters (.33 feet) below the drainage ditch. The drainage ditch received water flow during the entire year, except during the winter when everything was frozen. As can be seen in Figure 4.42, moisture contents at sensor 22 were relatively constant in the summers and winters between 2010 and 2014, and appeared to be unaffected by daily weather conditions. A possible explanation for this is that the moisture contents at sensor 22 were controlled by the drainage ditch, and were constantly saturated or nearly saturated. Sensor 22 was used as a reference for comparison purposes in the following figures.

Figure 4.42 shows the soil moisture changes at 0.45 meters (1.5 feet) below road surface. It is obvious that the moisture content at this depth was far below the moisture content at the reference location (sensor 22). In summer time, the moisture variation was neither influenced by rainfall intensity nor duration, primarily due to two processes: (1) the evaporation process at the soil surface was fast, and the water could be easily

evaporated to the open air; (2) the free water could effortlessly run off, due to gravitational force. Because the elevation of the ground adjacent to the roadway at the west side of the road is higher than elevation of the ground adjacent to the east side, it is reasonable that the moisture content of the soils on west side were higher than soils on the east side. It is also worth noting that it took nearly 2 months to thoroughly freeze the soil at this depth in winter months, but only took about 2 weeks to thoroughly thaw the frozen soil in early spring. The rate of thawing is determined by observing the volumetric moisture content. The average volumetric moisture content at this depth was approximately 0.09 on April 10, 2014 when the average daily air temperature was -15.5 °C; however, the moisture content increased to 0.14 on April 24, 2014, when the average daily air temperature changed to -1.1 °C. Therefore, even if the average daily air temperature was still below zero, the amount of solar energy during daytime was large enough to increase the unfrozen moisture content by 5%. Because the unfrozen water content increased dramatically in a relatively short period of time, which served as an additional water source that cannot be drained out of the roadway due to the frozen soil beneath, the thawing became the major deteriorating factor that softened the road surface.

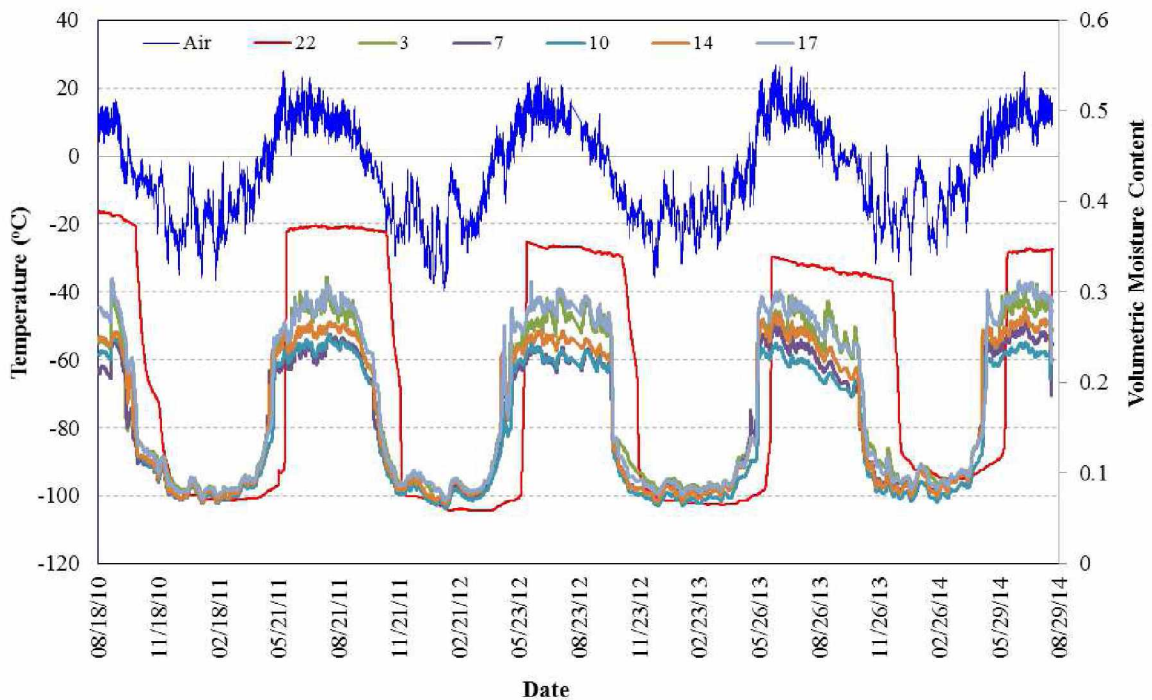


Figure 4.42 Soil Moisture Content 0.45 Meters (1.5 Feet) below the Road Surface

Figure 4.43 shows the soil moisture changes for sensors at 0.76 meters (2.5 feet) below road surface, where the first layer of wicking fabric was installed. In general, the soil moisture contents were not higher than the reference moisture content at the location of sensor 22, except as a result of some long and intensive rainfall events. Any sudden, large variation in soil volumetric moisture content change indicated a rainfall event. For the monitored 4-year period of data, the rainfall frequencies were decreasing and resulted in a decreasing volumetric moisture content trend for the reference location (sensor 22). Compared with Figure 4.42, soils at this depth, 0.76 meters (2.5 feet), were more affected by the rainfall events than soils at 0.45 meters (1.5 feet), likely because runoff water that is stored in the drainage ditch could flow into the soil easily, and the evaporation process was much slower for soils at 0.76 meters (2.5 feet) than for soils closer to the surface. However, the soil moisture content dropped back quickly after the rainfall events stopped, which indicates that the drainage condition at this depth was favorable.

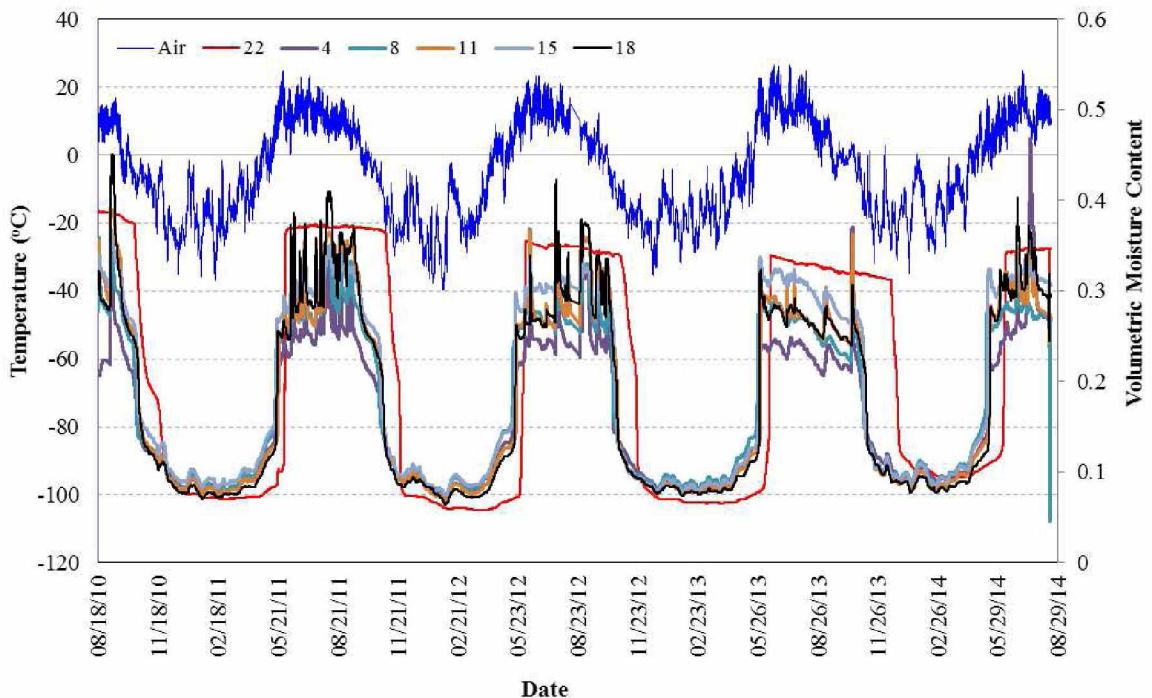


Figure 4.43 Soil Moisture Content 0.76 Meters (2.5 Feet) below the Road Surface

Figure 4.44 shows soil moisture changes at 1.06 meters (3.5 feet) below the road surface, where the second layer of wicking fabric was installed. Sensor 1 was buried on the east side of the road shoulder, and the moisture content was much lower than that for the reference sensor 22. Similarly, the moisture contents for sensors on the east side were all lower than at the location of the reference sensor, and the moisture content for sensors on the west side were all higher than at the location of the reference sensor. The amplitudes of moisture content changes were also higher at 1.06 meters (3.5 feet) than at the previous two depths discussed. This phenomenon could be a result of (1) accumulated water at the drainage ditch and (2) the one-month time lag to melt the frozen soil at this depth. Since the snow started to melt in early May, and the elevation of the ground adjacent to the road on the west side was higher than on the east side, a large amount of water was probably trapped in the drainage ditch, which provided a large quantity of water to the roadway structure. Additionally, the temperature at the center line of the road was lower than that at the edges. Soil at 1.06 meters (3.5 feet) and below would not start to melt until late May or early June. The freezing temperatures and excess moisture resulted in a hard, frozen core at the center of the road, impeding the drainage path. As a result, additional water was trapped in the area adjacent to and including the west side of the road, and resulted in higher moisture contents.

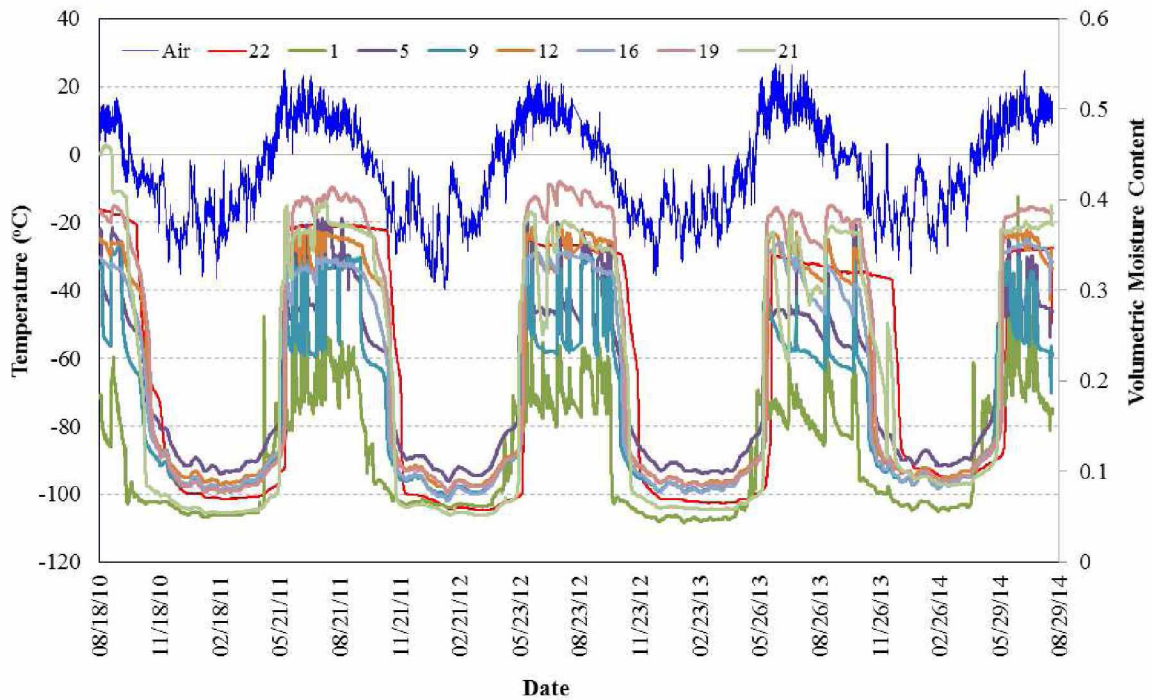


Figure 4.44 Soil Moisture Content 1.06 Meters (3.5 Feet) below the Road Surface

Figure 4.45 shows the moisture content changes for sensors at 1.97 meters (6.5 feet) below road surface. All of the sensors on the west side had moisture contents higher than those at the east side. It is noteworthy that soils around the location of sensor 13 did not fully melt until mid-August, which is nearly 3 months after snow melting began. As discussed previously, the frozen soil served as a hard core that impeded the natural water flow and caused excess water to become trapped in the west side of the road. Moreover, because the melting process took such a long time, soils in the west side of the road embankment could hold more water during the summer time, allowing the unfrozen moisture contents to remain approximately 4% higher than the moisture contents at the reference sensor location during winter months. In contrast, the moisture contents for sensors in the east side were much lower than at the reference sensor location, except for during some intense rainfall events.

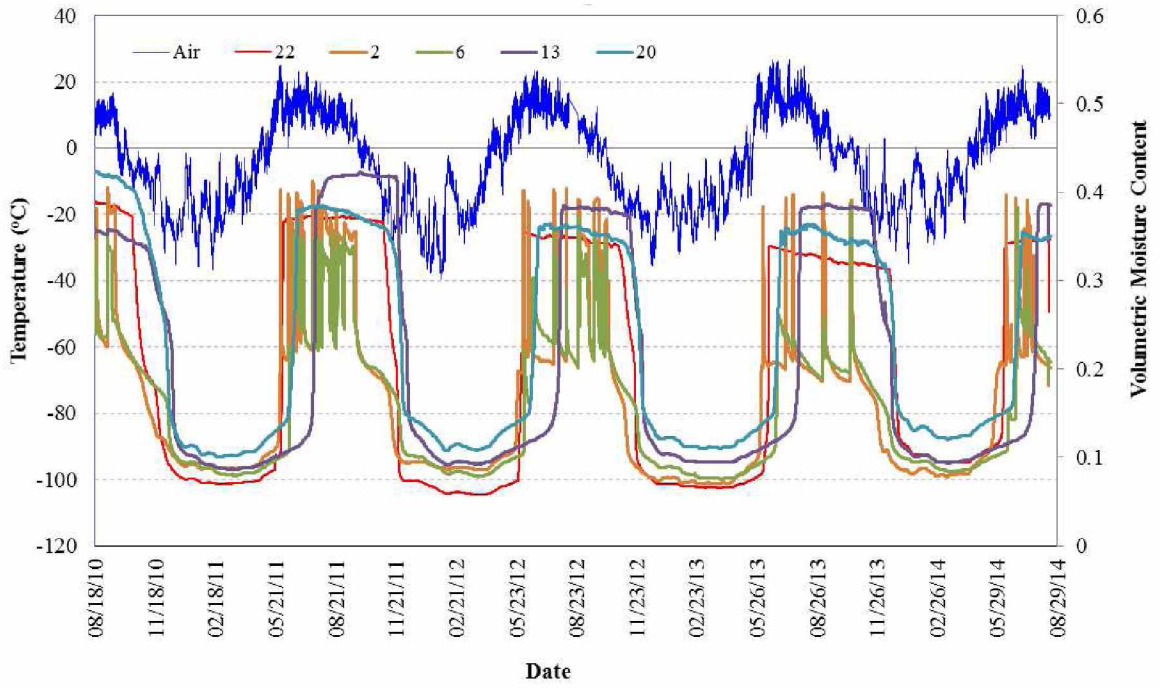


Figure 4.45 Soil Moisture Content 1.97 Meters (6.5 Feet) below the Road Surface

CHAPTER V

LONG-TERM PERFORMANCE OF WICKING FABRIC

The long-term performance of the wicking fabric can be visualized macroscopically via analyses under different climatic conditions (i.e. during rainfall events, during the freezing process, during the thawing process), and can be further analyzed by exploring the interaction between the wicking fabric and the surrounding soils on a microscopic level.

During Rainfall Events

Table 5.1 summarizes all of the major rainfall events for the four-year period monitored. Significant rainfall events were identified as the time periods when the relative air humidity exceeded 95% (winter months were not considered). Since the relative humidity in the air during the summer time is about 50% without rainfall, it is reasonable to assume that light rainfall events were not able to raise the relative humidity above 95%.

Table 5.1 Rainfall Event Summary

Event	Date	Duration (hours)
1	8/18/2010	3
2	8/18/2010	12
3	8/23/2010	6
4	8/24/2010	7
5	8/24/2010	12
6	9/4/2010	23
7	9/6/2010	2
8	9/7/2010	23
9	9/9/2010	10
10	10/2/2010	1
11	5/23/2011	2
12	6/8/2011	8
13	6/9/2011	1

(Table 5.1 Continued)

Event	Date	Duration (hours)
14	6/14/2011	4
15	6/15/2011	2
16	6/21/2011	11
17	6/22/2011	3
18	6/22/2011	3
19	6/22/2011	11
20	6/24/2011	6
21	6/26/2011	9
22	6/27/2011	2
23	6/28/2011	3
24	6/30/3011	6
25	6/30/2011	12
26	7/11/2011	39
27	7/16/2011	7
28	7/18/2011	7
29	7/24/2011	31
30	7/29/2011	43
31	8/1/2011	41
32	8/5/2011	4
33	8/5/2011	3
34	8/6/2011	2
35	8/7/2011	10
36	8/8/2011	8
37	8/10/2011	12
38	8/12/2011	4
39	8/13/2011	13
40	8/13/2011	15
41	8/20/2011	23
42	8/23/2011	16
43	9/1/2011	8
44	9/3/2011	8
45	9/3/2011	19

(Table 5.1 Continued)

Event	Date	Duration (hours)
46	9/4/2011	1
47	9/6/2011	16
48	9/7/2011	19
49	9/8/2011	15
50	5/13/2012	4
51	5/26/2012	27
52	5/29/2012	1
53	5/30/2012	2
54	6/2/2012	8
55	6/10/2012	12
56	6/27/2012	37
57	6/29/2012	28
58	7/4/2012	5
59	7/4/2012	11
60	7/17/2012	2
61	7/23/2012	8
62	7/24/2012	16
63	7/30/2012	8
64	8/2/2012	13
65	8/3/2012	6
66	8/4/2012	13
67	8/5/2012	8
68	8/6/2012	16
69	8/7/2012	5
70	8/25/2012	39
71	8/28/2012	3
72	8/29/2012	63
73	9/1/2012	30
74	9/3/2012	15
75	9/4/2012	11
76	9/5/2012	41
77	9/8/2012	12

(Table 5.1 Continued)

Event	Date	Duration (hours)
78	9/15/2015	14
79	9/18/2012	27
80	9/23/2012	10
81	9/28/2012	60
82	10/2/2012	32
82	10/5/2012	30
83	6/4/2013	3
84	6/4/2013	1
85	6/4/2013	5
86	6/9/2013	6
87	7/1/2013	4
88	7/8/2013	4
89	7/8/2013	12
90	7/9/2013	15
91	7/16/2013	5
92	7/16/2013	12
93	7/18/2013	1
94	7/19/2013	20
95	7/20/2013	1
96	7/24/2013	1
97	7/30/2013	3
98	7/31/2013	2
99	8/5/2013	2
100	8/10/2013	9
101	8/12/2013	4
102	8/14/2013	3
103	8/14/2013	13
104	8/16/2013	6
105	8/18/2013	11
106	8/19/2013	15
107	8/21/2013	4
108	8/24/2013	1

(Table 5.1 Continued)

Event	Date	Duration (hours)
109	8/28/2013	5
110	9/2/2013	16
111	9/3/2013	14
112	9/5/2013	15
113	9/7/2013	13
114	9/7/2013	4
115	9/9/2013	13
116	9/11/2013	7
117	9/11/2013	10
118	9/13/2013	6
119	10/13/2013	9
120	10/15/2013	11
121	5/17/2014	4
122	5/22/2014	3
123	5/31/2014	38
124	6/5/2014	5
125	6/6/2014	17
126	6/9/2014	14
127	6/11/2014	14
128	6/11/2014	16
129	6/18/2014	7
130	6/19/2014	3
131	6/22/2014	9
132	6/25/2014	54
133	7/8/2014	13
134	7/11/2014	15
135	7/15/2014	44
136	7/18/2014	10
137	7/19/2014	17
138	7/22/2014	31
139	7/23/2014	16
140	7/25/2014	9

(Table 5.1 Continued)

Event	Date	Duration (hours)
141	8/1/2014	13
142	8/2/2014	9
143	8/7/2014	2
144	8/7/2014	1
145	8/14/2014	3
146	8/15/2014	43

One important consideration is the effect that rainfall duration has on soil moisture distribution at the test section. Figures 5.1 through 5.3 and figures 5.4 through 5.6 show the comparison of a short rainfall and long rainfall event to demonstrate this mechanism. Figures 5.1 through 5.3 are a short duration event lasting several hours, and figures 5.4 through 5.6 are a long duration rainfall event lasting for several days. As shown in Table 5.1, there was a short rainfall event of 5 hours on August 28, 2013. By looking up the recorded data, it was determined that no other significant rainfall events occurred within a week prior to this event. The moisture contour figures presented in figures 5.1 through 5.3 show the soil moisture distribution before the rainfall, 1 hour after the rainfall and 1 day after the rainfall. It is apparent that the soil moisture distribution did not change significantly as a result of this event. This phenomenon indicated that a 5-hour rainfall is not long enough to change the water moisture distribution within the pavement structure.

In comparison, another rainfall occurred on July 8, 2013 and continued on the following day. The total rainfall duration was about 27 hours from July 8 to July 9. Figures 5.4 through 5.6 show the soil moisture distribution at the beginning of the rainfall event, 7 hours after the rainfall and about 1 day after the rainfall. The soils in the east side of the roadway were significantly drier than the soils in the west side of the roadway prior to the rainfall. 7 hours after the rainfall event, more water had accumulated in both the east and the west side of the road structure. The saturation zone in the west side was larger because water flowed into the pavement structure via a drainage ditch up-slope and adjacent to the west side of the embankment. Meanwhile, on east side of the road, the saturated zone was observed at the location of the wicking fabric layers. This

phenomenon indicated that the wicking fabric was able to suck the water from the surrounding soils and laterally transport it to the shoulder. The contours in figure 5.6 show that 1 day after the rainfall event, the saturation zone was smaller than before in the west side of the roadway. The soils near the wicking fabric were comparatively drier than the rest of the soils on the east side of the embankment, where no apparent saturation zone was observed.

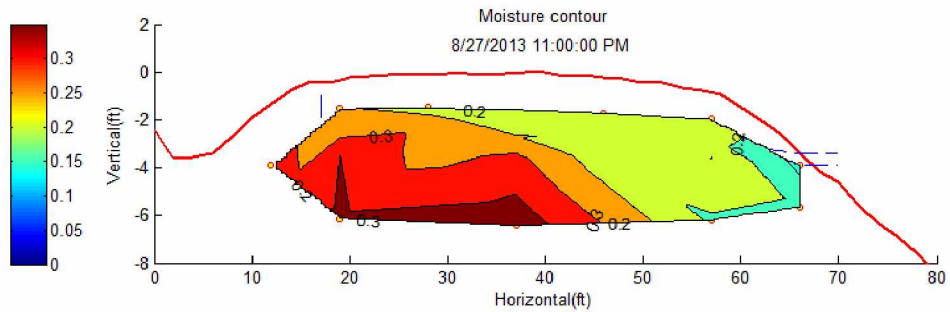


Figure 5.1 Soil Moisture Contours before Short Duration Rainfall

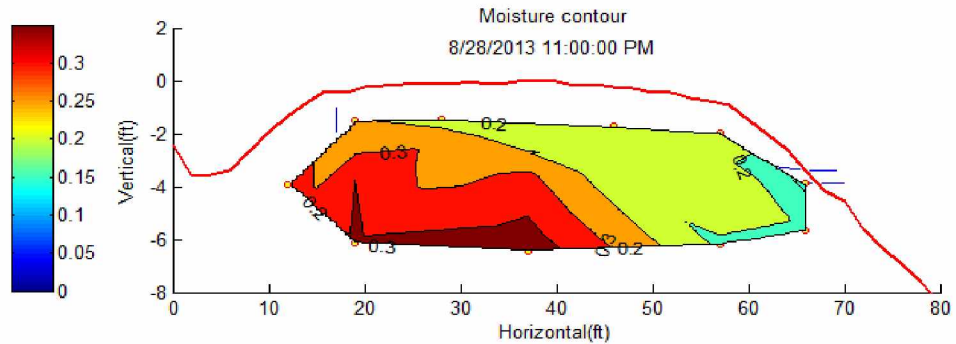


Figure 5.2 Soil Moisture Contours 1 Hour after Short Duration Rainfall

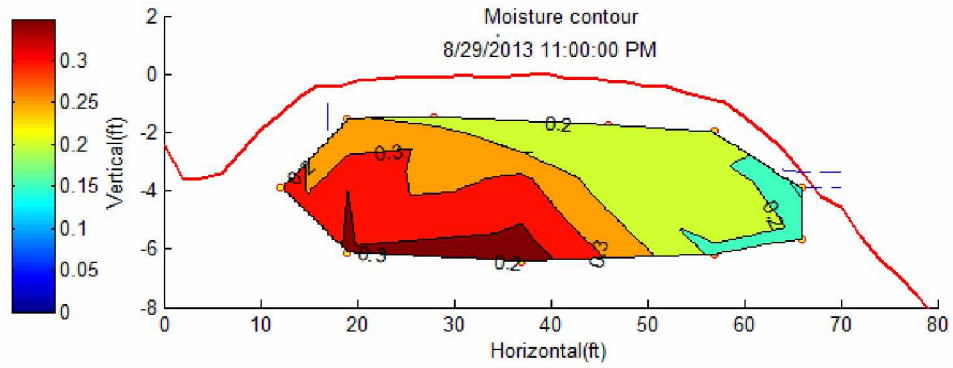


Figure 5.3 Soil Moisture Contours 1 Day after Short Duration Rainfall

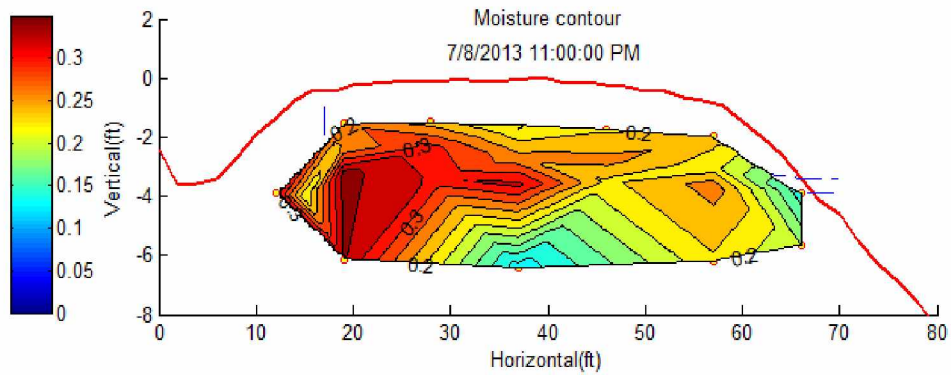


Figure 5.4 Soil Moisture Contours before Long Duration Rainfall

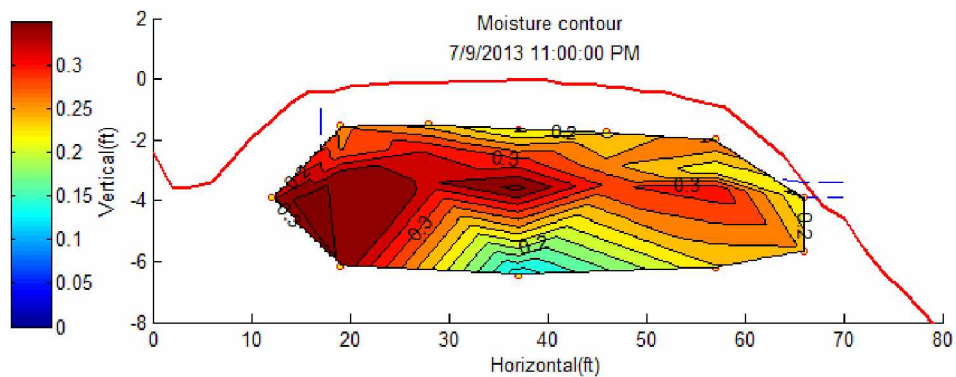


Figure 5.5 Soil Moisture Contours 1 Hour after Long Duration Rainfall

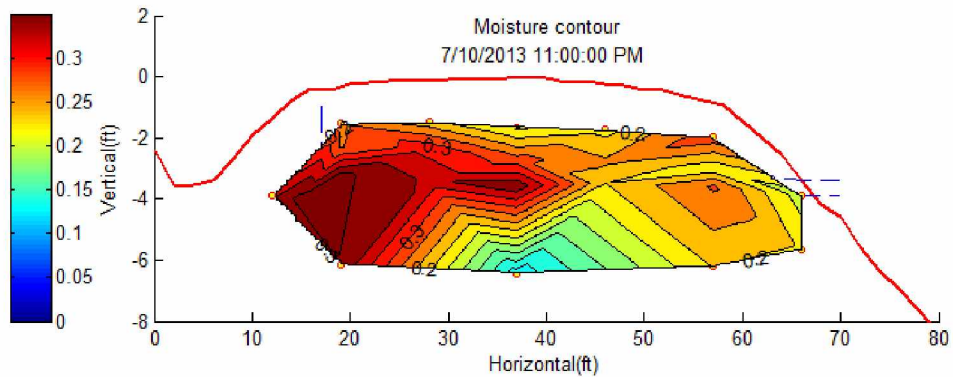


Figure 5.6 Soil Moisture Contours 1 Day after Long Duration Rainfall

During Freezing Process

For purposes of this discussion, we focused on 2012 data in our analysis of the freezing process. The air temperature dropped below 0°C on October 4, 2012; however, the temperature in the soil was still above 0°C , as shown in Figure 5.7.

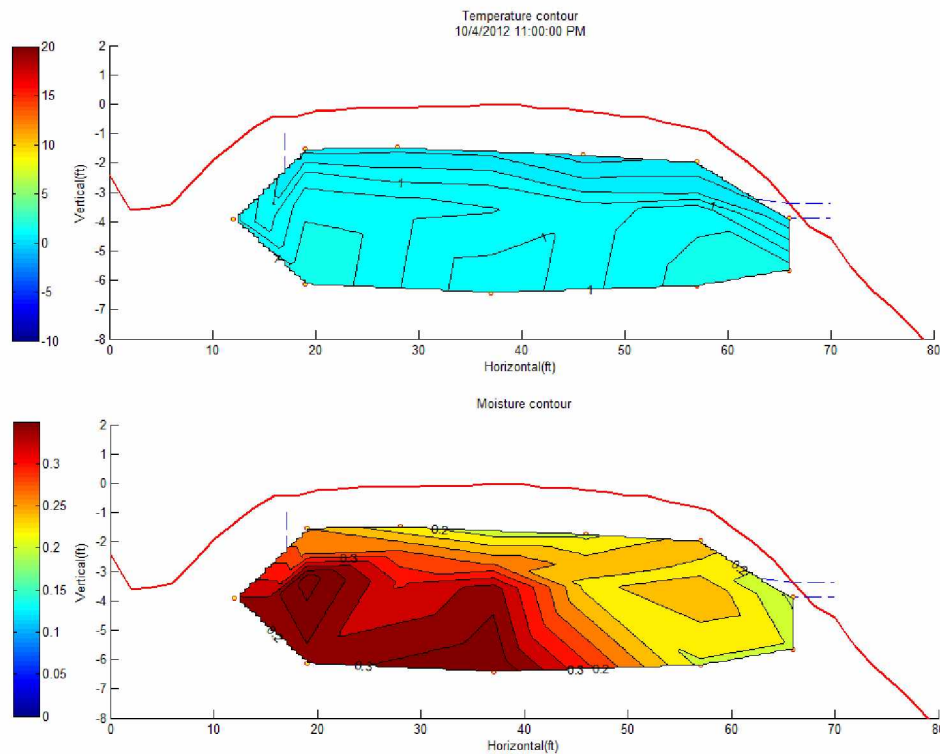


Figure 5.7 Temperature and Moisture Contours on October 4, 2012

It is critical to determine the moisture content distribution before the freezing front moves downward, because the water stored in the soil (both frozen and unfrozen) is the major factor influencing the severity of the “frost boiling” phenomenon in the subsequent spring. There were still two large saturation zones in the west side of the road; however, the moisture content in the east side was relatively low (about 0.2). This indicated that soft spots in the following spring, if frost boiling was observed, would be expected in the west lane of the road surface. Also, it would take a much longer time for the freezing front to move downward in the west side, as shown in Figure 5.8. It was discovered that the freezing front (0 °C isothermal curve) nearly coincides with the location of the 0.2 volumetric water content curve.

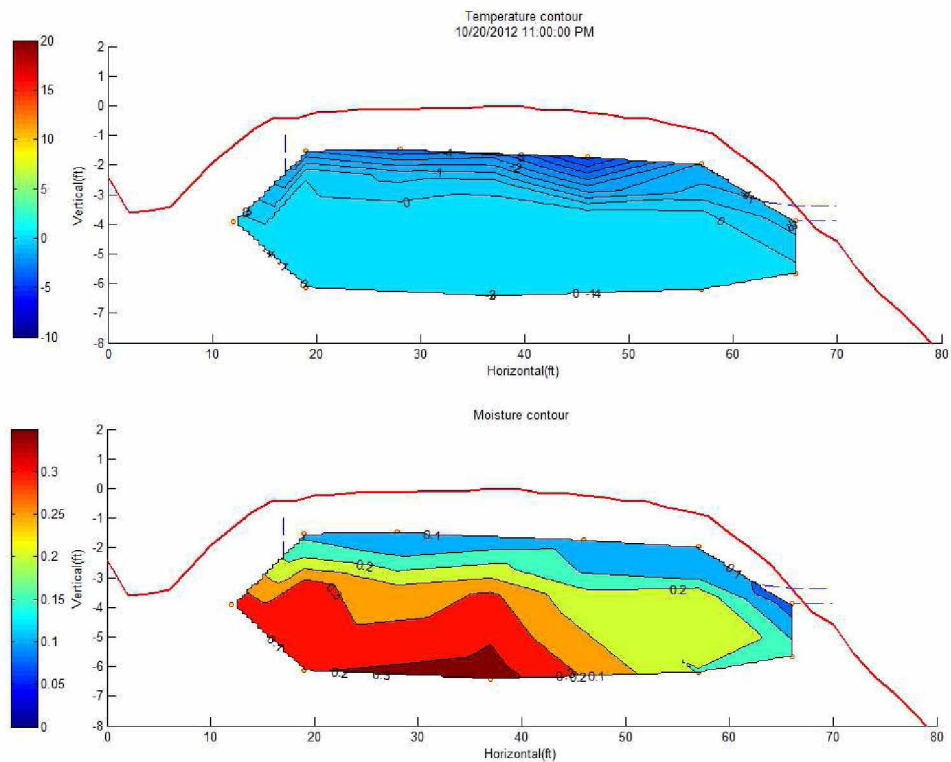


Figure 5.8 Temperature and Moisture Contours on October 20, 2012

The freezing front extended to about 0.76 meters (2.5 feet) below the road surface on October 20, 2012 on west side, and to approximately 1.07 meters (3.5 feet) on the east side. Moreover, the saturated zone was observed extending to the bottom sensor in the

west side. Since the specific heat capacity of water is relatively large compared with soil, it would take much more energy to freeze the soil on the west side, where the moisture content was higher. Furthermore, the area exposed to the freezing air on east side was larger than the west side, so it is reasonable to assume that the freezing front moved faster in east side of the road. If this holds true, the wicking fabric would stop functioning in early October, due to the frozen drainage paths where the fabric is exposed to the freezing air on the east side of the road. Figure 5.9 shows that the entire pavement structure was frozen on December 3, 2012, which was about two month after the air temperature dropped below 0°C . The unfrozen volumetric water content in the frozen soil was consistent, averaging about 0.07.

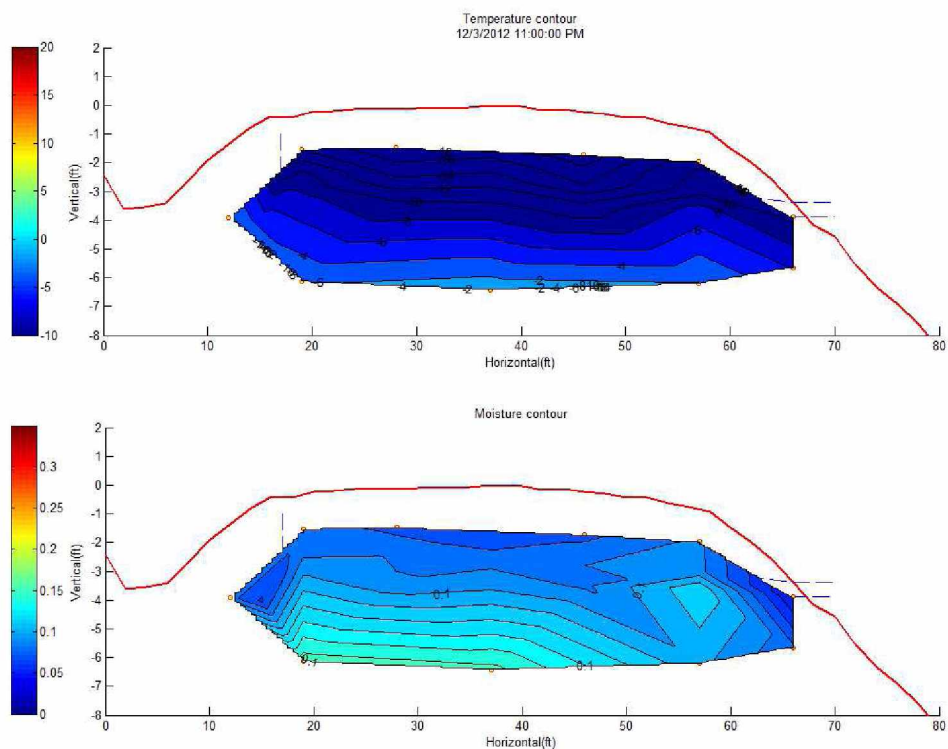


Figure 5.9 Temperature and Moisture Contours on December 4, 2012

Figure 5.10 through 5.13 show the temperature contours when the air temperature dropped below zero during the recorded four year period. It should be noted that the areas of the saturation zones decreased with time. For instance, there were two saturation zones that were connected together in 2010 and 2011; however, the saturation zones became

separated into two smaller zones on October 11, 2012. Because the soil moisture contents were lower than in previous years, it took less energy to move the freezing front downward. In comparison, the freezing front had already penetrated to 0.9 meters (2.95 feet) on October 11, 2012, which was about 0.3 meters (0.98 feet) deeper than the previous year. Furthermore, the saturation zone continued to decrease at the bottom of the roadway in year 2013.

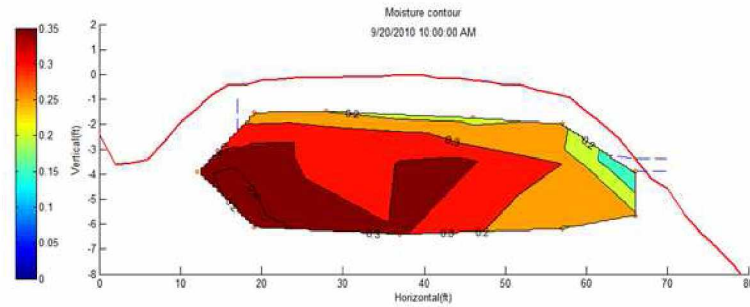


Figure 5.10 Moisture Contours on September 20, 2010

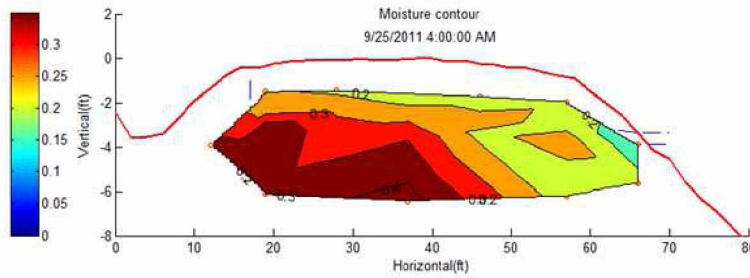


Figure 5.11 Moisture Contours on September 25, 2011

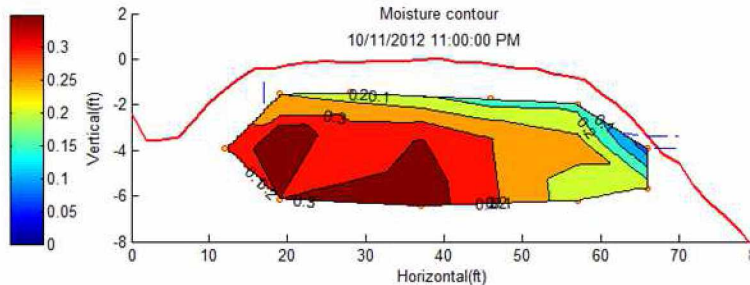


Figure 5.12 Moisture Contours on October 11, 2012

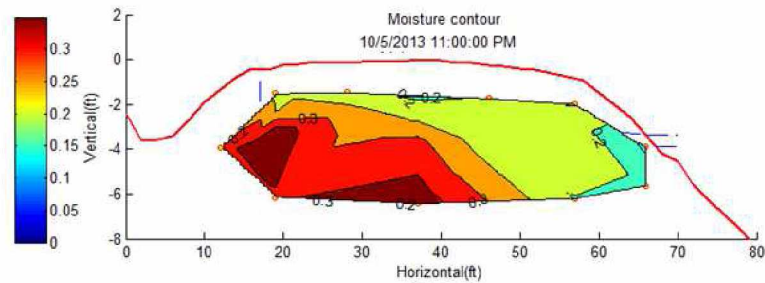


Figure 5.13 Moisture Contours on October 5, 2013

This phenomenon could be apparent because: (1) precipitation variation may cause such variations in the soil moisture content distribution, (2) the wicking fabric has worked effectively to reduce the moisture content in the soil. Because the rainfall event summary presented in Table 5.1 indicated that there were no significant rainfall events that occurred right before the selected days, precipitation was not the reason that caused the decrease in soil moisture contents. Therefore, the wicking fabric did reduce the water content in the east side of the roadway embankment, and reduced the size of saturation zone in the west side of the road. However, the performance of the wicking fabric to drain the water out needed to be further evaluated during the spring thawing process to validate its efficiency.

During Thawing Process

Figures 5.14 through 5.17 show the temperature and moisture contours during the thawing process in 2013. The mean daily air temperature raised above 0°C on May 9, 2013, as shown in Figure 5.14. The temperature in the soil was still below 0°C and the unfrozen water content of the soil was still about 0.07 to 0.10.

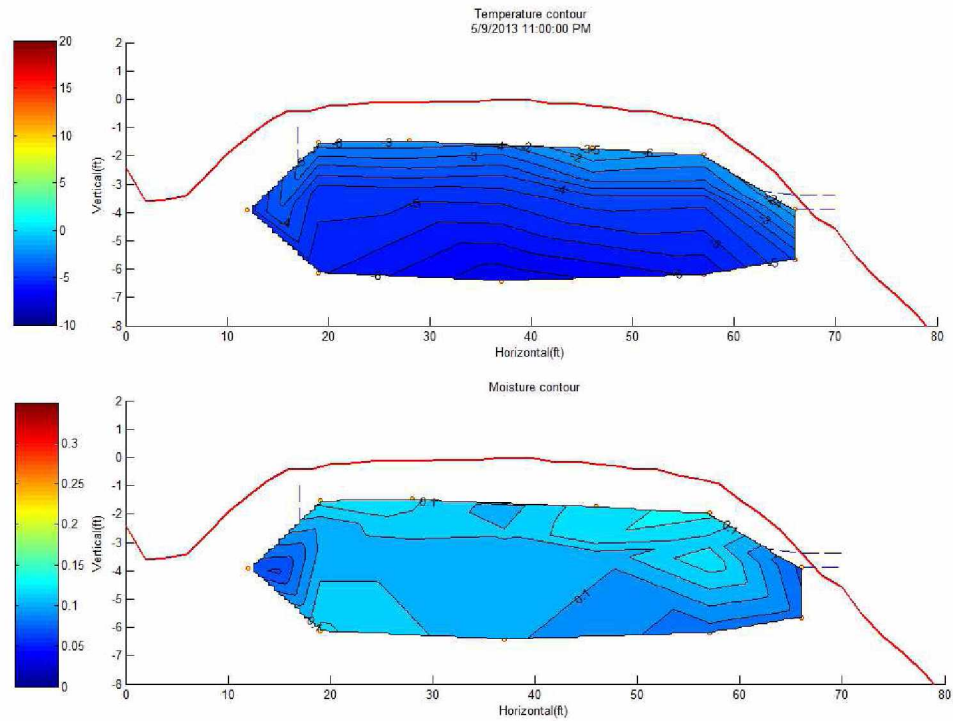


Figure 5.14 Temperature and Moisture Contours on May 9, 2013

Figure 5.15 shows the temperature and moisture contours on May 25, 2013. The thawing front had penetrated to about 0.61 meters (2 feet) near the west edge of the road, and to 1.06 meters (3.48 feet) at the east edge. It was mentioned previously that the frost boil phenomenon was observed during this time of the year. Similarly at sensor 22, located nearest to the drainage ditch, the unfrozen water content remained below 0.1, which indicated that the drainage ditch was still frozen at this time, and that there was no water supply from melting snow. All of the sensors showed that the moisture contents were far below saturation. This demonstrates that no soft spots could be observed at this time of the year.

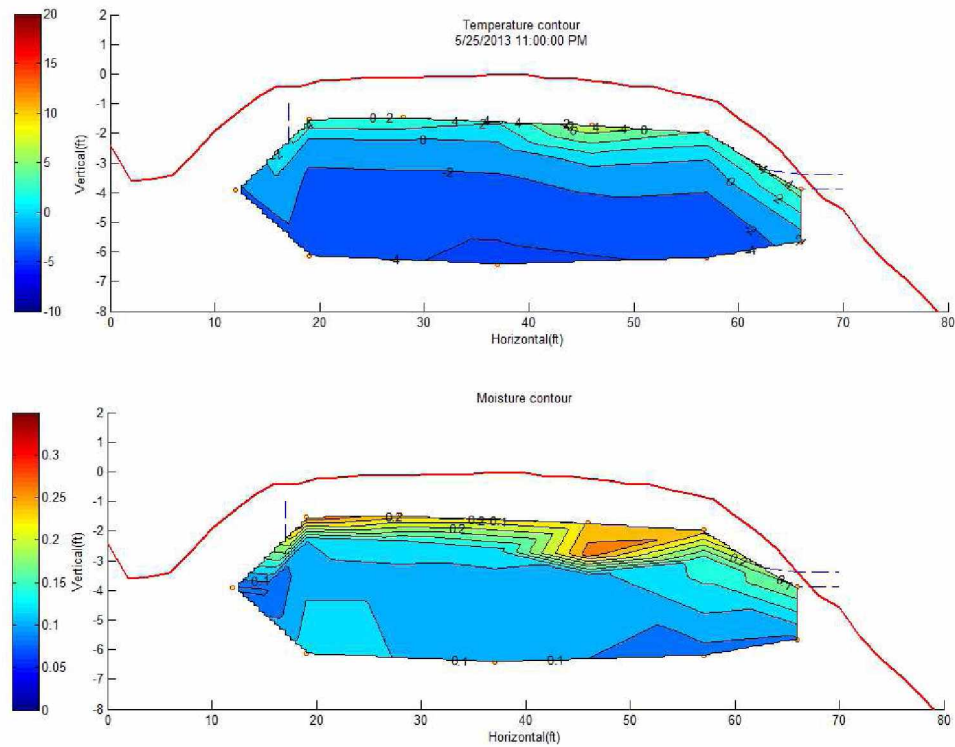


Figure 5.15 Temperature and Moisture Contours on May 25, 2013

Figure 5.16 shows the temperature and moisture contours on June 26, 2013. The thawing front had penetrated to 1.83 meters (6 feet) below the road surface, and a frozen core was evident in the center of the roadway. Again, since the moisture contents in the west side of the road embankment showed large amounts of stored water during the previous freezing process, and because the west side is located adjacent to the drainage ditch, the moisture contents were expected to be higher than those in the east side. Additionally, the frozen hard core in the center of the road embankment cut off the free water flow laterally and trapped the underground water at the east side of the roadway.

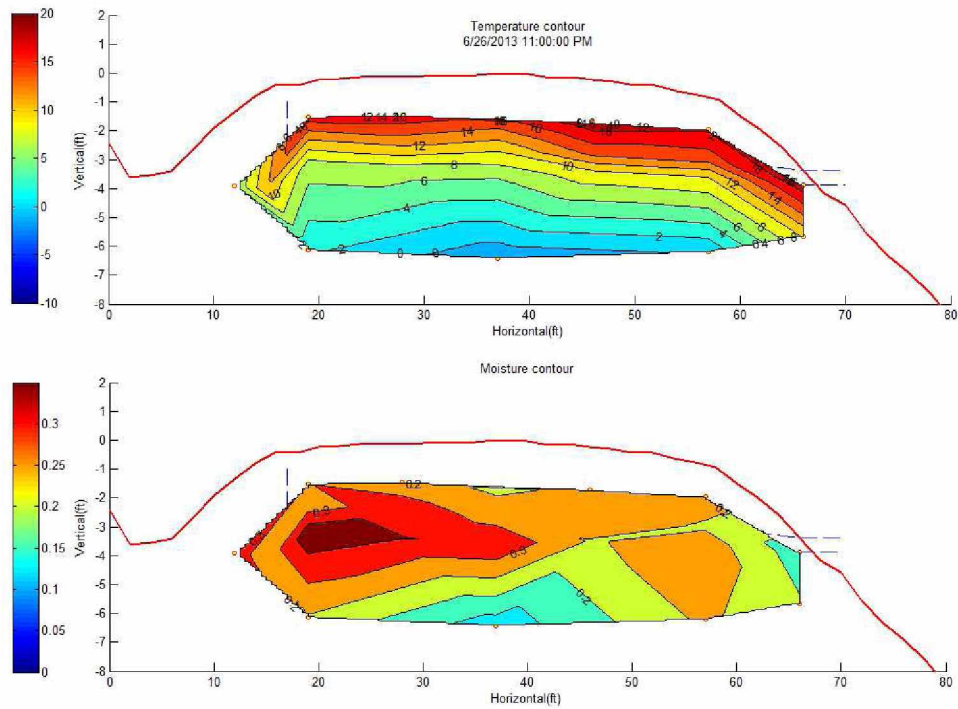


Figure 5.16 Temperature and Moisture Contours on June 26, 2013

Figure 5.17 shows the temperature and moisture contour on July 30, 2013. The thawing front had penetrated to 1.97 meters (6.4 feet) below the road surface, and the frozen core was thoroughly melted. The trapped saturation zone was released and was allowed to flow laterally out of the embankment. Meanwhile, the water stored in the drainage ditch and the ground water also provided additional water supply to the pavement structure; therefore, the saturation zone was expected to be even larger than before. Because of the presence of the wicking fabric, the east side of the embankment was relatively dry, demonstrating that the wicking fabric worked effectively to suck water out of the pavement structure.

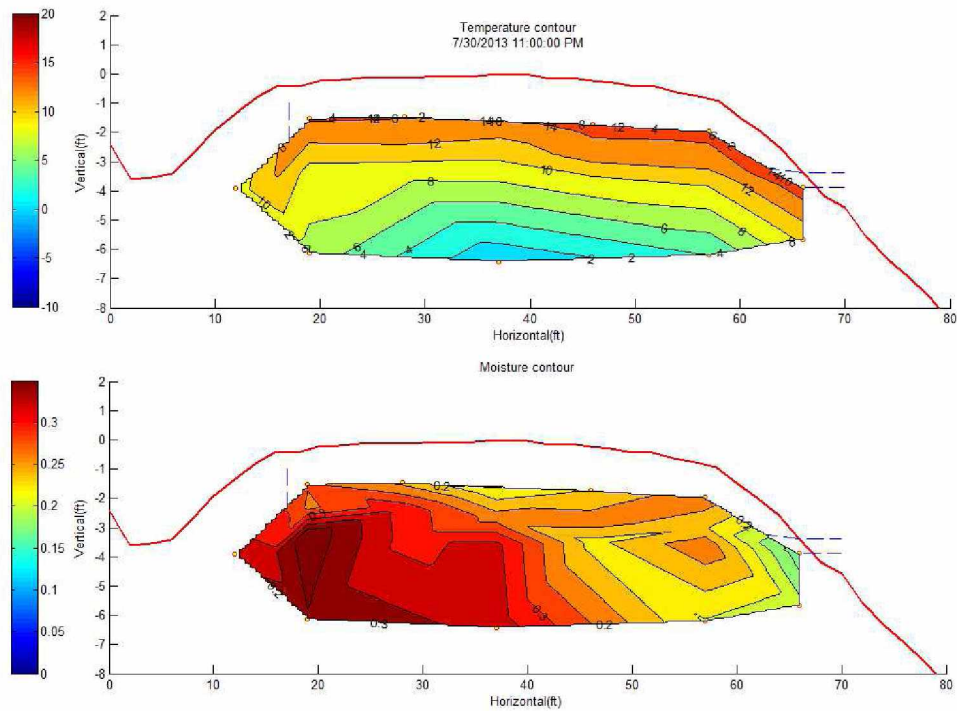


Figure 5.17 Temperature and Moisture Contours on July 30, 2013

Figures 5.18 through 5.21 show the moisture contours during the thawing process for the past four years. The mean monthly temperature for May, 2013 was lower than in previous years, so the thawing front only penetrated to 1.22 meters (4 feet) on the east side and 0.76 meters (2.5 feet) on the west side. For the other years studied, the penetration depth was relatively stable, corresponding to 1.06 meters (3.5 feet) on the west side and 1.37 meters (4.5 feet) on the east side. It has become evident that the wicking fabric effectively transported the water out of the roadway in the previous year and therefore reduced the amount of water that was stored in the frozen soil during the freezing process. The frost heave and subsequent thaw weakening issue did not occur in the following spring.

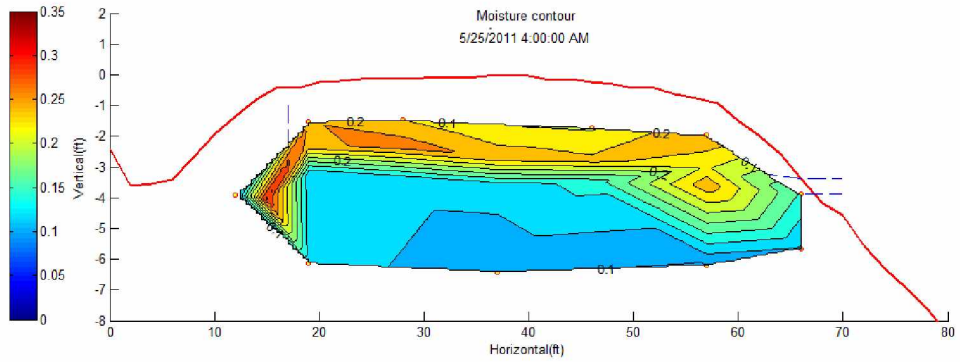


Figure 5.18 Moisture Contours on May 25, 2011

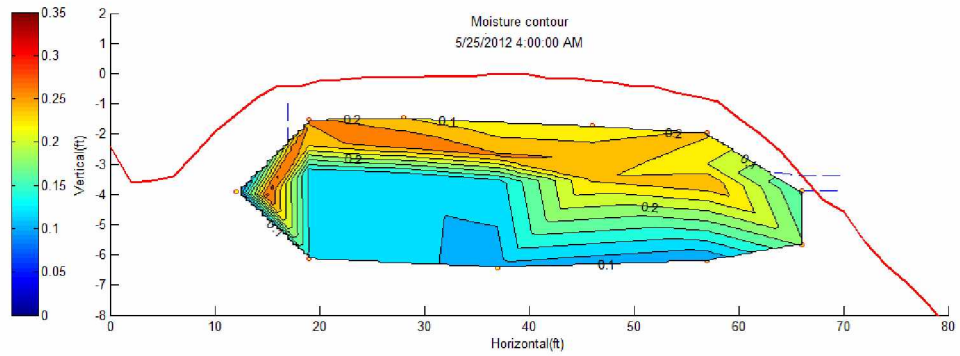


Figure 5.19 Moisture Contours on May 25, 2012

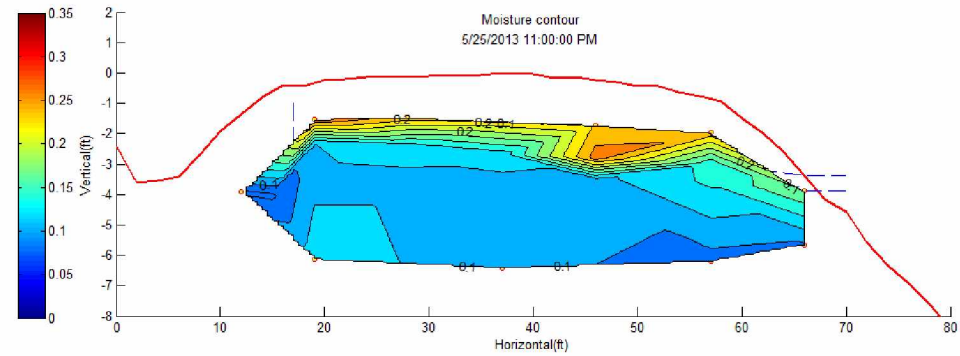


Figure 5.20 Moisture Contours on May 25, 2013

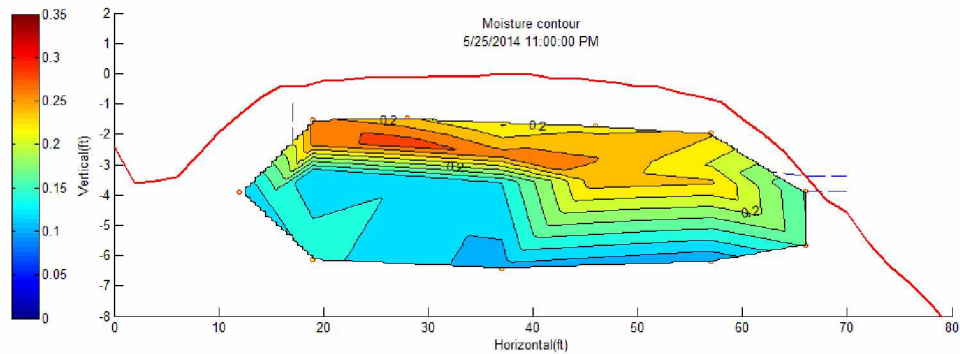


Figure 5.21 Moisture Contours on May 25, 2014

SEM Analyses

Field samples of the wicking fabric were collected from the Beaver Slide test site in July 2015. A JOEL JXA-8530F Electron Microprobe was used to analyze the wicking fabric microstructures. There were concerns about the long-term performance of the wicking fabric; specifically the clogging effect, permanent deformation, mechanical failure and aging effect. In total, 30 samples were analyzed; the detailed process and illustration regarding SEM analyses follows.

Clogging Effect

Figures 5.22 through 5.25 show some of the SEM images of samples collected from the Beaver Slide site. Figure 5.22 presents the woven structure of an intact sample with $\times 55$ magnification. It appears that large amounts of soil particles were detained on the surface of the wicking fabric. Figure 5.23 shows a closer view of the wicking fabric at the surface with $\times 350$ magnification. It further illustrates that the deep grooved drainage paths in the surface fibers were completely filled with fine soil particles. In comparison, Figure 5.24 shows the wicking fabric fibers just beneath the surface layer. The deep grooves beneath the surface were much cleaner than those above, and there were very few particles that had been detained in the drainage paths. In other words, the fibers of the wicking fabric at the surface served as a protective layer, preventing the fine soil particles from penetrating deeper into the fabric structure. Figure 5.25 shows the comparison of the wicking fibers on the surface and the fibers just beneath the surface. It can be visualized

from the figures that even though the wicking fabric fibers on the surface appeared to suffer from the clogging effect, the wicking fibers beneath the surface were relatively clean and still worked effectively to laterally drain water out of the pavement structure. Therefore, it is worth considering installing a layer of clean sand on top of the wicking fabric during the construction process in order to reduce the clogging effect, and improve the long-term performance of the fabric.

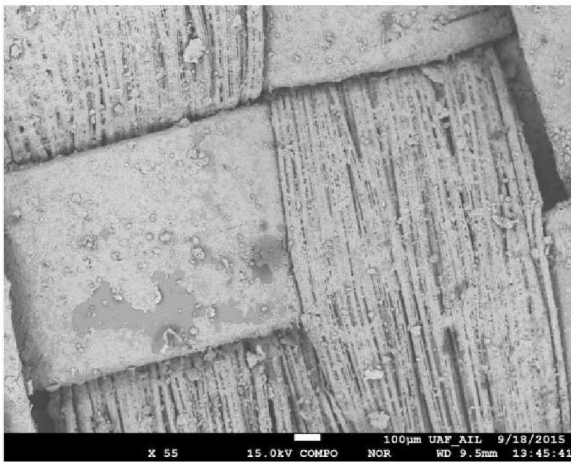


Figure 5.22 Intact Sample (Sample 4)

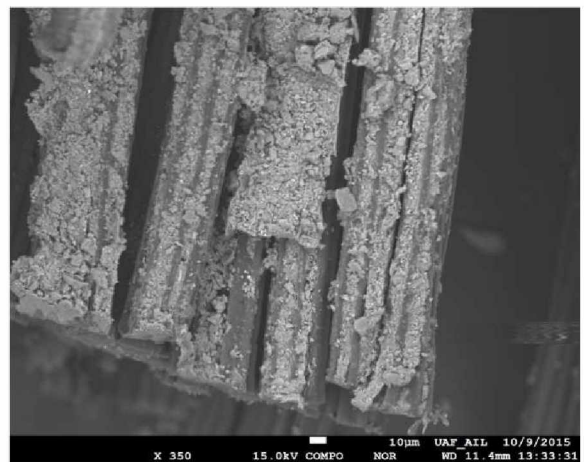


Figure 5.23 Surface Clogging (Sample 20)

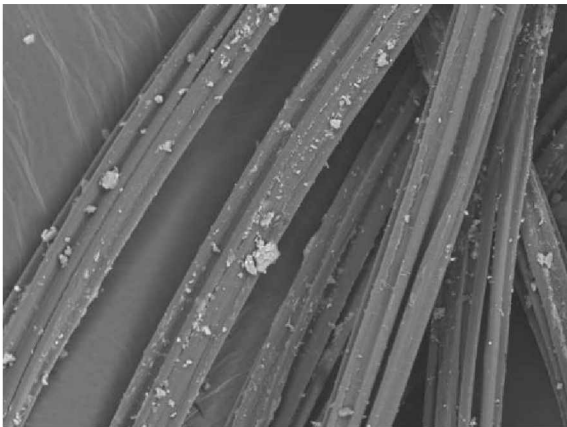


Figure 5.24 Beneath Sample (Sample 25)

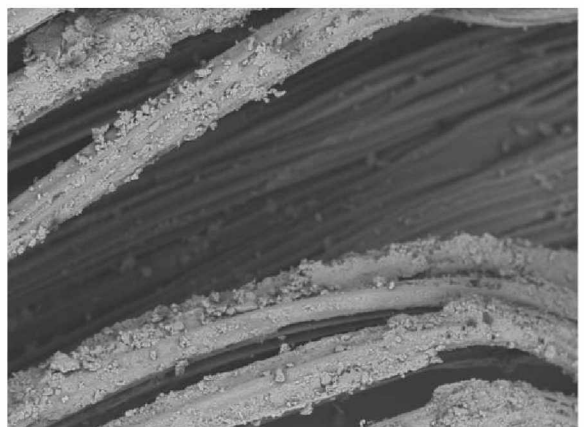


Figure 5.25 Wicking Fiber Comparison

Permanent Deformation and Mechanical Failure

Figures 5.26 through 5.29 present the SEM images of samples that suffered permanent deformation. Figures 5.26 and 5.27 present images of new wicking fabric, which were never used before. It was apparent that the wicking fabric fibers under the woven polypropylene yarns had already experienced some permanent deformation, and that the deformation was in the vertical direction. This deformation may have been caused by the pressure applied in the manufacturing process, or it may have occurred during the transportation process. Figures 5.28 and 5.29 show SEM images of the wicking fabric that was collected from the field. The permanent deformation observed in the new materials had further increased, as shown in these figures. Due to additional vertical pressure, the wicking fibers were nearly flattened, and the deep grooves were not able to hold water under unsaturated conditions. Furthermore, Figure 5.29 presents the front view of the wicking fabric; deep grooves are seen not only in the vertical direction, but deep grooves also tended to close in the horizontal direction.

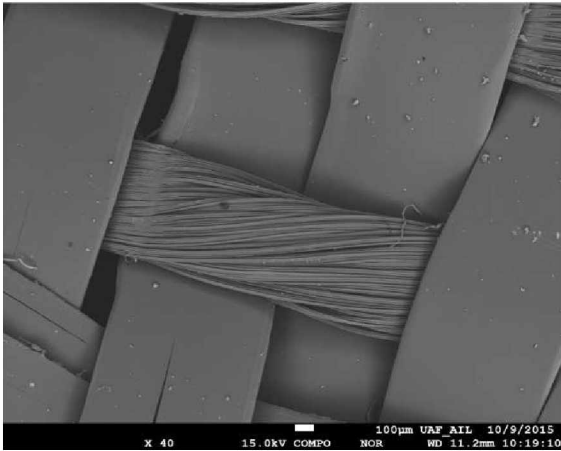


Figure 5.26 New Wicking Fabric

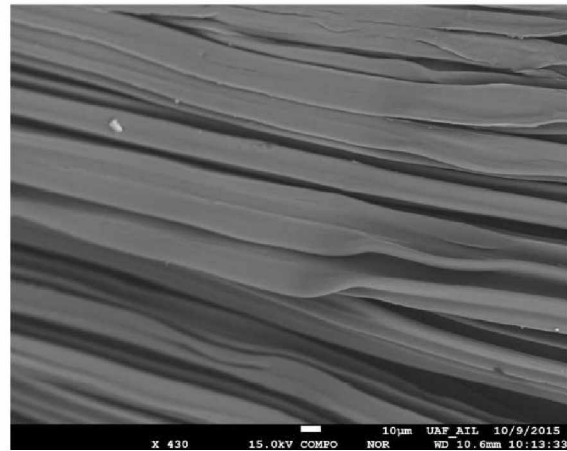


Figure 5.27 Permanent Deformation

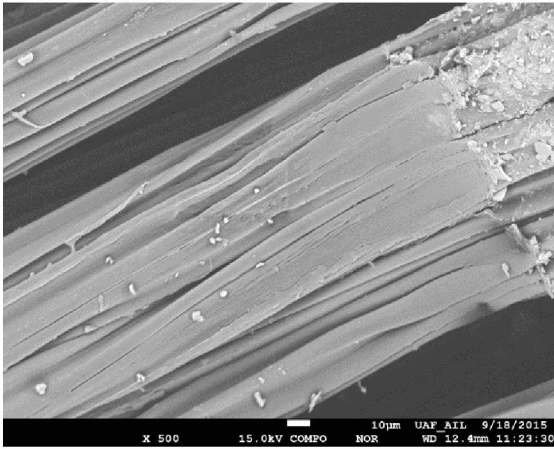


Figure 5.28 Top View

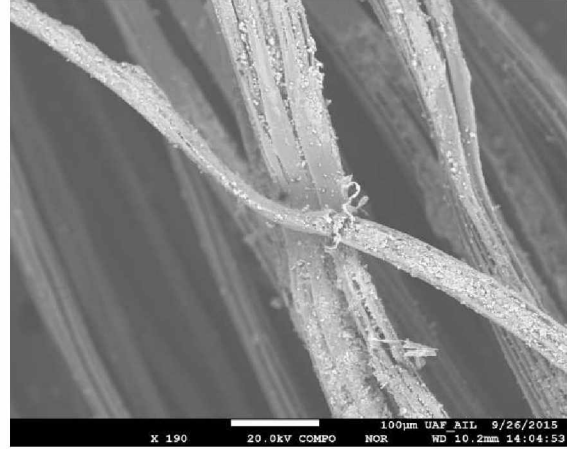


Figure 5.29 Front View

Another mechanical failure known as “puncturation” is illustrated in Figures 5.30 and 5.31. “Puncturation” refers to the puncturing of the soil fibers by the large soil particles that were detained on the wicking fabric surface. The large soil particles, especially those with sharp edges, acted as a cutting edge that severed the deep grooves of the wicking fabric. This likely occurred due to the high overburden soil pressures and the dynamic traffic loads applied to the road surface. The drainage paths were broken and became unable to continue to laterally transport water; however, this phenomenon was only observed in 5 of the 30 samples collected from the field.

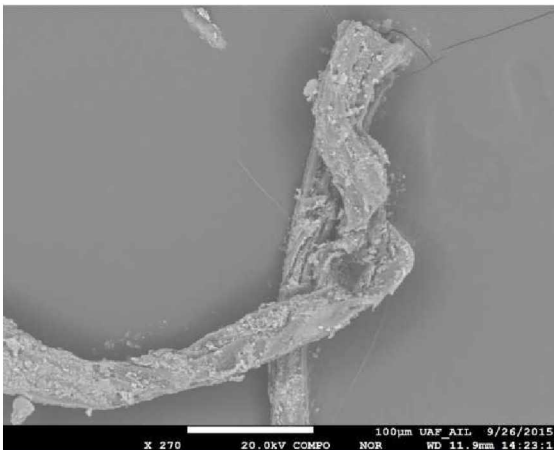


Figure 5.30 Sample 17

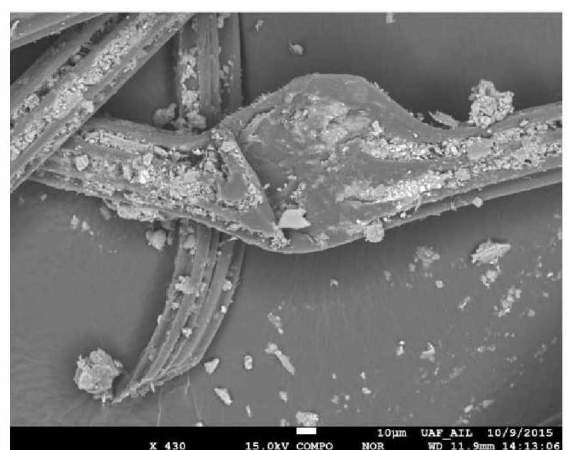


Figure 5.31 Sample 23

Aging

Because the wicking fabric is buried under the soil, another concern involves the wicking fabric's physical and mechanical aging issue, as shown in Figures 5.32 through 5.35. Figure 5.32 shows the aging severity of the wicking fabric fibers under the woven polypropylene yarns. Because the wicking fibers on the surface were directly in contact with the soil particles, the aging phenomena were usually observed in the fibers located at the surface of the fabric. Figure 5.33 shows the wicking fabric fibers at the surface without the woven polypropylene yarns. As believed, the aging phenomenon was likely due to direct contact with the soil particles. The aging effect at the bottom of the deep grooves was more severe than in the other areas of the wicking fabric. In comparison, Figures 5.34 and 5.35 show the wicking fabric fibers beneath the surface fibers. No obvious aging effect was observed below the surface layer of fibers, and the deep grooves were much cleaner than those of the fibers on surface of the fiber bundle.

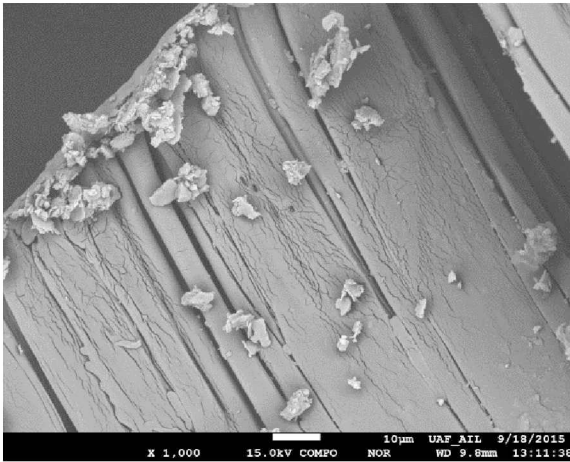


Figure 5.32 Sample 3

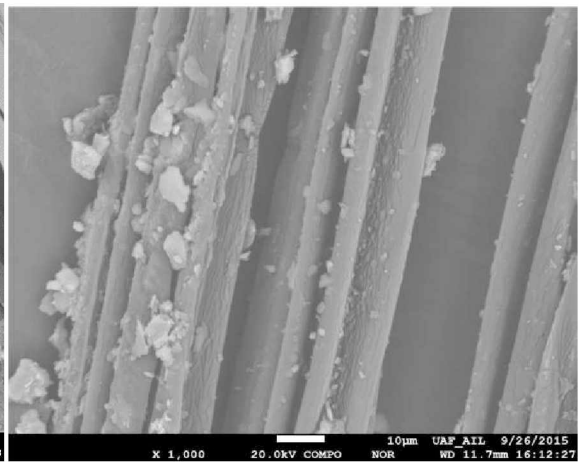


Figure 5.33 Sample 11

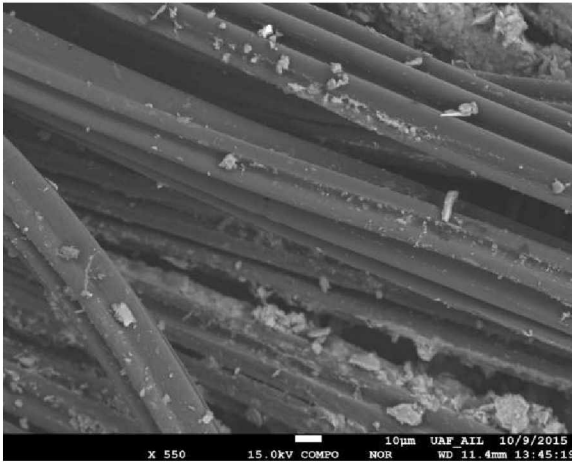


Figure 5.34 Sample 21

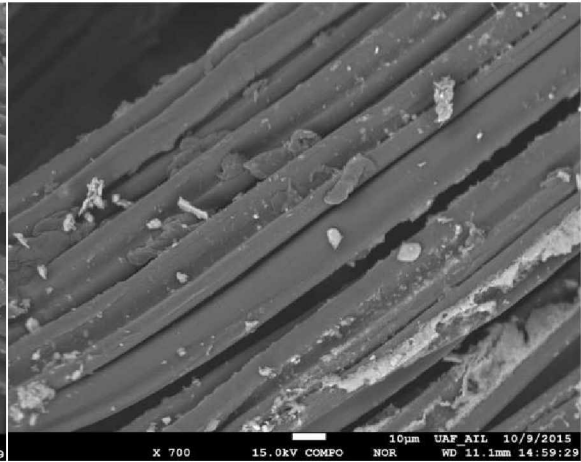


Figure 5.35 Sample 26

In general, all wicking fabric fibers on the surface of the fabric suffered from the clogging effect. However, only 6.67% of the wicking fabric fibers beneath the surface of the fabric suffered from the clogging effect. This indicates that even though the surface fibers were contaminated and the drainage paths were blocked, the wicking fibers beneath the surface of the fabric were well protected and worked effectively as a drainage material to transport water laterally under unsaturated conditions. Additionally, the permanent deformation was observed in every sample under the polypropylene woven area. The permanent deformations resulted from one, or both of the following two processes: (1) high pressure during the manufacturing process, and (2) high vertical overburden soil pressure and dynamic traffic load during its service life. The permanent deformation would likely affect the wicking fabric's long-term performance, since the drainage paths were either cutoff or narrowed down, and the deformation would continue to develop with time. The aging effect and mechanical failure were not considered to be major concerns that would influence the long-term performance of the wicking fabric.

CHAPTER VI

CONCLUSIONS

The Beaver Slide project has been monitored for more than five years, and the results indicate that the wicking fabric has successfully eliminated the ice formation and subsequent thaw weakening issues at the site.

Conclusions

The conclusions are listed as follows:

1. The soft spots observed during the early spring were caused by the ice formation and thaw weakening of the soils; however, the soft spots observed after heavy rainfall resulted from pressurized water flow. Although the phenomena were similar, the mechanisms were entirely different.
2. The severity of the thaw weakening in spring is relative to the moisture content present in the pavement structure before freezing begins at the start of the previous winter. The monitoring data shows that the moisture contents were decreasing, and that the saturated zones were smaller each year after the fabric was installed. Moreover, the moisture contents in the pavement structure were not observed to exceed the saturation moisture contents. This indicates that the wicking fabric worked successfully to eliminate the ice formation and subsequent thaw weakening issue during the past five years. The wicking fabric exhibits promising long-term performance results; however, additional monitoring and data analysis should be performed to establish long-term performance.
3. Clogging was only observed in the surface fibers of the wicking fabric. The wicking fabric fibers beneath the surface layer were relatively clean. The clogging effect was not considered to be a major issue for the application of the wicking fabric; however, it is recommended to use a protective layer above the wicking fabric so that the clogging effect can be further minimized at the surface of the wicking fabric.

4. The permanent deformation might be an issue that will affect the long-term performance of the wicking fabric. The deformed, deep grooves or drainage paths will reduce the amount of water that the wicking fabric can laterally transport. The permanent deformation may develop further over time due to high vertical pressure induced by the dynamic traffic loads and the overburden soils. The wicking fabric implementation depth and its influence on long-term performance should be studied further.
5. Mechanical failure and aging of surface fibers were observed in a limited number of samples. Mechanical failure may be caused by compaction during the construction process and high vertical pressure during its service life. Aging was observed in the surface fibers of the wicking fabric, where fibers were directly in contact with the surrounding soils.

REFERENCES

AKDOT&PF, (2004). Alaska Department of Transportation and Public Facilities Standard Specification for Highway Construction. 2004 Edition.

Allen, T., J. R. Bell, and T. S. Vinson. Properties of Geotextiles in Cold Regions Applications. Report 83-6. Transportation Research Institute, Oregon State University, Corvallis, 1983.

Beskow, G. (1946). "Supplement: some results of Scandinavian soil frost research 1935–1946." In Soil freezing and frost heaving with special applications to roads and railroads. Swedish Geological Society, Series Cv, No. 375, Year Book 3. Translated by J.O. Osterberg. CRREL Special Report 91-23, U.S. Army Corps of Engineers, Cold Regions Research and Engineering Laboratory, Hanover, N.H., pp. 161–169.

Casagrande, L. (1938). "Examination of the sub-soil of roads." In Proceedings of the 8th International Road Congress, The Hague, pp. 1–27.

Esch, D. (1994). "Long-Term Evaluations of Insulated Roads and Airfields in Alaska." FHWA_AK_RD_94_18 Final Report. Alaska Department of Transportation and Public Facilities. http://www.dot.state.ak.us/stwddes/research/assets/pdf/fhwa_ak_rd_94_18.pdf.

Guthrie, W. S. and Å. Hermansson (2006). "Saturation of Granular Base Material Due to Water Vapor Flow during Freezing." In Proceedings of the American Society of Civil Engineers Thirteenth International Conference on Cold Regions Engineering. CD-ROM. Orono, Maine, July 2006.

Henry, K.S. (1996). "Geotextiles to mitigate frost effects in soils: A critical review." 75th Annual Meeting of the Transportation Research Board, Washington, DC. Paper no 1534 (94 p.), pp. 5-11.

Henry, K.S. (1998). "The use of geosynthetics to mitigate frost heave in soils." Ph.D. dissertation, Civil Engineering Department, University of Washington, Seattle.

Henry, K.S., Holtz, R.D., (2001). "Geocomposite capillary barrier to reduce frost heave in soils." Canadian Geotechnical Journal 38, 678–694.

Henry, K.S. and J.C. Stormont (2002) "Geocomposite barrier drain for limiting moisture changes in pavement subgrades and base courses," Final Report for NCHRP-IDEA Project 68, The National Academies, Washington, D.C., 24p.

Holtz, R.D. and Kovacs, W.D. (1981). An Introduction to Geotechnical Engineering. Englewood Cliffs NJ: Prentice-Hall.

Hoover, J. M., J. M. Pitt, L. D. Handfelt, and R. L. Stanley. Performance of Soil-Aggregate-Fabric Systems in Frost-Susceptible Roads, Linn County, Iowa. In Transportation Research Record 827, TRB, National Research Council, Washington, D.C., 1981, pp. 6-14.

Rengmark, F. (1963). "Highway pavement design in frost areas in Sweden." Highway Research Record 33, Pavement Design in Frost Areas II. Design Considerations, pp. 137–157.

Taber, S. (1929). "Frost heaving." Journal of Geology, 38: 303–317. In Historical perspectives in frost heave research. CRREL Special Report 91-23, U.S. Army Cold Regions Research and Engineering Laboratory, Hanover, N.H., pp. 29–35.

Taivenen, O.A. (1963). "Preventive measure to reduce frost action on highways in Finland." Highway Research Record 33, pp. 202–216.

Zhang, X. and Belmont, N.(2009). "Use of Mirafi Nylon Wicking Fabric to Help Prevent Frost Heaving in Alaska Pavement: 1st, 2nd, 3rd, 4th and 5th progress reports." Progress reports to TENCATE GEOSYNTHETICS (North America).